MECHANICAL PROPERTIES OF HYDROXYAPATITE-MAGNESIUM ORTHOSILICATE COMPOSITE

JEFFREY CHIN KONG LEONG

FACULTY OF ENGINEERING
UNIVERSITY OF MALAYA
KUALA LUMPUR

2017

MECHANICAL PROPERTIES OF HYDROXYAPATITE-MAGNESIUM ORTHOSILICATE COMPOSITE

JEFFREY CHIN KONG LEONG

THESIS SUBMITTED IN FULFILMENT
OF THE REQUIREMENTS FOR THE DEGREE OF
DOCTOR OF PHILOSOPHY

FACULTY OF ENGINEERING
UNIVERSITY OF MALAYA
KUALA LUMPUR

2017

UNIVERSITI MALAYA

ORIGINAL LITERARY WORK DECLARATION

Name of Candidate: **Jeffrey Chin Kong Leong**

Registration/Matric No: **KHA110097**

Name of Degree: **Doctorate of Philosophy**

Title of Project Paper/Research Report/Dissertation/Thesis ("this Work"): Mechanical Properties of Hydroxyapatite-Magnesium Orthosilicate Composite

Field of Study: **Advance Materials/Nanomaterials**

I do solemnly and sincerely declare that:

(1) I am the sole author/writer of this Work;
(2) This Work is original;
(3) Any use of any work in which copyright exists was done by way of fair dealing and for permitted purposes and any excerpt or extract from, or reference to or reproduction of any copyright work has been disclosed expressly and sufficiently and the title of the Work and its authorship have been acknowledged in this Work;
(4) I do not have any actual knowledge nor do I ought reasonably to know that the making of this work constitutes an infringement of any copyright work;
(5) I hereby assign all and every rights in the copyright to this Work to the University of Malaya ("UM"), who henceforth shall be owner of the copyright in this Work and that any reproduction or use in any form or by any means whatsoever is prohibited without the written consent of UM having been first had and obtained;
(6) I am fully aware that if in the course of making this Work I have infringed any copyright whether intentionally or otherwise, I may be subject to legal action or any other action as may be determined by UM.

Candidate's Signature Date

Subscribed and solemnly declared before,

Witness's Signature Date

Name:
Designation:

ABSTRACT

Hydroxyapatite (HA) bioceramic has attracted a great deal of attention in the past two decades due to its similarity in terms of chemical structure to that of hard tissues. However, a major drawback of HA is the low fracture toughness (< 1 MPam$^{1/2}$) exhibited by the ceramic. Magnesium orthosilicate ceramic, on the other hand, possessed much higher fracture toughness and has recently been reported in the literature as a suitable biomaterial. However, limited studies have been conducted to investigate the combination of these two bioceramics, of which are crucial parameters needed to substantiate its suitability as a reliable nanocomposite material. Hence for the current research, the development of hydroxyapatite-magnesium orthosilicate composite with improved mechanical properties was investigated. The effects and implications of combining these two bioceramics were assessed in terms of linear shrinkage, phase stability, bulk density, Young's modulus, Vickers hardness, fracture toughness and microstructural evolution. In the present research, the hydroxyapatite powder was successfully synthesized through a novel wet chemical method and the magnesium orthosilicate powder was produced via combination of ultrasonification and mechanical ball milling method. Then the hydroxyapatite powder was mixed with magnesium orthosilicate accordingly to the concentration from 10wt. % to 50wt. % using the ultrasonification and mechanical ball milling method. Green samples were pressureless sintered at temperatures ranging from 1000°C to 1300°C at heating rate of 10°C / minute with a holding time of 2 hours.

A secondary phase known as whitlockite was found in all the hydroxyapatite-magnesium orthosilicate composites after sintering. In general, the ceramic composites exhibited low mechanical properties across all the composition investigated. However, a high fracture toughness of 2.5 MPam$^{1/2}$ was recorded for hydroxyapatite containing

20wt. % magnesium orthosilicate addition which indicated the potential of this composite to be used for load bearing biomedical applications. Moreover, the SEM graphs also demonstrated that formed whitlockite composite tends to form porous agglomerates. Such microstructure of calcium hydroxyapatite is one of the most frequently used bioceramics for bone and dental tissues reconstruction and for adsorption of hazardous materials from waste water and nuclear waste disposal.

ABSTRAK

Hydroxyapatite (HA) bioseramik mendapat banyak perhatian di sepanjang dua dekad yang lalu disebabkan struktur kimia yang sama dengan sepertimana yang didapati di dalam tisu keras. Walau bagaimanapun, HA mempunyai kekurangan yang utama di mana keliatan patahnya adalah rendah (<1 MPam$^{1/2}$) dipamerkan oleh seramik. Sebaliknya, seramik magnesium orthosilicate pula memiliki keliatan patah yang lebih tinggi dan sesuai untuk digunakan sebagai biobahan seperti yang dilaporkan di dalam kajian kesusasteraan kebelakangan ini. Namun, kajian penyelidikan berkaitan dengan pengabungan kedua-dua bioseramik ini, yang penting dalam menentukan kesesuaiannya sebagai bahan komposit yang boleh dipercayai adalah terhad. Justeru itu, kajian ini bertujuan menyelidik pembangunan hydroxyapatite-magnesium orthosilicate komposit dengan sifat-sifat mekanikal yang lebih baik. Kesan dan implikasi gabungan kedua-dua bioseramik ini akan dinilai dari segi pengecutan linear, kestabilan fasa, ketumpatan pukal, Young's modulus, nilai kekerasan, ketahanan patah dan evolusi mikrostruktur. Dalam kajian ini, serbuk hydroxyapatite telah berjaya disintesis melalui kaedah kimia basah novel dan serbuk magnesium orthosilicate dihasilkan melalui kombinasi ultrasonifikasi dan kaedah bola pengisaran mekanikal. Kemudian serbuk hydroxyapatite dicampurkan dengan forsterite mengikut kepekatan daripada 10wt. % kepada 50wt. % menggunakan ultrasonifikasi dan kaedah bola pengisaran mekanikal. Sampel hijau disinter tanpa tekanan pada suhu di antara 1000°C hingga 1300°C pada kadar pemanasan 10°C / minit dengan masa yang memegang 2 jam.

Selepas pensinteran, fasa kedua yang juga dikenali sebagai whitlockite didapati di semua komposit hydroxyapatite-magnesium orthosilicate. Secara umumnya, komposit seramik mempunyai sifat mekanik yang rendah berbanding dengan komposisi-komposisi yang diselidik. Walau bagaimanapun, hydroxyapatite dengan komposisi

20wt. % magnesium orthosilicate menunjukkan potensinya sebagai penanggung beban di dalam aplikasi bioperubatan dengan keliatan patahnya yang tinggi sebanyak 2.5 MPam$^{1/2}$. Di samping itu, graf SEM juga menunjukkan komposit whitlockite yang terbentuk mempunyai kecenderungan untuk membentuk gumpalan berliang. Mikrostruktur seperti kalsium hydroxyapatite adalah salah satu bioceramik yang paling kerap digunakan untuk pembinaan semula tulang dan tisu gigi dan untuk penjerapan bahan-bahan berbahaya daripada air kumbahan dan pembuangan sisa nuklear.

ACKNOWLEDGEMENTS

First and foremost, I would like to express my sincere gratitude and respect to my project supervisor, Prof. Ir. Dr. Ramesh Singh, for his continual guidance and encouragement given to me throughout the entire period of this research. His passion and drive in the research field in sharing his valuable knowledge had always been inspirational to me. He has not only shared with me his vast technical knowledge in the area of engineering ceramics but also molded me to be a competent researcher.

Next, I would also like to thank the kind Management of University of Malaya for the facilities support. Additionally, I would like to extend my appreciation to SIRIM Berhad Malaysia for providing the testing instruments such as XRD machine, Vickers hardness tester, etc.

Special thank you is also conveyed to my friends and colleagues who voluntary willing to spend their time to guide and motivate me during the research work: Natasha, Kelvin Chew, Ali Niakan and Christopher Chin. Their presents have made work and life more fun.

Finally, I would like to thank my loving family and my wife Carmen Tang who have been a great support right through the period of this research in providing endless words of encouragement, moral support and most importantly believing in me. I would not have made it without you people. All help, care and concern will forevermore be appreciated and remembered.

In memory of my late father

TABLE OF CONTENTS

LIST OF FIGURES

LIST OF TABLES

LIST OF SYMBOLS AND ABBREVIATIONS

A-W	Apatite wollastonite
ACP	Amorphous calcium phosphate
Al_2O_3	Alumina
AP	Apatite
BCP	Biphasic calcium phosphate
Ca/P	Calcium phosphorus ratio
$Ca_{10} (PO_4)_6 (OH)_2$	Hydroxyapatite
$Ca_3(PO_4)_2$	Tricalcium phosphate
$CaSO_4$	Calcium sulphate
$CaZrO_3$	Calcium zirconate
CDHA	Calcium deficient hydroxyapatite
CHAp	Carbonate apatite
CIP	Cold isostatic pressing
CPC	Calcium phosphate ceramic
DCPA	Dicalcium phosphate anhydrous
DCPD	Dicalcium phosphate dehydrate
E	Young’s modulus
EDX	Energy dispersive X-ray
FTIR	Fourier transform infrared
HA	Hydroxyapatite
HA-MO	Hydroxyapatite-magnesium orthosilicate
H_2O	Water
Hv	Vickers hardness
i.e.	that is (id est)
JCPDS	Joint Committee of Powder Diffraction Standard

K_{Ic}	Fracture toughness
MCPA	Monocalcium phosphate anhydrous
MCPM	Monocalcium phosphate monohydrate
Mg	Magnesium
MgO	Magnesium oxide
Mg_2SiO_4	Magnesium orthosilicate/forsterite
MO	Magnesium orthosilicate
OCD	Octacalcium
PMMA	Polymethyl methacrylate
Q	Action energy
Rpm	Revolution per minute
SC-HA	Hydroxyapatite scaffold
SEM	Scanning electron microscopy
Si	Silicon
SiO_2	Silicon oxide/quartz
TCP	Tricalcium phosphate
TTCP	Tetracalcium phosphate
UHMWPE	Ultra high molecular weight polyethylene
wt. %	Weight percentage
XRD	X-ray diffraction
Y-TZP	Yttria stabilized zirconia
ZrO_2	Zirconia
α-TCP	Alpha tricalcium phosphate
Β-TCP	Beta tricalcium phosphate
σ	Strength

CHAPTER 1 - INTRODUCTION & OBJECTIVES

1.1 Introduction

Ceramics in general are consists of inorganic and nonmetallic materials that include clay products, porcelain, refractory materials, pottery, abrasives, nonmetallic magnetic materials, and glasses. In the recent 30 years, ceramics and glasses have been in the interest as candidates for implant material since these materials exhibit highly desirable characteristics for applications as shown in Figure 1.1. These ceramics materials which are specially engineered for use as dental and medical implants are termed bioceramics. The material's characteristic of being inert in aqueous conditions and high biocompatibility makes it as an advantage to be used in bioceramic application. Bioceramics can be classified into three types such as materials that are implanted inside bodies, materials that are implanted outside bodies that will be in contact with mucous membranes and skins and materials that are used without direct contact with the human body. The three types of materials are represented by artificial bones, crowns and column fillers for high performance liquid chromatographies. Basically, bioceramic have been incorporated into products used in biochemical, pharmaceutical and medical fields.

One of the bioceramic from calcium orthophosphates family widely used by researchers, the hydroxyapatite (HA) material, is known to have a chemical formula (Ca_{10} $(PO_4)_6$ $(OH)_2$) that correlates well with the mineral component of human such as the hard tissues and has been widely commercialized as an artificial bone prosthetic material that directly interface with living bones (Zhang et al., 2016). The strength (porosity) and shapes are adjusted to supplement various bone defects and reconstruct bone tissues. The use of dense bodies can be applied in area where strength is required, while high porosity bodies are used in areas where involved integration with living bone tissues. The HA are also used to replace bone or as supplement throughout the body and are usually processed into various sizes and shapes. Moreover, the stability in aqueous medium with pH above 4.3 has been regarded as excellent as it was well within the range for blood which has a pH of 7.3 (Best et al., 2008; Kalita et al., 2007).

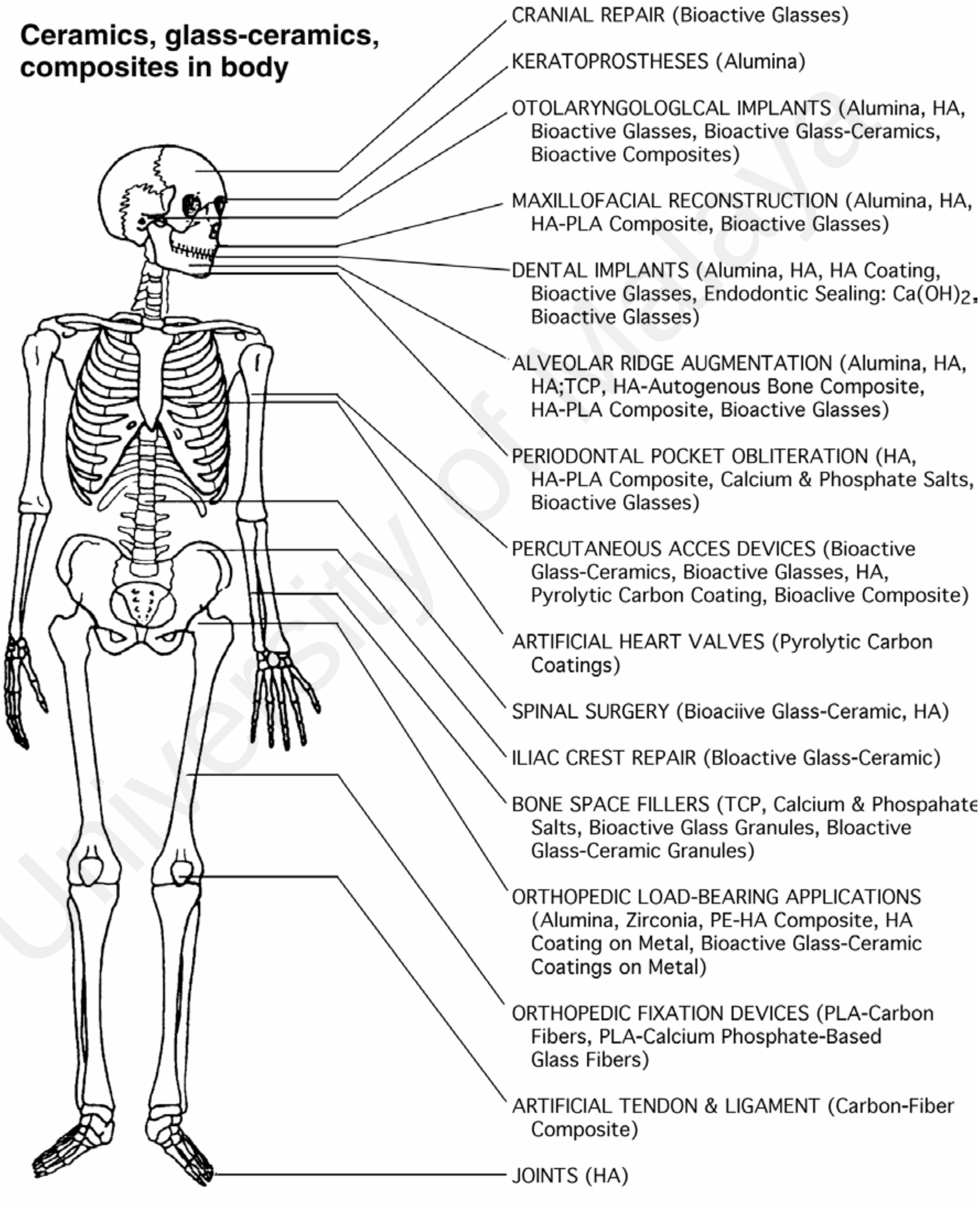

Figure 1.1: The applications of glasses, ceramics and composites in the human anatomy (Hench and Wilson, 1993).

Although hydroxyapatite is a promising biomaterial, its poor and unsatisfactory mechanical properties have constraint its fullness in clinical orthopedic and dental applications which researchers are continuously working on the improvements.

1.2 Problem Statement

Hydroxyapatite with its high biocompatibility and chemical similarity with natural bone was introduced to be a material of interest for biomedical applications (Zakaria et al. 2013). However, due to processing difficulties and the lower mechanical properties of HA, the applications have been limited to coatings, powders, and non-load bearing implants only. The low mechanical properties such as poor fatigue resistance, inherent brittleness and strength, especially its low fracture toughness (K_{Ic}) of < 1 $MPam^{1/2}$ are the major drawback for load bearing applications (Khorsand et al., 2014). Some studies have been carried out previously by addition of dopants to enhance the low mechanical properties of HA, however the findings showed little improvement in the fracture toughness.

Amongst the materials which have a crucial roles in human are the magnesium and silicon. Studies have shown that in skeletal development, silicon is necessitous and is usually uniquely localized in the active areas of young bone (Tavangarian & Emadi, 2011). The findings from the literatures (Tavangarian & Emadi, 2011; Kharaziha & Fathi, 2010; Siyu et al., 2007; Carlisle, 1988) showed that silicon (more than 5wt. %) is found in the active growth areas in the bones which have a Ca/P ratio of 0.7 in the young rats and involved in the early stage of bone calcification in physiological conditions. Schwarz and Milne (1972) also reported that the addition of silicon in the rats' diet has influenced its growth. Besides silicon, magnesium is considered as the next important element in human body as this element is closely associated with mineralization of calcined tissues and indirectly influences mineral metabolism which influence the control of bone growth (Schwarz & Milne, 1972).

To improve the low mechanical properties of hydroxyapatite, there is a need to reinforced the HA with other ceramics having better mechanical properties. Magnesium orthosilicate (Mg_2SiO_4), also known as forsterite, could be a material of interest because of the biocompatibility and higher fracture toughness. The fracture toughness of magnesium orthosilicate ceramic has been proclaimed to be about 2.4 $MPam^{1/2}$ which is much higher than 1 $MPam^{1/2}$ reported for bone implants and hydroxyapatite ceramic (Sebdani et al., 2011; Fathi & Kharaziha, 2009).

1.3 Objectives of Research

The main objective in conducting this research is to develop a hydroxyapatite – magnesium orthosilicate (HA-MO) composite that exhibits better mechanical properties while preserving its phase stability. The three-fold objectives of this research are as follows:

1) To synthesize a HA-MO composite.
2) To establish the optimum sintering conditions of the composite that exhibits superior mechanical properties at lower temperature suitable for biomedical applications.
3) To establish the factors that control the properties of the composite and elucidate the sintering mechanism of the composite.

This combination of HA-MO has not been reported widely in the literature, therefore it is envisage that this research would generate new knowledge in the area of biomaterials. In addition, the understanding of the various process parameters governing the sinterability of the composites would be gained.

1.4 Scope of Project

The research will commence with an extensive literature review covering the area of magnesium orthosilicate and hydroxyapatite in order to establish better understanding and awareness of the current work being performed in this field. The composite will be prepared in various compositions, by varying the magnesium orthosilicate content from 10wt. % to 50wt. % via mechanical ball milling and conventional pressureless sintering at 1000°C to 1300°C, with ramp rate of 10°C/minute (heating and cooling) and holding time of 2 hours for each firing. Upon sintering, the phase analysis will be carried out using an X-ray Diffraction (XRD) machine to evaluate the phase stability of HA. For the grain size measurement and phase composition of HA-MO nanocomposite will be examined through scanning electron microscope (SEM) and Energy-dispersive X-ray (EDX) machine. Finally, the HA-MO nanocomposite will also be evaluated in terms of mechanical properties by measuring the relative density, Vickers hardness, Young's modulus and fracture toughness.

1.5 Thesis Structure

In Chapter 1, a brief overview and introduction of the research area is presented. The problem statement which lead to this research is highlighted followed by the objectives to achieve.

Chapter 2 gives an extensive literature review on biomaterial and other researchers' work related to HA and MO are presented. There are not many literatures available for HA-MO composite, hence it is important to establish the fundamental of combining these two materials.

Chapter 3 describes the framework on the synthesis technique to produce HA and MO powder for the present work. Besides that, the experimental testing and analysis techniques of the sintered composites will be written too. Any descriptions of the equipment used will be included here.

The results and discussion are presented in Chapter 4. The hydroxyapatite, magnesium orthosilicate and HA-MO powders' characterization are discussed here, follow with discussion on the mechanical properties and microstructural analysis. This chapter will gives a clearer picture on the achievement of this research work.

Finally Chapter 5 concludes the current research findings and some suggestion for future work are given here. The appendices will contain carious experimental results, equipment used, sample calculation including research publications.

CHAPTER 2 - LITERATURE REVIEW

2.1 Human Bone Structure

The bulk of the human skeleton consists of bony framework which assists locomotion, and also acts as a protective cage for internal organs. The bony framework is usually strong and lightweight, but is also a constantly changing tissue which undergoes a remodeling process in the entire life. Structurally, the skeleton consists of bone tissue whereby it is formed by the inorganic and organic phases and water in the nanoscale. Bone can be mentioned in terms of weight basis (60% inorganic, 30% organic and 10% water) or volume basis (proportions broken down into 40%, 35%, and 25%) respectively. (Tony, 2003; Chen et al. 2004). The bone with the inorganic phase is referring to the ceramic that consists of mineral type of crystalline, commonly referred to as hydroxyapatite, $Ca_{10}(PO_4)_6(OH)_2$ (Tony, 2003). The tiny apatite crystals in bone hydroxyapatite contain impurities such as carbonate (as substitute of the phosphate ions), potassium, magnesium, stronchloride or fluoride (as substitute of the calcium ions), and fluoride or chloride (as subsitute of hydroxyl ions). For the bone with organic phase, it comprises of type I collagen (90wt. %), collagen types (III and VI), and some variety of noncollagenous proteins such as bone sialoprotein, osteonectin, osteocalcin, and osteopontin (Boskey, 2010). Table 2.1 summarized the elements found in bones.

The hierarchical composite of the bone tissue at the micron scale and above is as shown in Figure 2.1. At the lowest level (0.1µm) is where the mineralized collagen fibrils are located, follow by the next level in the range of 1 to 10µm scale where two forms of the fibrils can be arranged into known as lamellae (about 7µm thick) that contain unidirectional fibrils in alternating angles between layers or as woven fibrils. Naturally, the lamellar bone is commonly found in the adults (human), while the woven bone is found in children and large animals where rapid growth takes place, and also in the initial healing stage of a fracture.

At the millimeter scale in different types of histological structures, lamellar bone can be found. The primary lamellar consists of large concentric rings of lamellae similar to the growth rings on a tree that circle the outer (2 to 3 mm) of diaphysis. In human adults, the cortical bone is known as Haversian bone or oeteonal, where the central Haversian canal consists of lamellae arranged in concentric cylinders, a vascular channel about 50 µm in diameter that contains nerves, variety of bone cells, and blood vessel capillaries.

Table 2.1: Elements found in an adult's bone (Orlovskii et al., 2002; LeGeros & Legeros, 1993).

Elements	**Weight (%)**
Calcium	34.8
Phosphorus	15.2
Sodium	0.90
Magnesium	0.72
Potassium	0.03
Carbonates	7.40
Fluorine	0.03
Chlorine	0.13
Pyrophosphates	0.07
Other elements	0.04

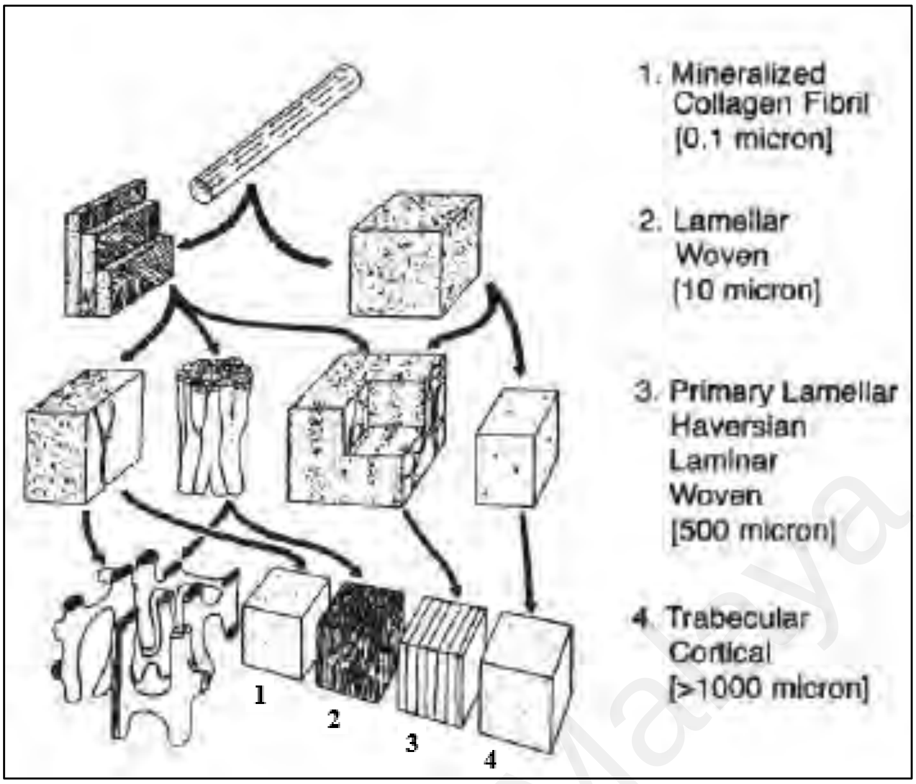

Figure 2.1: The hierarchy levels of bone microstructure (Paul, 2004).

Lastly, the tightly packed lamellar which is known as the cortical bone and highly porous cellular solid woven bone and trabecular bone are commonly found at the highest level of the hierarchical in the range of 1 to 5mm Basically the cortical surrounds the trabecular bone giving that forms the bone shape or shell. For load bearing condition, the cortical component of the bone is markedly thickened to form a strong shaft. The internal porous framework of bones is supported by the trabecular bone. The trabecular bone consists of stem-cell-rich bone marrow. For the growth of new connective tissue such as muscle, cartilage, bone and tendons will require the bone marrow. Figure 2.2 shows a typical bone structure of a human femur.

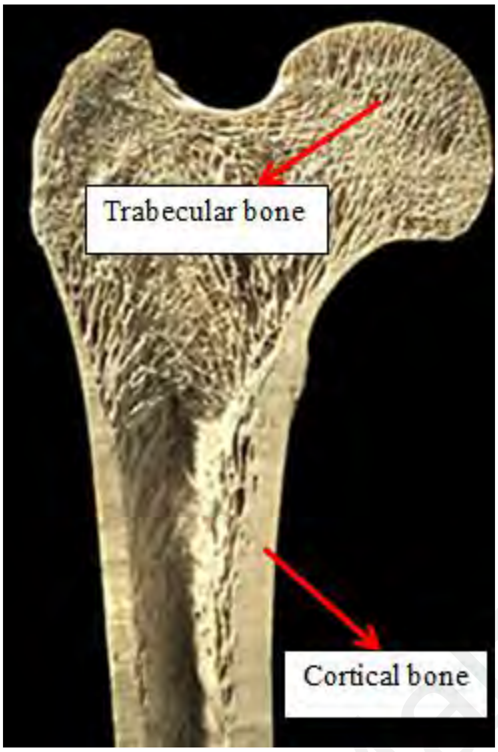

Figure 2.2: Bone structure of a human femur (Paul, 2004).

2.2 Biomaterials

About 50 years ago, biomaterials at the present state that are broadly used throughout dentistry, medicine and biotechnology did not exist. Biomaterials have evolved over the years to the greater understanding for the functions and characteristics. Initially, biomaterials were considered by researchers as medical devices that requires reliability and should be non-toxic in nature (Carlisle, 1970; Shirtliff & Hench, 2003). Researchers were able to investigate and understand better the biological interactions with biomaterial surfaces along the way when they improved their knowledge on human biological mechanisms.

Since the implantation of biomaterials comes in contact with the interior of the body and body fluids, the selection of suitable materials that can be used are limited (Agrawal, 1998a; Chai & Ben-Nissan, 1999 ;Williams, 2003). For any materials to be considered as a biomaterial, the main criteria is to be biocompatible (Williams, 2008).

Biocompatibility is the interactions between biomaterial and the tissue of the human body without causing any adverse response that affects the body.

Besides, biomaterials should exhibit characteristics of being chemical inertness, non-thrombogenic, non-immunogenic, non-carcinogenic, non-irritant, non-toxic and stable within the living body (Suchanek & Yoshimura, 1998; Williams, 2008), Cao et al., 2008) that serve its functions as implant. The interactions between biomaterials and living tissue can be summed as shown in Figure 2.3 while the factors relating to the biocompatibility of biomaterials are indicated in Figure 2.4 (Yamanaka et al., 2006).

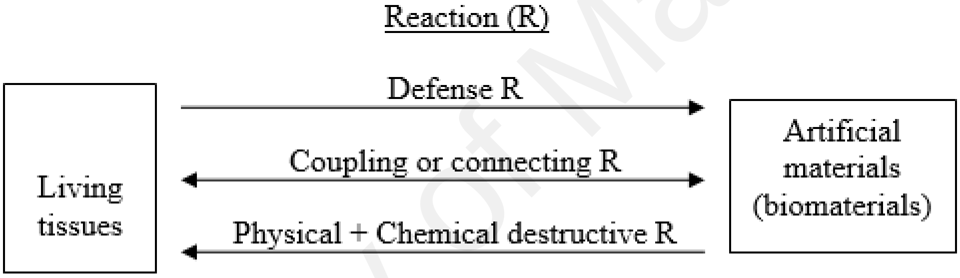

Figure 2.3: Interactions between living tissues and artificial materials (biomaterials) (Yamanaka et al., 2006).

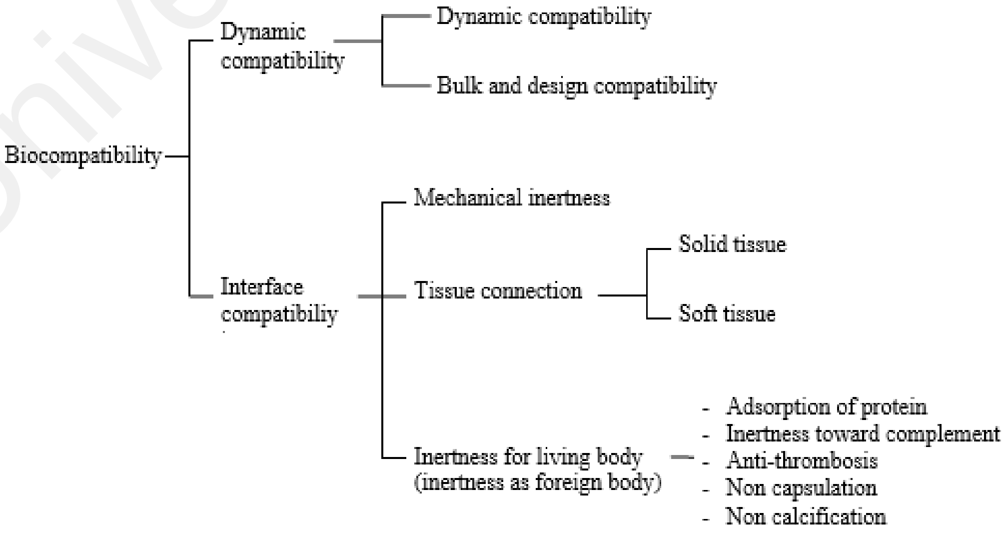

Figure 2.4: Biocompatibility factors (Yamanaka et al. 2006).

Generally, the biomaterials can be grouped such as metal, polymers, ceramics and composites. Each of these biomaterials has different properties which gives each material its advantages and disadvantages. The following Table 2.2 shows the different types of biomaterials with its application in medical devices.

Table 2.2: The advantages and disadvantages of various biomaterials in medical devices (Sivakumar, 1999; Wang, 2003; Thamaraiselvi & Rajeswari, 2004; Mano et al., 2004; Binyamin et al., 2006; Roeder et al. 2008).

Classification	Advantages	Disadvantages	Applications
Metal (Fe, Co, Ni, Mg, Zn, Cr, etc.)	Tough, ductile. strong, malleable, good conductor of heat and electricity	Corrosion, dense, difficult to make, heavy, constant maintenance	Orthodontic wires, anti-bacterial material, fracture fixation, joint replacement, orthopaedic fixation devices.
Polymer (Teflon, nylon, silicone, rubber, polyester polytetrafuoroethylene, PVC, HDPE, LDPE etc.)	Insulator, easy to produce, resilient, easy to fabricate, can form any shape easily, light	Deforms with time, may degrade, not strong, nonrenewable	Vascular grafts, trocars, tubing, catheters, drug delivery, bone cement, non-resorable sutures, heart valves, wound dressing hernia mesh, heart – lung machine, as exchange membrane.
Ceramic (steatite, alumina, zirconia, calcium phosphate including HA, carbon)	Very biocompatible, high wear, heat, pressure and chemical attack resistance, low density	Brittle, not resilient, weak in tension, poor shock resistance, can be expensive to fabricate	Dental implants, orthopaedic prostheses, heart valves, joint replacement, heart valves, bone filler, coating dental, bone cement filler, implant coatings.
Composite (carbon carbon, wire- or fiber – reinforced bone cement)	Strong, tailor – made, light weight	Difficult to make, expensive	Socket correction, ear implant, orbital floor reconstruction, tissue engineering scaffolds, total hip replacement, spinal implants, screws, plates, nails, orthopaedic fixation.

One of the widely used biomaterials for implants is the metallic materials. Its applications include simple wires and screw, to fracture-fixation plates and total joint prostheses (artificial joints) for hips, knees, shoulders and even elbows (Dorozhkins, 2015). It is used for these applications due to attributes of stiffness, strength, toughness and also impact resistance properties (Kulkarni et al., 2013). The metallic materials that were initially considered as a biomaterials includes aluminum, silver, gold, stainless steel, tantalum, vanadium steel, platinum group elements, cobalt based alloys and titanium alloys, however due to concerns of biocompatibility and corrosion resistance, most of the metallic materials were found to be ineffective as biomaterials (Habibovic & Barralet, 2011). The factors mentioned have also put metallic materials less suitable for load bearing applications thus making its usage limited. The following Table 2.3 shows some of the widely used metallic materials' mechanical properties compared to cortical bone.

Table 2.3: Mechanical properties of selected metallic materials compared to cortical bone (Dee et al., 2003).

Materials	Young's modulus, E (GPa)	Tensile strength, σ_{UTS} (MPa)	Yield strength, σ_y (MPa)	Fatigue limit, σ (MPa)
Cortical bone	15-30	70-150	30-70	-
Co-Cr alloys	210-253	655-1896	448-1606	207-950
Stainless steel	190	586-1351	221-1213	241-820
Titanium	110	760	485	300
Ti-6Al-4V	116	965-1103	896-1034	620

On the other hand, polymers are also used for various biomedical applications as well such as implantable devices, vascular grafts, injectable biomaterials, surgical tools and device coatings (Dobradi et al., 2015). The use of polymers as biomaterials began due to the need for synthetic tissue substitutes. Polymers are also used in diagnostic aids, drug delivery and as a material for scaffolding in tissue engineering applications. However, clinical complications will arise when the possibility of polymers releasing hazardous chemicals occur. The hazardous chemicals can be from some unspecified additives or chemical compounds needed for the synthesis of the polymers. It is also not suitable to be used in biomedical applications that bear loads. Table 2.4 shows some mechanical properties of selected polymers.

Table 2.4: Mechanical properties of selected polymers (Dee et al., 2003).

Material	Tensile strength, σ_{UTS} (MPa)	Young's Modulus, E (GPa)	Elongation %
Silicone rubber	2.8	Up to 10	160
Polylactic acid	28-50	1.2-3	2-6
Polyethylene terephthalate	53	2.14	300
Nylon 6/6	76	2.8	90
Polypropylene	28-36	1.1-1.55	400-900
Polytetrafluoroethylene	17-28	0.5	120-350
Ultra high molecular weight polyethylene (UHMWPE)	≥ 35	4-12	≥ 300
Polymethyl methacrylate (PMMA)	30	2.2	1.4

The choices of implant materials changes as well as researchers established more in depth understanding of the biomaterial mechanism and biocompatibility. Therefore, ceramics or bioceramics became the choice as biological implants in part due to its biocompatibility to replace and restore the function of bones (Hench, 1998; Fathi & Hanifi, 2007; Dorozhkin, 2015). Some of the common bioceramics mechanical properties are shown in Table 2.5. For any bioceramics to be implanted well with the living host tissue, it needs to show a solid interface (Hench, 1998). Furthermore, the type of materials used as implant dictates the response of tissue at the implant interface as listed below (Hench, 1998; Dorozhkin, 2015):

a. The surrounding tissues will die if the implant material is toxic.
b. An interfacial bond forms with living tissues if the implant material is bioactive and nontoxic.
c. A fibrous tissue of variable thickness will form if the material is biologically inactive and nontoxic.
d. The surrounding tissue will be replaced if the implant material is biodegradable and nontoxic.

Table 2.5: Mechanical properties of common bioceramics (Hench, 1998).

Ceramic	Density (g/cm^3)	Young's Modulus, E (GPa)	Fracture Toughness, K_{Ic} ($MPa.m^{1/2}$)	Compressive Strength (MPa)	Hardness, (Hv)
Alumina	3.98	420	3 - 5.4	4400	2300
Zirconia	5.74 - 6.08	210	6.4 - 10.9	1990	1400
Hydroxyapatite	3.05 - 3.15	80 -110	0.7 - 1.2	500 - 1000	600
Bioglass 45S5	2.6572	35	0.7	500	458
TCP	3.07	33–90	-	460 - 680	138 - 229

Lastly, composites are materials that were developed due to the need to eliminate stress shielding of bone and elastic modulus mismatch present in other biomaterials (Hench, 2000; Liu & Wang, 2007). It comprises of two or more combination of biomaterials chosen from the metal, bioceramics or polymer type (Wang, 2003; Thamaraiselvi & Rajeswari, 2004). Moreover, this material was designed with the aim of incorporating the best characteristics from each material used (Goller et al., 2003; Binyamin et al., 2006).

Initially, composites for biomedical applications are classified based on the type of matrix material used (Wang, 2003). The different types of composites are classified as polymer matrix, metal matrix or ceramic matrix composites (Wang et al., 1993; Bhaduri & Bhaduri, 1998; Mano et al., 2004). The examples of these composites are shown in Table 2.6 (Cao & Hench, 1996; Wang, 2003). Later, researchers used bioactivity as the basis of classifying the different types of composites mentioned above. It can be classify into three types such as the bioinert, bioactive and bioresorbable composites as shown in Table 2.6 (Hench, 1991; Wang, 2003).

Originally, carbon based bioinert composite are thought to be ideal for load-bearing orthopaedic devices as it exhibit characteristics such as lightweight, strong and have low modulus. However, delamination under cyclic loading and chronic inflammatory response that occurs rendered it an unsuitable biomaterial (Hench, 2000; Han et al., 2006). Subsequently, bioactive composite which does not degrade was researched. The research resulted in material that produces bioactive bond to bone when implanted. Furthermore, it has mechanical properties that closely matched that of bone. The bioresorbable composites were produced due to the need for bioactive material that degrades and replaced by natural bones (Hench, 2000; Best et al., 2008).

Table 2.6: Classification of composite materials (Cao & Hench, 1996; Wang, 2003).

Basis of classification	Material Matrix	Examples
Material	Metal	HA/TiO2, HA/Ti-6Al-4V
	Ceramic	HA/stainless steel, HA/glass
	Polymer	Carbon/PEEk, HA/HDPE
Bioactivity	Bioinert	carbon/carbon, carbon/PEEK
	Bioactive	HA/HDPE, HA/Ti
	Bioresorable	TCP/PLA, TCP/PHB

2.3 Bioceramics

Bioceramics has been used for medical devices and implants for millennia. In general, bioceramics materials can be categorized into two large groups, usually known as the bioinert and bioactive materials (Best et al., 2008; Cao & Hench, 1996). The bioinert materials when used as implants are considered as good biocompatibility when it retained its mechanical and physical properties. Typical bioinert materials include alumnia (Al_2O_3), zirconia (ZrO_2), carbon (C), and silicon nitrades (Si_3N_4) (Cao & Hench, 1996). Alumina possesses characteristics such as high hardness, high abrasion resistance, strength and chemical inertness including good biocompatibility. This has allowed it to be used as dental and bone implants. However, it was found that alumina apart from being bioinert, it also induces weak tissue reaction which leads to loosening of the implant (Best et al., 2008; Hafezi et al., 2013). On the other hand, zirconia ceramic is known for its high toughness, high mechanical strength and good biocompatibility. These characteristics have caught the interest to use zirconia in orthopaedic applications and structural support (Aykul et al., 2013). Carbon, one of the more versatile elements, exists in many forms. It exhibit good biocompatibility with similarity in mechanical properties as the carbon content in bones. Apart from that it does not suffer from fatigue like other metals, polymers or even ceramics. However, as in the case of ceramic material, it suffers from low tensile strength and brittleness limiting its use in major load bearing application (Cao & Hench, 1996). Even though bioinert materials are non-carcinogenic, it lacks biological response with living tissue.

The bioactive materials on the other hand can be classified further into non-resorbable and resorbable types (Best et al., 2008; Rabiee et al., 2015). For non-resorbable bioceramics, the bioactive materials will encourage the formation of a biological bond between tissues and the material without degradation. Calcium phosphate ceramics, bioactive glass-ceramics and bioactive glass are considered under this category of material (Rabiee et al., 2015).

For calcium phosphate ceramics (CPC), the non-resorbable type is the hydroxyapatite (HA). The HA have a chemical formula of $Ca_{10}(PO_4)_6(OH)_2$, which bear resemblance the mineral constituent of bone and teeth (Kalita et al., 2007; He et al., 2008). Apart from that, HA also shows excellent biocompatibility with hard tissue, skin and muscle tissues. In addition, it can directly bond to the bone without much complication (Hsieh et al., 2001; Murugan & Ramakrishna, 2005). Hence, it is used in various medical applications such as periodontal treatment, alveolar ridge augmentation, dental implants and maxillofacial surgery (Pramanik et al., 2007; Ramesh et al., 2007a). Even though HA has been found to be beneficial for many medical application, its mechanical properties are still low when compared to that of bone (Chu et al., 2004).

Another well-known material of bioceramics is the bioactive glass. It is a material that derives excellent bioactivity and biocompatibility coupled with good mechanical properties (Thamaraiselvi & Rajeswari, 2004; Chen et al., 2006). Hench and colleague were the first to develop a bioactive glass that uses SiO_2, Na_2O, CaO and P_2O_5 as base component. They successfully synthesized a bioactive glass known as Bioglass® 45S5 that contains 45wt. % of SiO_2, 24.5wt. % of Na_2O and 24.5wt. % of CaO with addition of 6wt. % of P_2O_5 to simulate the Ca/P constituents of HA (Shirtliff & Hench, 2003). Subsequently, different compositions of bioglass were synthesized based on a SiO_2-Na_2O-CaO system as shown in the compositional diagram in Figure 2.5 (Hench, 2006). These variations of bioglass have a constant 6 wt % of P_2O_5 with varying SiO_2-Na_2O-CaO wt. % (Hench, 1991; Cao & Hench, 1996; Hench et al., 1998; Vitale-Brovarone et al., 2008).

Bioactive glass-ceramics are known for its high compressive strength, bending strength, fracture toughness, interfacial bonding to bone and excellent resistance to degradation of properties (Shirtliff & Hench, 2003). This composition of glass-ceramics phase was modified and used by many researchers. However, the most important modification was developed by Yamamuro and Kokubo (1992). They developed A/W (apatite/wollastonite) bioactive glass-ceramics which have excellent mechanical properties, biocompatible, bioactive and it is non-toxic (Kokubo et al., 2003; Best et al., 2008). Subsequently, many variations of glass-ceramics were developed as shown in Table 2.7 (Cao & Hench, 1996). Though glass-ceramics have been used in various medical applications, it is still unsuitable to be used in load-bearing applications (Kokubo et al., 2004).

Table 2.7: Types of bioactive glass-ceramics (Cao & Hench, 1996).

Component (wt %)	Types of glass-ceramics				
	A/W glass-ceramics	KG Cera Ceravital®	Mina 13 Ceravital®	KGy213 Ceravital®	M8/1 Ceravital®
SiO_2	34.2	46.2	46.0	38.0	50.0
$Ca(PO_3)_2$	-	25.5	16.0	13.5	7.1
CaO	44.9	20.0	33.0	31.0	-
P_2O_5	16.3	-	-	-	-
Na_2O	-	4.8	-	4.0	5.0
MgO	4.6	2.9	5.0	-	-
CaF_2	0.5	-	-	-	-
K_2O	-	0.4	-	-	-
Al_2O_3	-	-	-	7.0	1.5
Ta_2O_5	-	-	-	5.5	-
TiO_2	-	-	-	1.0	-
B_2O_3	-	-	-	-	4.0
$Al(PO_3)_3$	-	-	-	-	2.4
SrO	-	-	-	-	20.0
La_2O_3	-	-	-	-	6.0
Gd_2O_3	-	-	-	-	4.0

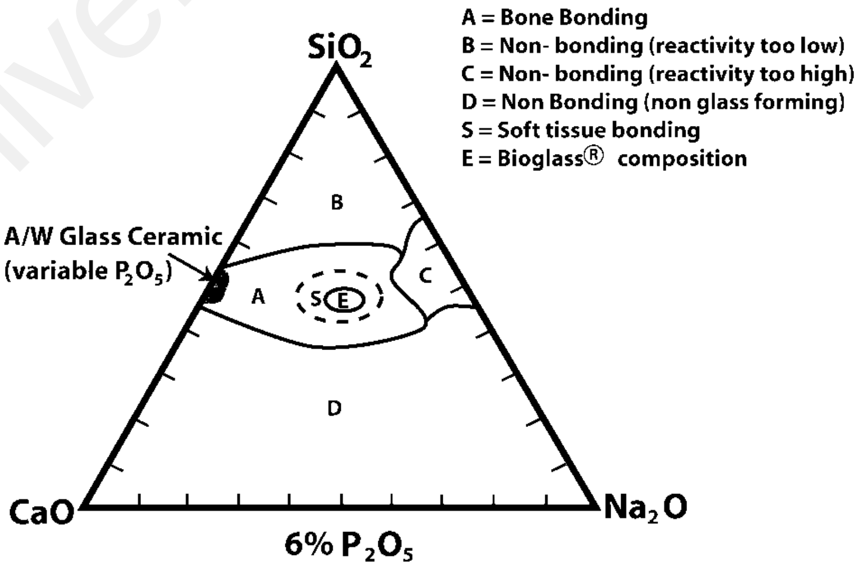

Figure 2.5: Bone bonding in terms of compositional (wt. %) (Hench, 1991; Hench, 2006).

Resorbable bioceramics are ceramics that progressively degrade over time when implanted in physiological environment. As degradation occurs, it will slowly be replaced by the host's natural tissues (Binyamin et al., 2006). The resorbable bioceramics includes corals, calcium sulphate and calcium phosphates ceramics (CPC) in the form of tricalcium phosphates (TCP) (Le Huec et al., 1995; Adamopoulus & Papadopoulus, 2007). Moreover, these ceramics also exhibits characteristics such as bioactivity and also biocompatibility ensuring no formation of fibrous tissues layer (Giannoudis et al., 2005; Viswananth et al., 2007).

Tricalcium phosphate (TCP) have a chemical formula of $Ca_3(PO_4)_2$. Typically, TCP is used in applications such as periodontal corrections, augmentation of bony contours and drug delivery devices (Heymann & Passuti, 1999; Liu et al., 2008). On the other hand, natural corals have cancellous pore that provide exceptional structure for ingrowths of bone while allowing adsorption of nutrients and metabolism (Xu et al., 2001; Zhang et al., 2007). Therefore, it is used for repairing of traumatised bone and replacement of diseased bone including correction of various bone defects (Ben-Nissan et al., 2004). Calcium sulphate ($CaSO_4$) has been used successfully in periodontal therapy due to its regenerative behaviour. Apart from that, it can also create barriers which isolate connective tissues while allowing bone regeneration to occur during healing (Adamopoulus & Papadopoulus, 2007).

2.4 Calcium Phosphate

Calcium phosphate is one of the largest and most important inorganic parts that make up hard tissues of bone. It is similar to the crystallographic and chemical composition of materials found in bones (Pramanik et al., 2007; Best et al., 2008). This similarity contributes to the properties such as bioactivity and biocompatibility (Calafiori et al., 2007; Cengiz, et al., 2008). Therefore it is used widely in various medical applications such as facial and oral surgery, drug carriers, dentistry and orthopaedics (Rodriguez-Lorenzo et al., 2001; El Briak-BenAbdeslam et al., 2008).

The calcium phosphates can be grouped according to its Ca/P ratio ranging from 0.5 to 2.0 as summarized in Table 2.8. The significant of Ca/P ratio is reflected in the acidity and the solubility of the mixture. For mixture with Ca/P < 1, the acidity and the solubility are exceptionally high. As the Ca/P ratio increases, solubility would decreased (with exception of TTCP and α-TCP) while acidity moves towards basicity. Furthermore, the in vivo solubility of the material can be predicted in the order as shown (Fernandez et al., 1999a; Aizawa et al., 1999; Bohner, 2000; Best et al., 2008):

MCPM > TTCP, α-TCP > DCPD > DCPA > OCP > β-TCP > CDHA > HA

In biomedical industry, the commercially available of calcium phosphate includes hydroxyapatite (HA), β-tricalcium phosphate (β-TCP), biphasic calcium phosphate (BCP), monocalcium phosphate monohydrate (MCPM) and unsintered apatite (AP) (Kalita et al., 2007). Among those mentioned, the most widely used calcium phosphate based ceramics are the HA and β-TCP (Slosarcyzk et al., 1996 ; Santos et al., 2004; Thamaraiselvi & Rajeswari, 2004).

Hydroxyapatite (HA) is one of the most studied phases of calcium phosphate due to excellent stability in aqueous media especially for pH above 4.3. Moreover, researchers have established human blood pH to be at ~7.3 (Cao & Hench, 1996; Kalita et al., 2004; Best et al., 2008; Ramesh et al., 2008). Apart from that, HA's chemical formula of $Ca_{10}(PO_4)_6(OH)_2$, correlates well with the mineral component of human hard tissues as shown in Table 2.9 (LeGeros & LeGeros, 1993; Suchanek et al., 1998; Suchanek et al., 2002; Liu et al., 2004; Dorozhkin, 2007).

In addition to that, HA has a Ca/P ratio of 1.67 that is similar to stoichiometric hydroxyapatite (Landi et al., 2000; Afshar et al., 2003; Sung et al., 2004; Kumta et al., 2005). Moreover, it has a hexagonal crystal structure with a P63/m space group which refers to a space group with a six-fold symmetry axis with a three-fold and a microplane. Furthermore, the lattice constants of the hexagonal HA are a = 9.422 Å and c = 6.883 Å, matches that of hard tissues as given in Table 2.8 (Narasaraju & Phebe, 1996; Zhang & Gonsalves, 1997; Jokanovic et al., 2006; Kalita et al., 2007; Suchanek et al., 1997).

These similarity of HA to bone's mineral phase has given it excellent biocompatibility and bioactivity properties. What's more, these properties allows HA to bond with living tissues without showing any adverse effects such as toxicity, inflammatory and immunogenic (Murugan & Ramakrishna, 2005; Wang, et al., 2005; Mobasherpour et al., 2007; Fathi et al., 2008).

Even though HA exhibits properties that causes no adverse effect on living tissues, there are concern with regards to its mechanical properties. Inherently, HA is brittle, thus, this translates into low fracture toughness (< 1 MPam$^{1/2}$), low flexural strength (< 140 MPa) and high elastic modulus (~ 120 GPa). Consequently, the usage of HA is limited to non-load bearing applications (Ruys et al., 1995a; Muralithran & Ramesh, 2000; Donadel et al., 2005; Ramesh et al., 2007a; Ramesh et al., 2007b; He et al., 2008).

Table 2.8 The various calcium phosphates solubility product constants at 25°C and 37°C (Fernandez et al., 1999a; Bohner, 2000; Vallet-Regí & González-Calbet, 2004; Bandyopadhyay et al., 2006; Kalita et al., 2007; Dorozhkin, 2007 & 2008).

Ca/P ratio	Compound	Chemical formula	Acronym	Solubility at 25°C – log(K_S)	Solubility at 37°C – log(K_S)	pH stability range in aqueous solution at 25°C
2.0	Tetracalcium phosphate	$Ca_4O(PO_4)_2$	TTCP	38-44	37-42	[a]
1.67	Hydroxyapatite	$Ca_{10}(PO_4)_6(OH)_2$	HA	116.8	117.2	9.5-12
1.5-1.67	Calcium-deficient hydroxyapatite [e]	$Ca_{10-x}(HPO_4)_x(PO_4)_{6-x}(OH)_{2-x}$ [f] $(0 < x < 1)$	CDHA	~85.1	~85.1	6.5-9.5
1.2-2.2	Amorphous calcium phosphate	$Ca_xH_y(PO_4)_z \cdot nH_2O$, n = 3-4.5; 15-20% H_2O	ACP	[b]	[b]	~5-12[d]
1.50	β-Tricalcium phosphate	$\beta\text{-}Ca_3(PO_4)_2$	β-TCP	28.9	29.5	[a]
1.50	α-Tricalcium phosphate	$\alpha\text{-}Ca_3(PO_4)_2$	α-TCP	25.5	25.5	[a]
1.33	Octacalcium	$Ca_8H_2(PO_4)_6 \cdot 5H_2O$	OCD	96.6	95.9	5.5-7.0

Table 2.8 (continued)

Ca/P ratio	Compound	Chemical formula	Acronym	Solubility at 25^{o}C – log(K_S)	Solubility at 37^{o}C – log(K_S)	pH stability range in aqueous solution at 25^{o}C
1.00	Dicalcium phosphate dehydrate	$CaHPO_4 \cdot 2H_2O$	DCPD	6.59	6.63	2.0-6.0
1.00	Dicalcium phosphate anhydrous	$CaHPO_4$	DCPA	6.90	7.02	[c]
0.50	Monocalcium phosphate monohydrate	$Ca(H_2PO_4)_2 \cdot H_2O$	MCPM	1.14	-	0.0-2.0
0.50	Monocalcium phosphate anhydrous	$Ca(H_2PO_4)_2$	MCPA	1.14	-	[c]

[a] Hard to precipitated from aqueous solutions.

[b] Some values found were: 25.7 ± 0.1 (pH = 7.40), 29.2 ± 0.1 (pH = 6.00), 32.7 ± 0.1 (pH = 5.28).

[c] Stable level of temperature > 100^{o}C.

[d] In metastable condition

[e] Commonly known as precipitated HA.

[f] When x = 1, (the boundary condition with Ca/P = 1.5).

Table 2.9: Composition of physical and mechanical properties of human bone, enamel and hydroxyapatite (HA) ceramic (LeGeros & LeGeros, 1993; Suchanek et al., 1998; Dorozhkin, 2007).

	Enamel	Bone	HA
Constituents (wt%)			
Calcium, Ca^{2+}	36.0	24.5	39.6
Phosphorus, P	17.7	11.5	18.5
Ca/P molar ratio	1.62	1.65	1.67
Sodium, Na^{2+}	0.5	0.7	-
Potassium, K^{+}	0.08	0.03	-
Magnesium, Mg^{2+}	0.44	0.55	-
Carbonate CO_3^{2-}	3.2	5.8	-
Flouride, F^{-}	0.01	0.02	-
Chloride, Cl^{-}	0.30	0.10	-
Total inorganic (mineral)	97.0	65.0	100.0
Total organic	1.0	25.0	-
Absorbed H_2O	1.5	9.7	-
Traces elements: Sr^{2+}, Ba^{2+}, Pb^{2+}, Fe^{3+}, Zn^{2+}, Cu^{2+} etc.			
Cyrstallographic properties			
Lattice parameters (±0.003 Å)			
a-axis	9.441	9.419	9.422
c-axis	6.882	6.880	6.880
Crystallinity index	70-75	33-37	100
Crystallite size, Å	1300 x 300	250 x 25-50	-
Sintering products			
@ 800°C – 950°C	β-TCP + HA	β-TCP + HA	HA + CaO
Mechanical properties			
Elastic modulus (10^6 MPa)	0.014	0.020	0.01
Tensile strength (MPa)	70	150	100

2.5 Magnesium Orthosilicate

Magnesium orthosilicate (Mg_2SiO_4), also known as forsterite, is traditionally used as an industrial ceramic and is often sought after for its favorable refractory properties. In view of its low heat conductivity, creep stability and good refractoriness under load, magnesium orthosilicate is often used as thermal insulators or refractory material for heat preservation (Xu and Wei, 2005; Li et al., 2009). Following recent developments on magnesium orthosilicate, studies revealed that magnesium orthosilicate is chemically stable in fuel cell environments; thus making it suitable to manufacture manifolds made of solid oxide fuel cell (SOFC) (Kosanovic et al., 2005).

Moreover to its favorable thermal properties, Sugiyama et al. (2006) revealed that magnesium orthosilicate possessed excellent dielectric properties, thus making it a material suitable for millimeter-wave communication. Additionally, it was also discovered that magnesium orthosilicate is an excellent active medium for tunable lasers (Kosanovic et al., 2005; Tavangarian and Emadi, 2010). For instance, chromium-doped magnesium orthosilicate (Cr_{4+}: Mg_2SiO_4) lasers have a broad tunable region of 1.1 – 1.3 μm (Tavangarian & Emadi, 2011) which are also found to be ideal for optical coherence tomography due to the lower scattering in biological tissues (Kharaziha & Fathi, 2010; Tavangarian & Emadi, 2011; Sara et al, 2012).

Nevertheless, recent findings have established potential biomedical applications for magnesium orthosilicate ceramics. Based on the chemical formula of magnesium orthosilicate (Mg_2SiO_4), this ceramic was found to be composed from essential minerals which are heavily involved in bone development. Studies have shown that in skeletal development, silicon is an important element and is uniquely found in the active areas of young bone (Xie et al., 2009; Jagdale & Bamane, 2011). The findings from the literatures (Schwarz & Milne, 1972; Lugo et al., 2016) showed that young rats' bone having a Ca/P ratio of 0.7 consists of more than 5 wt. % of silicon. The role of silicon is mainly involved in bone calcification in the early stage of physiological conditions. Schwarz and Milne (1972) also reported that the addition of the silicon in the rats' diet has an influence towards the growth. Another essential mineral which controls the bone growth in human body and also oxidation of calcined tissues is magnesium (Legeros, 1991; Nikaido et al., 2015). Besides the significance of its minerals towards bone development, magnesium orthosilicate was also found to exhibit bioactivity when experimented in SBF solution (Kharaziha and Fathi, 2009).

In addition to its favorable magnesium silicate composition, magnesium orthosilicate also demonstrated high mechanical properties; whereby recent data suggests that magnesium orthosilicate possessed a maximum fracture toughness of 4.3 MPa·m$^{1/2}$ (Kharaziha and Fathi, 2010) and this is much higher than HA. According to documented figures, the fracture toughness of magnesium orthosilicate was established to be within the region of 3.6 – 4.3 MPa·m$^{1/2}$ (Juang & Hon, 1996; Fathi and Kharaziha, 2009; Kharaziha and Fathi, 2010). Hence, at a maximum of 4.3 MPa·m$^{1/2}$, the fracture toughness of magnesium orthosilicate is approximately 3 MPa·m$^{1/2}$ more when compared to HA (K_{Ic} = 1.18 – 1.25 MPa·m$^{1/2}$ (Akao et al., 1981; Gu et al., 2002; Kalmodia et al., 2010).

2.6 Hydroxyapatite Composites

Hydroxyapatite is a material commonly utilized in biomedical applications and regenerative medicines for bones because of its biocompatibility and structural analogy which are found in bone and dental tissues. However, the material has limitation where it cannot be used in high load bearing conditions due to low mechanical properties such as low strength, low fracture toughness and poor resistance. To fulfil the function of hydroxyapatite as a biological and structural material, HA composites have been developed.

In general, no synthetic material will be completely harmonious with the living environment. However, there are different levels of inertness associated with bioceramic. Few factors are taken into account when it comes to the biocompatibility when implanted such as charge, roughness, composition of material, surface wettability, implants size and shape. For a bioceramic composite to be used as a material in implantation, the composite must not cause any adverse effects to the blood or tissue-material bonding, and most importantly biocompatible. This requires the bioceramic composite to integrate naturally in the presence of blood and tissue upon implantation. The bioceramic composites can be categorized as bioinert, bioactive and biodegradable.

2.6.1 Hydroxyapatite – Bioinert Composites

Inert bioceramics are stable materials which do not interact with tissue activity when implanted within human body. When implanted into living organism or tissue, they show high chemical stability or even if minor non-toxic degradation products are released, they can be readily assimilated by the body. Some bioinert ceramics like zirconia and alumina ceramics are used for load bearing implants as these materials exhibited better mechanical properties than bioactive ceramics.

Knowing that mechanical properties of hydroxyapatite is unsatisfactory, the incorporation of zirconia and alumina to form hydroxyapatite – bioinert composites can help to improve its mechanical strength and fracture toughness.

2.6.1.1 Hydroxyapatite – Zirconia

Hydroxyapatite is mainly used as a hard tissue implant in non-load bearing areas due to its excellent biocompatibility in the human body. It can only be used in non-load bearing areas because of its brittle nature. However, inert crystalline ceramics such as zirconia can be mixed with hydroxyapatite to make composites that take advantage of the biocompatibility of hydroxyapatite and high strength of zirconia (Evis, 2007). Zirconia (ZrO_2) is a well-known material for its mechanical properties and low toxicity, which makes it as a viable biomaterial for dental implants and is expected to be a new bone restorative material (Evis, 2007; An et al., 2007; Chiu et al., 2007; Drdlik et al., 2015).

Chiu (2007) studied the ramification incorporating zirconia into the microstructural evolution of porous hydroxyapatite. The calcium zirconate ($CaZrO_3$) is a compound formed from the product reaction of HA and zirconia and is bio-inert towards human tissue (Chiu et al., 2007). The retribution of such a reaction is the consumption of the Ca from Ha. As the amount of ZrO_2 is large, HA would be consumed completely after sintering, and α- or β- tricalcium phosphate formed (Chiu et al., 2007). In this study, 0 – 5 vol.% of 230 nm zirconia particles was added into hydroxyapatite (HA). The XRD trends of the sintered HA and HA-ZrO_2 specimens at 1300°C is shown in Figure 2.6. No ZrO_2 peaks are found in the patterns, instead calcium zirconate is found in the sintered specimens which indicated that the reaction between HA and ZrO_2 has taken place to form $CaZrO_3$.

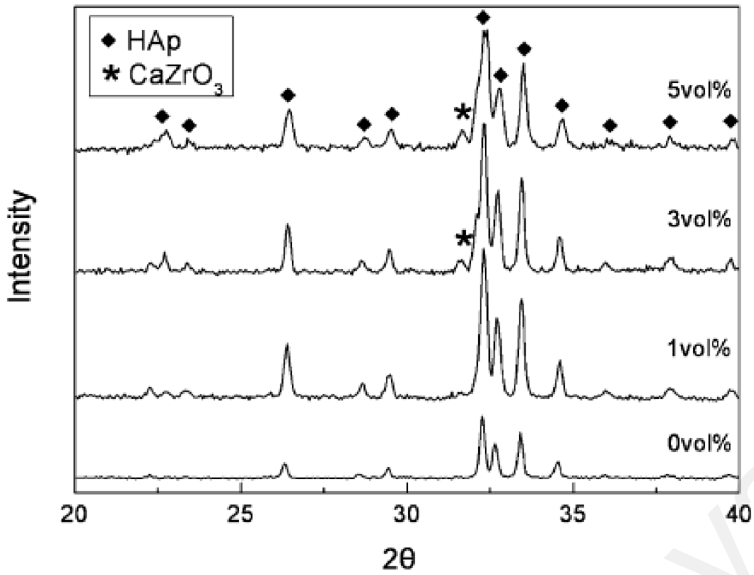

Figure 2.6: XRD trends for HA and HA-ZrO_2 specimens after sintering at 1300°C for 2 h (Chiu et al., 2007).

It was reported by Chiu (2007) that the $CaZrO_3$ can thus act as an effective grain growth inhibitor for the HA grains. Figure 2.7a and Figure 2.7b show the typical micrographs of HA and HA-$CaZrO_3$ samples after sintering and Figure 2.8 shows the average size of HA grains in the sintered composites as a function of ZrO_2 content. The addition of ZrO_2 particles reduces the size of HA grains. Moreover, as the pores are smaller, the $CaZrO_2$ particles can act as microstructure refiner to HA.

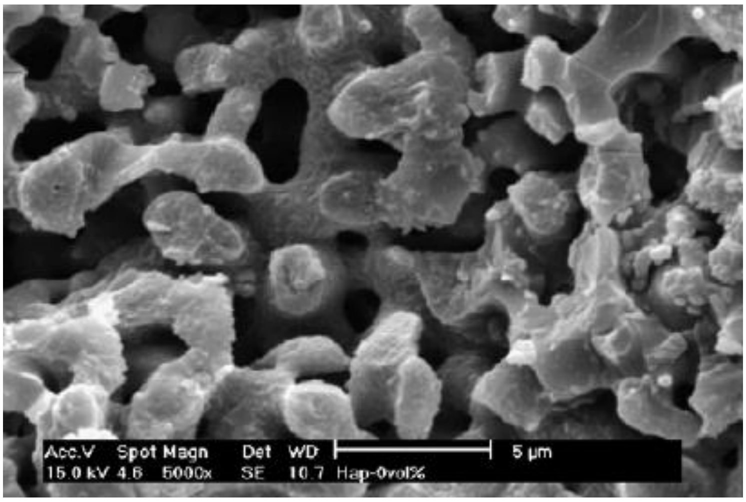

(a)

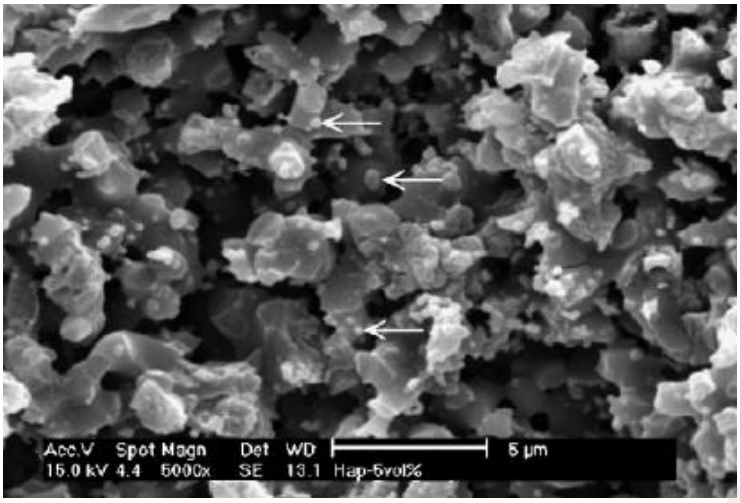

(b)

Figure 2.7: Typical micrographs of (a) HA and (b) HA-ZrO_2 samples after sintering at 1300°C for 2 h. Several $CaZrO_3$ particles in (b) are indicated by arrows (Chiu et al., 2007).

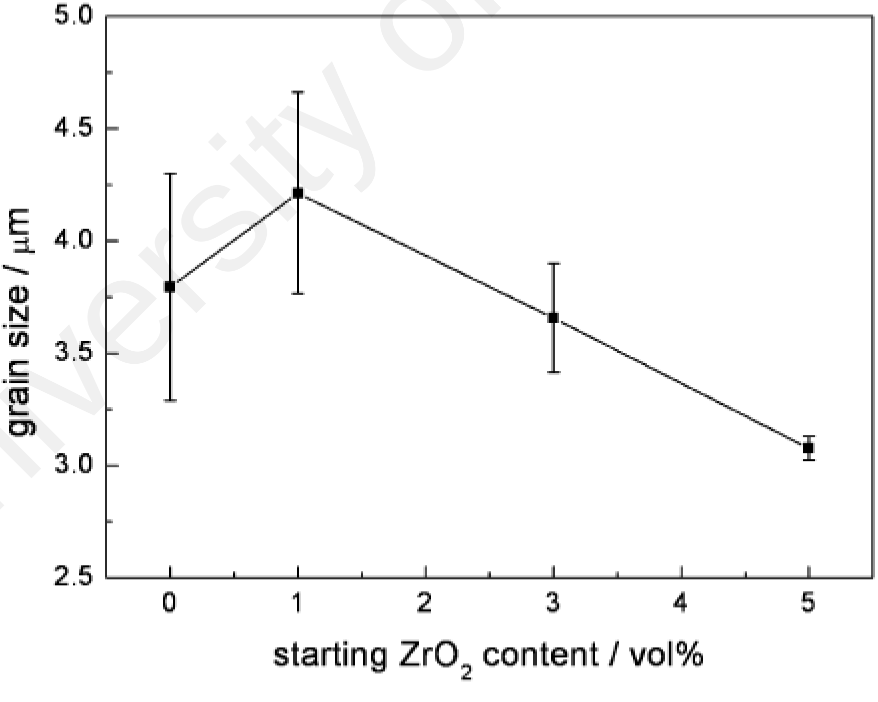

Figure 2.8: Size of the HA grains in the HA-$CaZrO_3$ composites as a function of starting ZrO_2 content (Chiu et al., 2007).

However, the strength and toughness of the HA-$CaZrO_3$ composites decreased as the ZrO_2 content increased as shown on Figure 2.9 which corresponded to the increase in porosity in the composites. This indicated that the presence of porosities have an adverse effect on the mechanical properties of the composite.

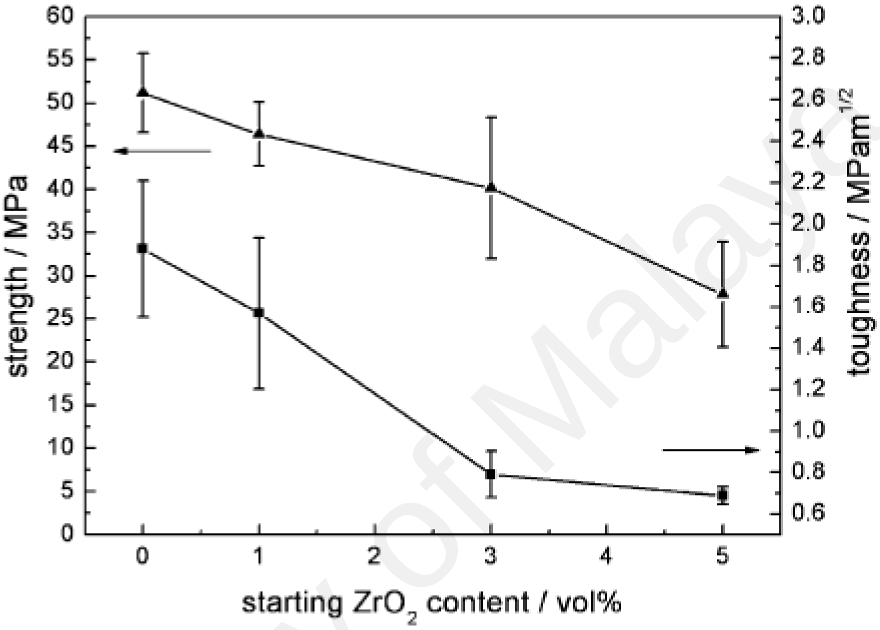

Figure 2.9: Strength and toughness of the HA-$CaZrO_3$ composites as a function of starting ZrO_2 content (Chiu et al., 2007).

Evis (2007) studied the reactions in hydroxyapatite – zirconia composites sintered at 1100°C and 1300°C using XRD and SEM. The HA – ZrO_2 composites (more than 92% of the theoretical density) were produced after the synthesis by precipitation method and sintered in air at 1100° and 1300°C without any need to pressure sintering. However, the author reported that due to the increase of zirconia, the HA decomposed when sintered at 1100°C and 1300°C. The decomposition rate of HA is based on the strain that is caused by the exchange of Ca^{+2} and ZrO^{2+} ions from the HA and zirconia. The water from the decomposition actually led to the increased of porosity in the sintered samples (Evis, 2007). The porosities of the composites as determined from SEM are presented in Table 2.9.

Table 2.10: Porosity in HA-zirconia composites (%) (Evis, 2007).

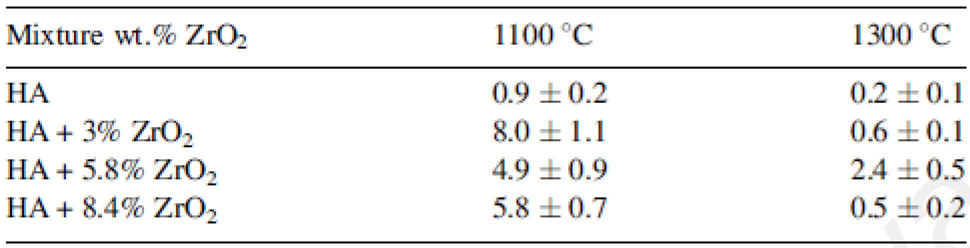

Mixture wt.% ZrO_2	1100 °C	1300 °C
HA	0.9 ± 0.2	0.2 ± 0.1
HA + 3% ZrO_2	8.0 ± 1.1	0.6 ± 0.1
HA + 5.8% ZrO_2	4.9 ± 0.9	2.4 ± 0.5
HA + 8.4% ZrO_2	5.8 ± 0.7	0.5 ± 0.2

More recently, Jadwiga et al. (2016) also reported that zirconia additive promotes decomposition of both hydroxyapatite of natural origin as well as the synthetic one. The reaction led to the formation of β-TCP and the CaO-ZrO_2 solid solution. The research was based on pressureless sintering performed at 1000-1300°C and hot pressing at 1050-1300°C. Table 2.10 shows the phase composition of hydroxyapatite matrix-zirconia composites pressureless sintered and hot pressed. No free CaO was observed as it was assume that it has dissolved in zirconia.

Table 2.11: XRD phase composition of hydroxyapatite matrix-zirconia composites pressureless sintered and hot pressed (Jadwiga et al., 2016).

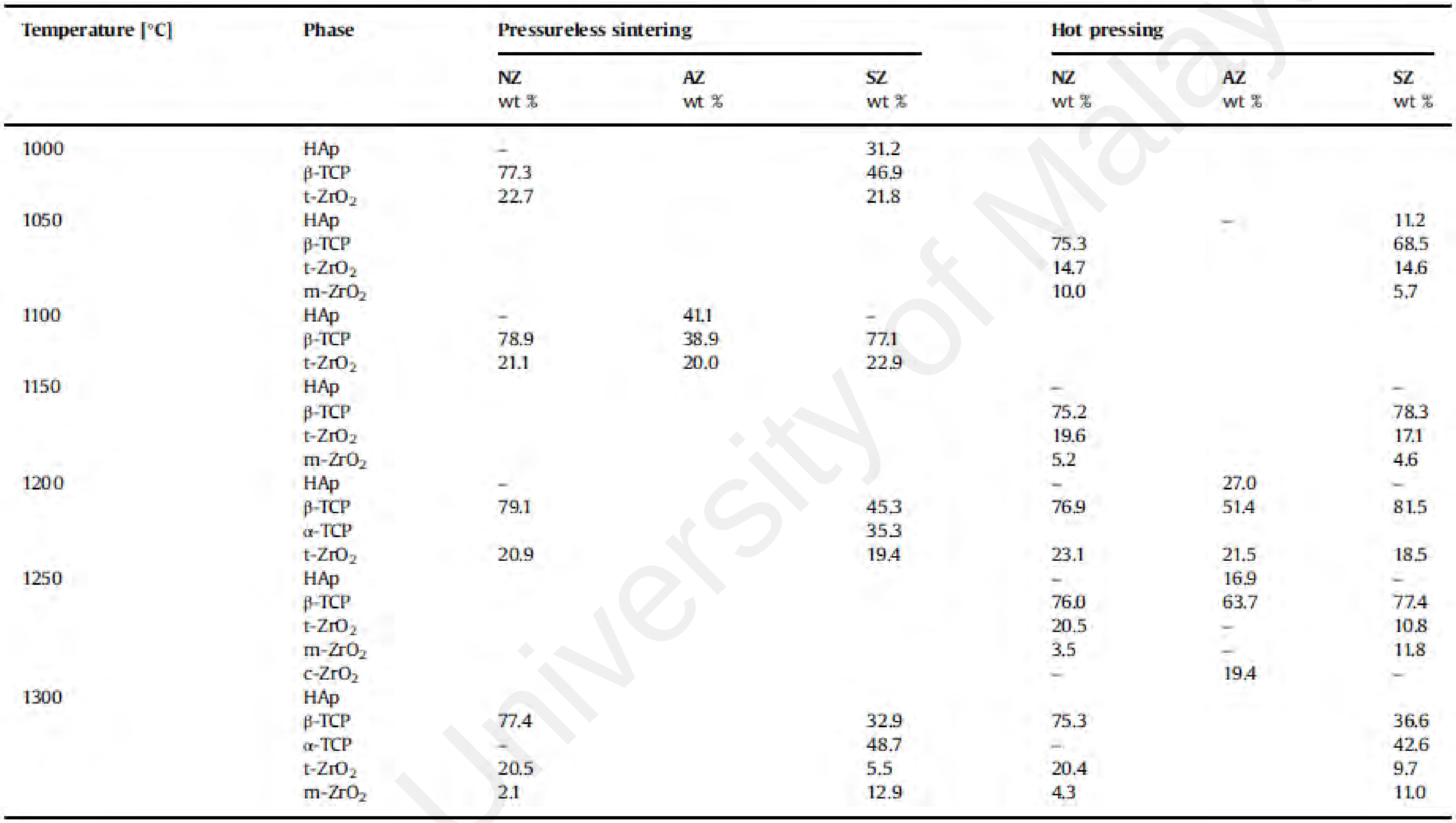

Temperature [°C]	Phase	Pressureless sintering			Hot pressing		
		NZ wt %	AZ wt %	SZ wt %	NZ wt %	AZ wt %	SZ wt %
1000	HAp	–		31.2			
	β-TCP	77.3		46.9			
	t-ZrO_2	22.7		21.8			
1050	HAp					–	11.2
	β-TCP				75.3		68.5
	t-ZrO_2				14.7		14.6
	m-ZrO_2				10.0		5.7
1100	HAp	–	41.1	–			
	β-TCP	78.9	38.9	77.1			
	t-ZrO_2	21.1	20.0	22.9			
1150	HAp				–		–
	β-TCP				75.2		78.3
	t-ZrO_2				19.6		17.1
	m-ZrO_2				5.2		4.6
1200	HAp	–			–	27.0	–
	β-TCP	79.1		45.3	76.9	51.4	81.5
	α-TCP			35.3			
	t-ZrO_2	20.9		19.4	23.1	21.5	18.5
1250	HAp				–	16.9	–
	β-TCP				76.0	63.7	77.4
	t-ZrO_2				20.5	–	10.8
	m-ZrO_2				3.5	–	11.8
	c-ZrO_2				–	19.4	–
1300	HAp						
	β-TCP	77.4		32.9	75.3		36.6
	α-TCP	–		48.7	–		42.6
	t-ZrO_2	20.5		5.5	20.4		9.7
	m-ZrO_2	2.1		12.9	4.3		11.0

2.6.1.2 Hydroxyapatite – Alumina

In total joint replacement, alumina (Al_2O_3) ceramics are being used because of excellent biocompatibility, inertness and high wear resistance (Li et al., 1995; Carolina et al., 2016). However, in many natural bone replacement, this material does not bond easily. On the other hand, hydroxyapatite ceramics which have the competence to be implanted inside bone are used as implant materials because it also helps to promote the formation of new bone in osseointegration implant (Li et al., 1995; Mobasherpour et al., 2009; Zhang et al., 2016). Therefore, mechanical properties of HA and HA coatings can be improved by addition of alumina (Zhang et al., 2016).

Li et al. (1995) studied the hydroxyapatite alumina composites, with HA compositions of 15wt. %, 25wt. %, 30wt. %, 70wt. % and pure HA. The specimens were sintered at 1275°C and implanted into 12 New Zealand White rabbits' femoral cortical bones for duration of 3 months. The results indicated that the bonding strength of the implants increased as the HA content increases in the composite which indicated the significant role of HA to the implants thru the new bone apposition. However, no linear relationship can be drawn from HA content and bonding strength. Among the other composites, the similar fracture interfaces and same level of bonding strength were obtained from the pure HA and 70% HA composite through SEM. This supports the high bonding strength transfer ability of the contact zone. For the mechanical strength of the composites, a three-point bending test method was used to measure the strength. The bending strength of the materials decreased with increasing HA content as shown in Figure 2.10. The mechanical strength of HA containing ceramics increased with increasing alumina content. The reinforcement effect of alumina can be observed in the composite with 30% alumina in HA, where the strength was doubled compared to pure

HA. When the volume of alumina exceeded 50%, the strength of the composites was determined by the distribution of the HA phase in the alumina matrix.

Li et al. (1995) also reported that densities decreased with increasing HA content as shown in Table 2.11.

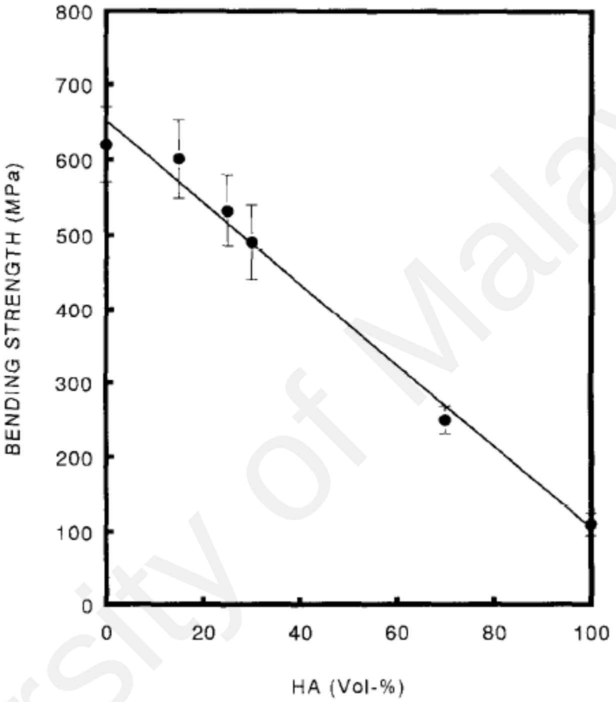

Figure 2.10: Bending strength of HA-alumina composites (Li et al., 1995).

Table 2.12: Density and surface profile of selected implant cylinders (Li et al., 1995).

Materials	**Density (gcm^{-3})**
Al_2O_3	3.97
HA	3.15
15HA/Al_2O_3	3.85
25HA/Al_2O_3	3.75
30HA/Al_2O_3	3.73
70HA/Al_2O_3	3.39

Viswanath & Ravishankar (2006) carried out experimentation on the interfacial reactions in hydroxyapatite – alumina nanocomposite. The composite mixtures containing 10wt. %, 20wt. %, and 30wt. % of alumina were sintered from 1000 to 1200°C for a constant duration of 1 hour. The amount of alumina and sintering temperature plays a major role in the interfacial reaction. This can be observed from the XRD in Figure 2.11 that the decomposition of HA into tricalcium phosphate (TCP) increased as the alumina content increased. Moreover, the decomposition of HA increased too as the sintering temperature increased as shown in Figure 2.12. The outcome of the analysis indicated that the alumina reacted with HA and formed alumina-rich calcium aluminates and TCP phases at relatively low temperatures (1000°C).

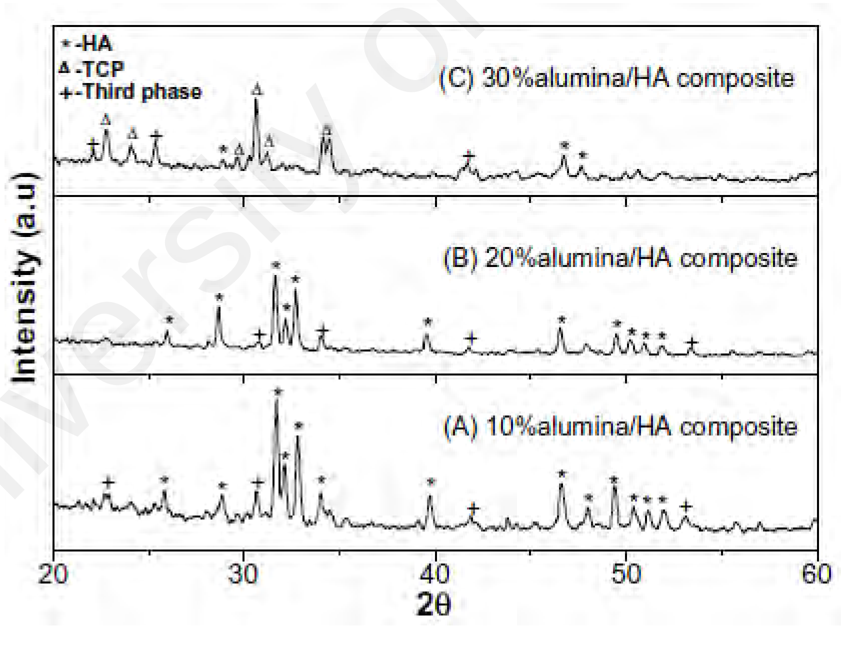

Figure 2.11: XRD trends of HA-alumina composites of different composition sintered at 1100°C (Viswanath & Ravishankar, 2006).

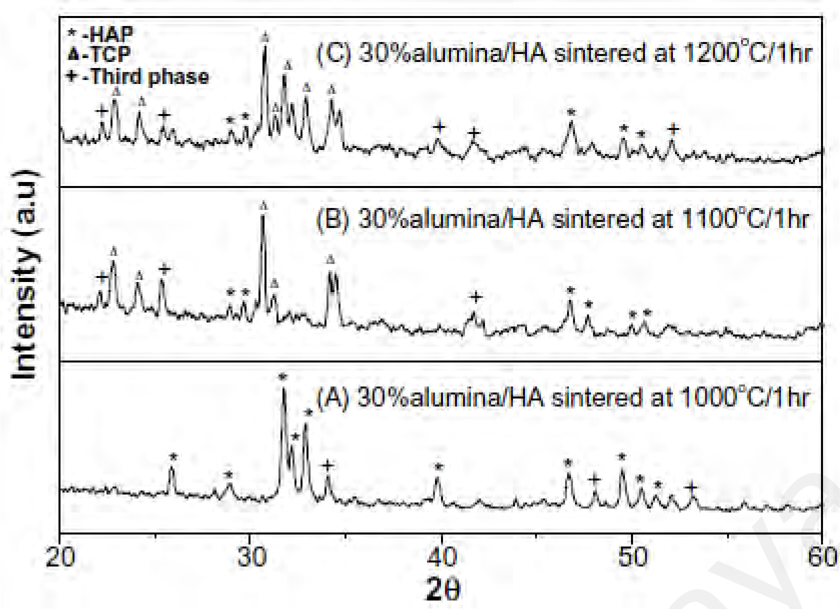

Figure 2.12: XRD trends of 30wt. % alumina sintered at different temperatures (Viswanath & Ravishankar, 2006).

In another work, Aminzare et al. (2013) used biomimetic method to synthesize the hydroxyapatite-alumina nanocomposite. In this work, 20wt. % alumina nanopowder was mixed with HA before sintered at the rate of 5°C/minute to 1400°C. The results showed that the addition of alumina was beneficial in enhancing the bending strength by 40% and improved the hardness from 2.52 (pure HA) to 5.12 (HA-Al_2O_3 composite) (Aminzare et al., 2013).

2.6.2 Hydroxyapatite – Bioactive Composites

Bioactive materials are engineered for a specific biological activity that will give strong bonding to bone. During the implantation in the living bone, the kinetic modification of the surface which is time dependent will takes place in the biological activity (Kim, 2001). An ion exchange reaction takes place between the bioactive implant and surrounding body fluids which results in the formation of a biologically active calcium phosphate layer on the implant. The layer is chemically and crystalographically equivalent to the mineral phase of bone (Kim, 2001). Prime examples of bioactive materials are bioceramics such as synthetic hydroxyapatite, glass ceramic (A-W) and bioglass. Figure 2.13 shows the clinical uses of the bioceramics mentioned earlier in bone repairs and replacements.

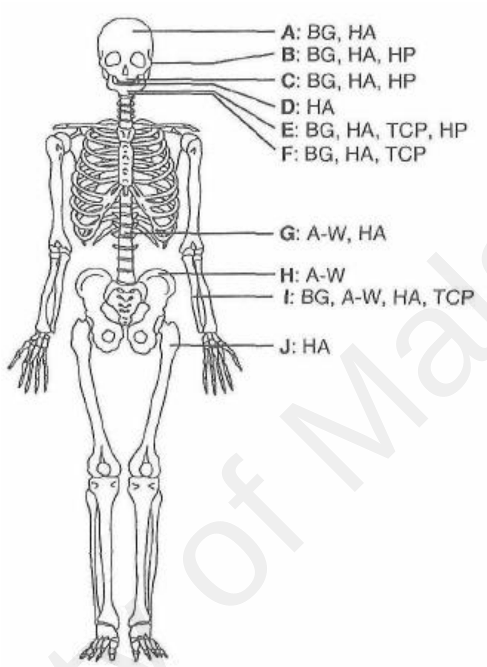

Figure 2.13: Bioglass: BG, Cerabone A/W: A-W, Sintered hydroxyapatite: HA, Sintered β-tricalcium phosphate: TCP, HAPEX: HP (A- cranial repair, B – middle ear bone replacement, C – maxillofacial reconstruction, D – bioactive coating on dental root, E – alveolar ridge augmentation, F – periodontal pocket obliteration, G – spinal surgery, H – iliac crest repair, I – bone filler, and J – bioactive coating on joint stem (Kim, 2001).

The mechanical strength of bioactive ceramics is generally lower than that of bioinert ceramics. Therefore, over the years there are many research on uplifting the limitation of bioactive ceramics thru combination of biomaterials to improve the mechanical properties aspect of it.

2.6.2.1 Hydroxyapatite – Bioactive Glass

In the SiO_2 – CaO – P_2O_5 system, the design of bioactive glass ceramic plays an important role as it is used for repair and replacement of diseased and damaged bone tissue (Bogdanov et al., 2008; Rabie et al., 2015). In initial discovery, Hench et al. (2006) explored the glass ceramic (Bioglass®), and found to bond with the living bone without the fibrous tissue formed on the bone surfaces. The important feature of bioactive glass is their biological activity which promotes their usage for some specific application. Hence, the formation of hydroxyapatite on material surface can be observed from the active materials which will be able to produce a stable bond when in contact with bone tissue from implantation (Bianco et al., 2007; Laczka et al., 2016). It can also be defined as their ability to induce specific cell responses leading to faster regeneration of bone tissue. The main drawback from being used in load-bearing applications was due to the amorphous three dimensional glass network which is believed to be the cause of low fracture toughness and low bending strength which was reported in the range of 40-60 MPa (Dobradi et al., 2015).

Tancred et al. (1998) performed a study on the sintering of HA with glass additions. According to the authors, the objectives for sintering HA with a glassy phase were to enhance the densification and to improve the bioactivity of the composite (Kangasniemi, 1993; Chern et al., 1993). In this study, synthetic hydroxyapatite was prepared using a wet method and phosphate glass was prepared using conventional glass-forming techniques. The HA was mixed with phosphate glass with composition of 2.5, 5, 10, 25 and 50wt. % and sintered at 4°C/minute with holding time of 3 hours at desired temperatures of 1100°C to 1350°C. A maximum of 97.8% theoretical density was achieved by HA at 1300°C as shown in Figure 2.14. On the other hand, composites containing 2.5 and 5wt. % glass additions attained maximum densification above

1250°C. For composites containing above 10wt. % achieved slightly lower densification.

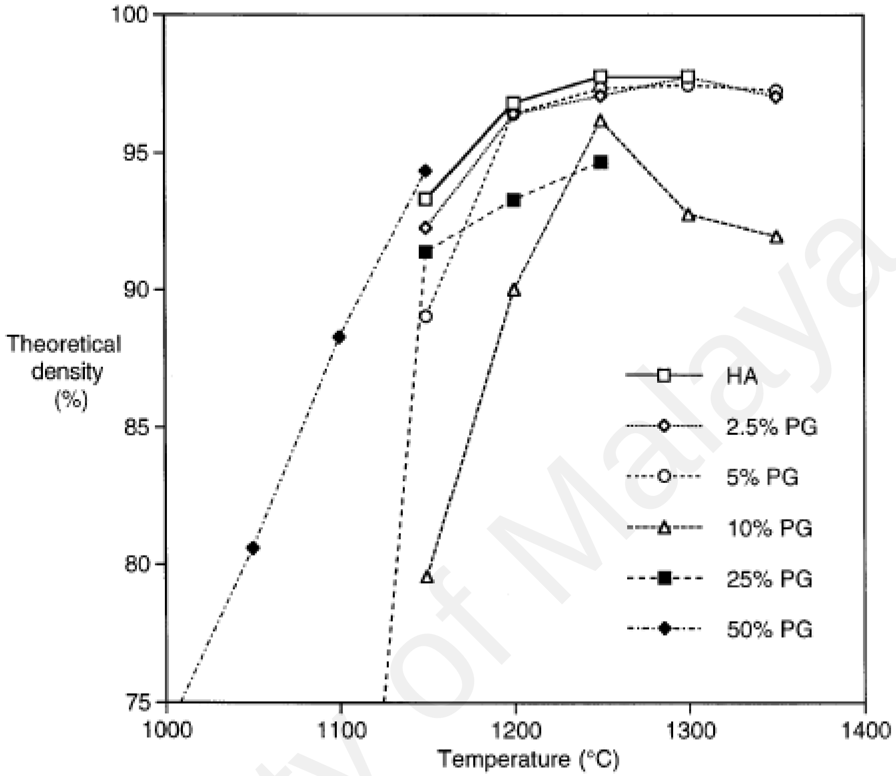

Figure 2.14: Theoretical density of HA/phosphate glass composites

(Tancred et al., 1998)

For microstructure evaluation, rapid grain growth was observed for pure HA at above 1200°C (Figure 2.15). It was reported that the average grain size increased from 1.0 ± 0.05µm at 1200°C to 2.47 ± 0.13 µm at 1350°C. Subsequently, HA with phosphate composition up to 10wt. % resulted in high porosity when sintered at 1200°C, probably due to reaction between the glass and HA. However, between 1200 and 1250°C, there was a decreased in porosity for each composite as the materials reached almost maximum density.

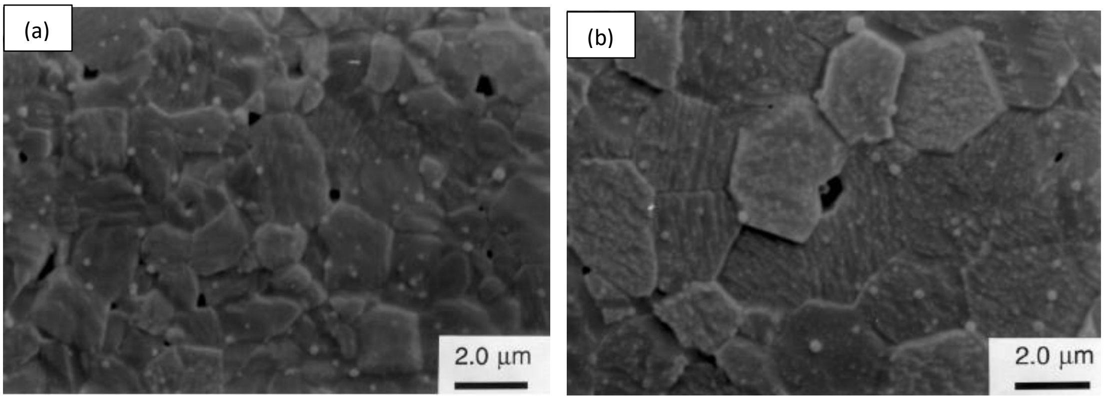

Figure 2.15: Microstructure of HA sintered at (a)1250°C and (b)1350°C

(Tancred et al., 1998)

An improvement in the for fracture toughness was also observed for composites containing up to 10wt. % glass additions as shown in Figure 2.16. Author reported that extensive lateral vent crack formation was found for samples containing 10wt. % and above, therefore no results were obtained from this point.

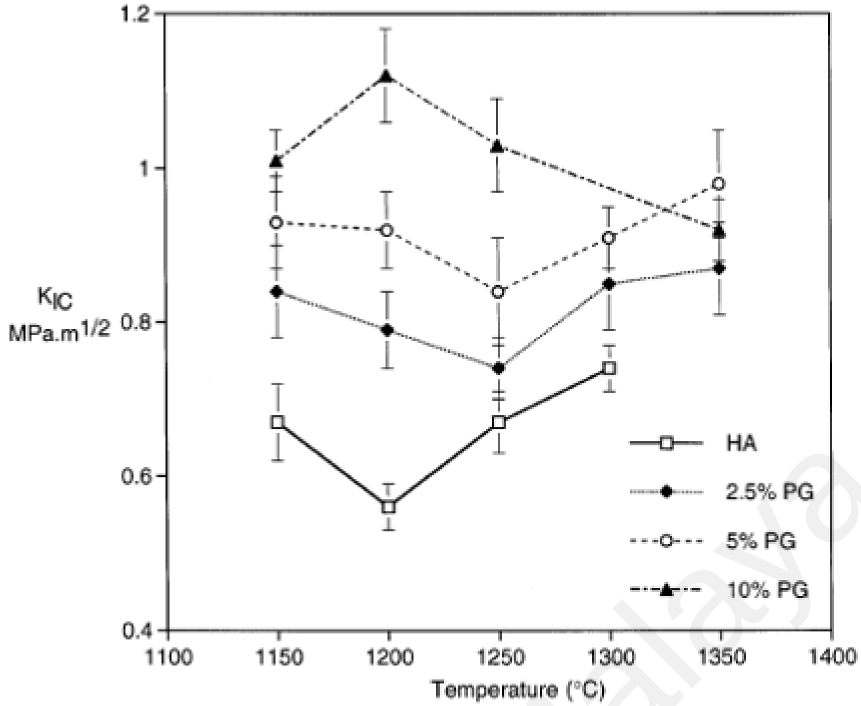

Figure 2.16: Fracture toughness of HA/phosphate glass compositions (Tancred et al., 1998)

In another work, Goller et al. (2003) sintered the naturally produced HA from human teeth with addition of 5wt. % and 10wt. % bioglass at 1200°C and 1300°C for 4 hours. The density of the composites varied depending on the reinforcement contents and sintering temperatures as shown in Figure 2.17. The authors found that the bioglass reinforcement content from 5 to 10wt. % resulted in increasing density from 2.66 to 2.72 g/cm^3 when sintered at 1200°C. However, the density improvement did not show much variation when composites were sintered at 1300°C, which was about 2.72 g/cm^3 for 5 and 10wt. %.

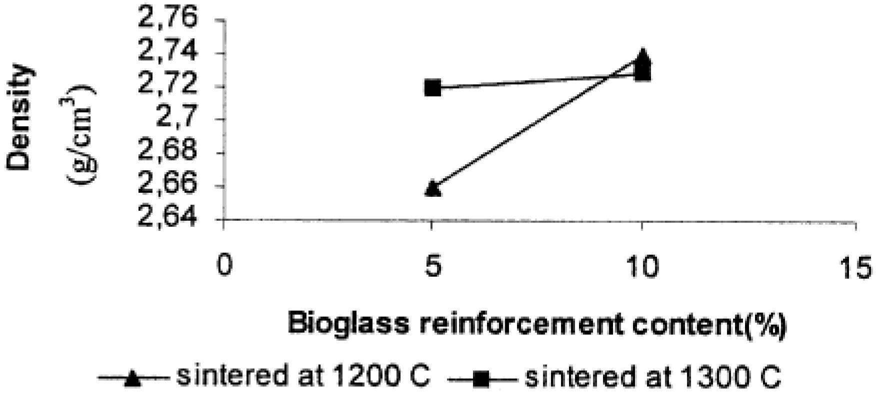

Figure 2.17: Density of composites sintered at 1200°C and 1300°C (Goller et al., 2003).

When composites sintered at 1200°C and 1300°C, the microhardness also displayed a trend of decrement. The authors reported that increasing the bioglass content from 5 to 10wt. % caused the decrease in hardness from 474 to 383 HV when sintered at 1200°C and 365 to 234 HV when sintered at 1300°C.

2.6.2.2 Hydroxyapatite – AW Glass

Since the discovery and introduction of bioactive ceramic concept (later named as Bioglass®) by Hench and his co- workers in early 1970s for clinical applications, it has opened new avenue to other researchers to develop further in bioactive glass which could spontaneously bond to and integrate with living bone with improved mechanical properties. Another researcher, Kokubo et al. (1982) reported on the discovery of a bioactive glass ceramic, named glass-ceramic A-W (appatine-wollastonite) which has higher mechanical strength as well as high bone bonding capability. This glass ceramic was introduced to be the first load bearing bioactive bone substitute which it has been in used in bulk, granular and porous forms in mainly spinal surgery (Kokubo et al., 1982). It was later commercialized as Cerabone®. The glass ceramic A-W has two crystalline phases; 38wt. % of oxyfluorapatite $Ca_{10}(PO_4)_6(O,F_2)$ and 34wt. % wollastonite ($CaOSiO_2$) 50-100nm in size and a residual vitreous phase of MgO-CaO-SiO_2. The authors also developed a simulated body fluid (SBF) test in 1990 to examine the behavior of glass-ceramic A-W. This technique was also used to rank other materials in terms of their bioactivity.

Kokubo (1990) observed that an apatite layer that is capable of bonding to the bone was formed when the glass-ceramic A-W was placed in the body. The findings of the authors showed that the bonding was so strong that when the mechanically tested samples were retrieved, there were no signs of fracture found on the interface of the bone implant, but rather inside of the bone structure (Kokubo, 1990). The author believed that silanol groups were formed at the glass-ceramic surface since no amorphous silica layer was observed between hydroxyl-carbonate apatite (HCA) layer and the glass-ceramic A-W when tested in a simulated body fluid (SBF) as shown in Figure 2.18. Silanol groups are believed to be the cause of the apatite layer formation as these groups provide favourable sites needed for apatite crystal nucleation and growth. The apatite crystals form rapidly on the surface of the glass-ceramic A-W and the calcium and phosphate ions in the surrounding media will be consumed.

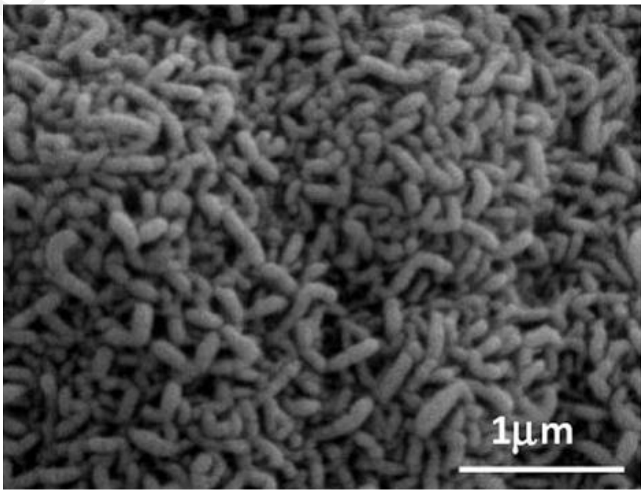

Figure 2.18: Apatite formation tested in simulated body fluid (SBF) (Kokubo, 1990)

Other authors, such as Ryu et al. (2005) and Jun et al. (2007) experimented with hydroxyapatite scaffolds reinforced with glass ceramic A-W coating. The authors reported that the glass coating improved the strength as well as the bioactivity of the HA scaffolds. It was observed that the higher alkaline phosphatase activity of the cells successfully cultured on the scaffold coated with A-W glass than on HA scaffold alone, which indicated that the bioactivity had been improved (Jun et al., 2007).

In another work, Encinas-Romero et al. (2010) studied the HA-wollastonite composite powders via sol-gel processing method. The ratios of 20, 50, and 80wt. % were synthesized and processed thru sol-gel method before evaluated through thermal analysis, FTIR, XRD, Raman spectroscopy and SEM. The hydroxyapatite was observed to have formed in the composites at relatively low temperature accompanied by calcium carbonate formation between 400 to 420°C, while wollastonite remained the same. Heat treatment and hydrochloric acid were used to produce the B-type carbonated hydroxyapatite-wollastonite composites as final products. The compounds of the composites experienced no decomposition upon heating between 1000°C to 1400°C. The authors investigated and concluded on the addition of 80wt. % wollastonite had tremendously improved the hardness by 200% when compared to pure HA, and the reduced elastic modulus is also 45% higher as shown in Figure 2.19. In summary, the incorporation of wollastonite has contributed to the improvement of the mechanical properties.

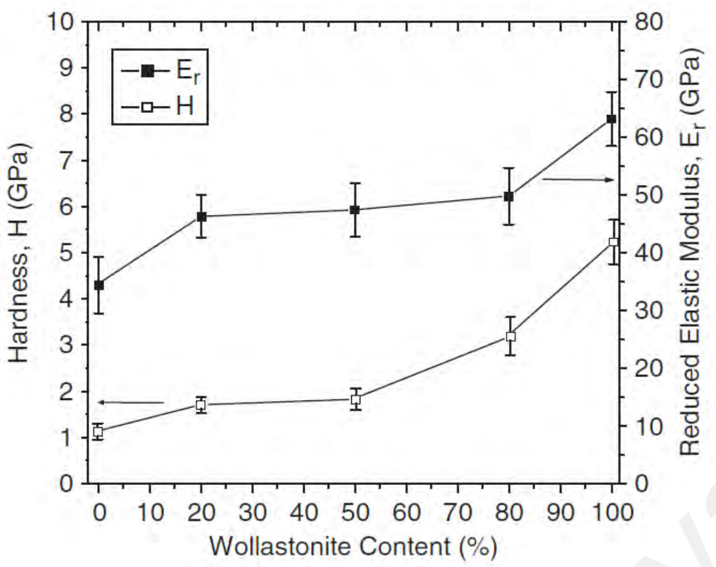

Figure 2.19: Hardness (H) and reduced elastic modulus (Er) values of HA-wollastonite composite vs. different compositions of wollastonite (Encinas-Romero et al., 2010)

2.6.2.3 Hydroxyapatite- Magnesium Orthosilicate

In the recent developments, magnesium orthosilicate (MO) or also known as forsterite was incorporated into HA to improve its mechanical properties (Sebdani & Fathi, 2011). Magnesium orthosilicate shows considerable fracture toughness and hardness. Sebdani & Fathi (2011) experimented the hydroxyapatite-magnesium orthosilicate-bioglass by sol-gel method by adding MO and bioglass to hydroxyapatite sol. The gels were sintered at 600°C, 700°C and 800°C, followed by immersion in simulated body fluid solutions for 1 day, 7 days, 14 days and 28 days. The authors reported that the optimum temperature for synthesizing the composite was at 600°C to produce the particle size of composite nanopowder in the range of 60-70 nm. Apatite layer was formed after soaking for a day, which conclude that the composite can be good candidate for biomedical applications (Sebdani & Fathi, 2011).

Tavangarian & Emadi (2011) also reported on the improvement of bioactivity and mechanical properties in hydroxyapatite-magnesium orthosilicate-bioactive glass nanocomposite when compared to single hydroxyapatite. The composites were prepared in varying amount of MO (10wt. %, 20wt. %, 30wt. %) by sol-gel method. The authors summarized the findings as shown in Table 2.13. The results had determined that with the addition of MO amount can possibly help improve the mechanical properties, and concluded the findings as a good composite material with potential for biomedical implantation purpose in future.

Table 2.13: Hardness, fracture toughness and Elastic modulus of prepared composites (Tavangarian & Emadi, 2011).

	Hardness (MPa)	Elastic Modulus (GPa)	Fracture toughness ($MPa\cdot m^{1/2}$)
HA	2384	46	0.56
HA-10MO	2812	70	0.68
HA-20MO	3293	85	0.75
HA-30MO	3388	96	0.97

2.6.3 Hydroxyapatite – Biodegradable Composites

One of the criteria for a restorable implant is that the repair and resorption rate must be the same or at least close to body tissues' repair rates. Therefore, the changes of the bio-fluid in terms of compositional and the capability of biomolecules adsorption will influence the healing process. Various types of cell that reach the $CaPO_4$ surface and adsorbed layer will dictate the ways the cells respond during this process (Bogdanoviciene et al., 2006; Witte et al., 2007; Dorozhkin, 2010; Veljovic eet al., 2011). Tricalcium phosphate (TCP) with the chemical formula, $Ca_3(PO_4)_2$ is one of the family under calcium phosphates known to be biodegradable. During implantation, TCP can be dissolved with time and replaced by bone. The most common polymorphs of TCP are the α and β forms. The formation of these phases rely on the Ca/P ratio; the α or β tricalcium phosphate exist if Ca/P ratio is found lower than 1.67 after processing. If the Ca/P ratio is higher than 1.67, then calcium oxide (CaO) will be found in the HA phase (Ioku et al., 1996; Tampieri et al., 2000).

2.6.3.1 Hydroxyapatite – β-TCP

In one of the most frequently used bioceramics for dental replacement and bone is the calcium hydroxyapatite including beta-tricalcium phosphate (β-TCP) and biphasic calcium phosphate (BCP) which are widely used for grafts, augmentation, bone repair or even substitution (Legeros et al., 2003; Galea et al., 2008). Calcium hydroxyapatite is widely used for implant due to their similarity in composition to bone mineral, bioactivity (formation of bone apatite like material on their surfaces) and their osteoconductivity (ability to provide the appropriate scaffold for bone formation (Lala et al., 2016). The β-TCP possesses stoichiometry similar to amorphous biologic precursors to bone mineral, displays a Ca/P molar ratio of 1.5 (Wang et al., 2006).

In one of the interesting research work by Akira et al. (2004), the authors studied the implantation of hydroxyapatite and β-TCP as bone substitutes after excision of bone tumors. There were 23 patients involved for the long term study (97 months) and 30 patients for the short term study (26 months) with bone tumors treated by curettage or resection followed by implantation of hydroxyapatite (HA) or highly purified β-TCP. The authors found that HA was successfully incorporated into host bone in all but two cases; moreover, no obvious evidence of HA biodegradation was observed. A single patient exhibited late deformity following implantation of HA, while for β-TCP, at least partially, absorbed and replaced by newly formed bone. For HA, it took about 17 weeks for the disappearance of radiolucent zones between the ceramics and host. The authors concluded that highly purified β-TCP has the advantages over HA for surgical intervention in bone tumors due to the nature of remodeling and osteoconductivity.

In another research, Nursen et al. (2004) also revealed that β-TCP ceramic was appropriate for repair of cortical defects. One of the commonly used method to fabricate porous calcium phosphate ceramics is by using isostatic compaction and sintering of powders which contains granules of organics such as naphthalene, and polymer, however the pressing method is limited to simpler geometric forms which eventually leads to problem of polymer springback that involved cracks. Therefore, the authors investigated the importance of pore size and pore distribution of β-TCP ceramics. The ceramics were produced using a modified slip casting technique, and sintered for 2 hours at 1000°C. The presence of micropores in the sintered samples affect the bioresorption of TCP based ceramic implants which, therefore it is important to control the size and amount of macro and micro porosity during fabrication (Nursen et al., 2004). From Figure 2.20, the authors revealed that there was a change in the morphology of pore structure as the amount of the porosifier increased through slip casting. The micrographs in Figure 2.20 indicated a uniform pore distribution in all the samples examined under SEM, which supported the fact that polymer beads were suspended properly in the slip. Figure 2.20 (a) indicated that the ceramic had about 65% porosity by volume which was prepared from a slip using 70% polymer beads in the size range of 210-250μm. On the other hands, Figure 2.20 (b) and (c) belong to the slips prepared from solid containing 75 and 85 vol. % polymer. The size of the pore interconnections increased proportionally as the amount of polymer beads increased. The benefit of this porosity is to allow free circulation of body fluids. Hence, these findings on porosity will be a desirable feature since it facilitates the diffusion of calcium and phosphorus ions for mineralization (Nursen et al., 2004).

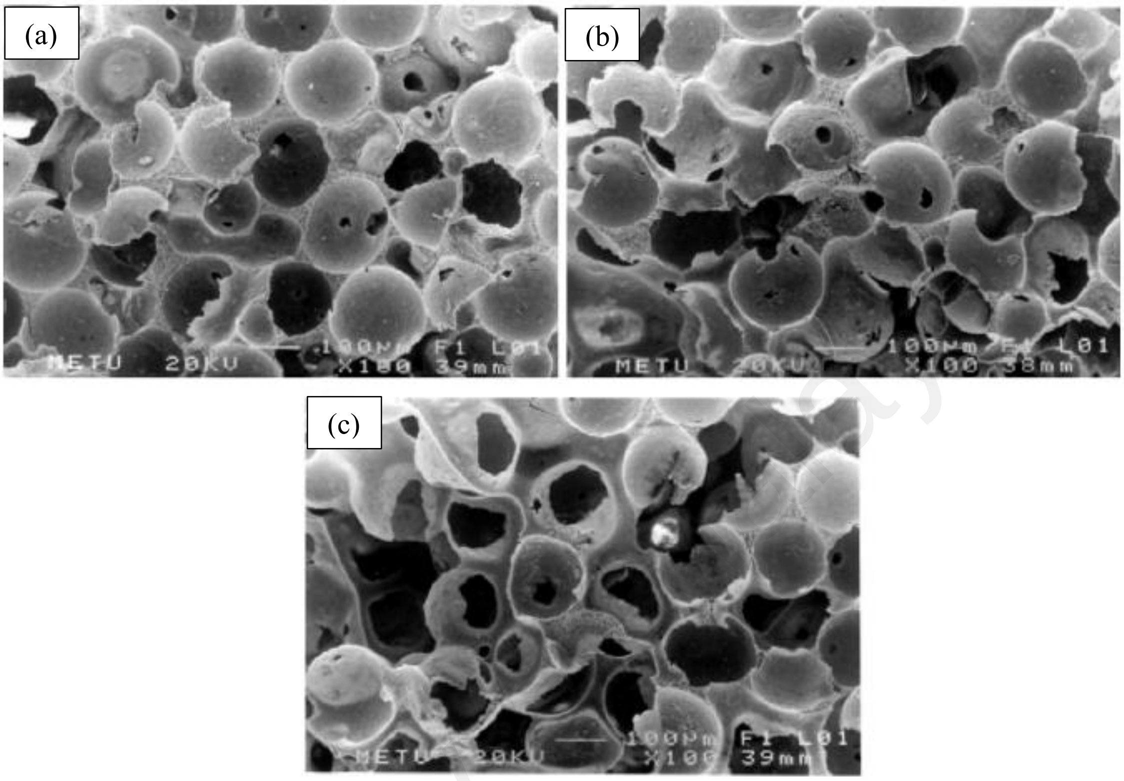

Figure 2.20: SEM micrograph of porous β-TCP (a) 65 vol. % porosity (b) 75 vol. % porosity (c) 85 vol. % porosity (Nursen et al., 2004).

Kobayashi and Murakoshi (2013), experimented the combination of HA/β-TCP composites. The composites were synthesized and sintered with different β-TCP content (0, 10, 20, and 30wt. %). Based on the observation, the authors reported that a trend of porosity increased with β-TCP content increases from 0 – 30 wt. %. The porosity indicated the poor sinterability of HA/β-TCP powder mixture which also reflected the low mechanical properties. For the 30 wt. % β-TCP composite, the bending strength decreased by ~20% and Vickers hardness decreased by ~40% compared to pure HA. However, the fracture toughness was found to have improved from 1MPa·m$^{1/2}$ to 1.3 MPa·m$^{1/2}$ with the 30 wt. % β-TCP composite. Moreover, Kobayashi and Murakoshi

(2013) also established the grain size relationship where mechanical properties such as Vickers hardness, strength and elasticity decreased with increasing grain size when β-TCP content was increased as shown in Figure 2.21. The grain size was reported to have increased with increasing β-TCP content, 0 wt. % (1.86μm) > 10 wt. % (2.59μm) > 20 wt. % (2.81μm) > 30 wt. % (2.44μm).

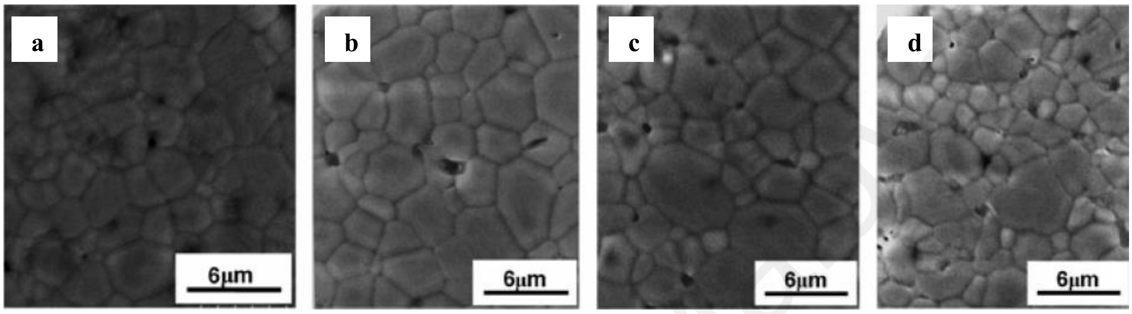

Figure 2.21: SEM images of HA/β-TCP grains (a) 0 wt. % (b) 10 wt. % β-TCP (c) 20 wt. % β-TCP (d) 30 wt. % β-TCP (Kobayashi & Murakoshi, 2013).

2.6.3.2 Hydroxyapatite – α-TCP

Among the possible candidate materials for bone regeneration and engineering scaffolds, calcium phosphates displayed several advantages due to their similarity and high compatibility with natural bone (Almirall et al., 2004). One of the phosphate material, known as alpha-tricalcium phosphate (α-TCP) has been gaining popularity due to its high solubility and osteoconductivity when implanted in the body (Thurmer et al., 2016). New bone tissue are able to replace the implant, preventing complications such as inflammatory or foreign body reactions.

With both HA and α-TCP's advantages as the materials for bone implant, it is believe that the combination of HA and α-TCP is expected to enhance faster bone growth than HA alone (Kien et al., 2015). Yasuda et al. (2002) studied the behavior of the HA and α-TCP combination in ratios of 20wt. % and 40wt. % of α-TCP. The mixed powders were prepared through colloidal processing with 30 vol. % HA/α-TCP mixed powder and 70 vol. % aqueous solution containing polycarboxlic from the anion dispersant. Then, the synthesized samples were sintered at 1200°C and 1500°C for 2 hours. The authors discovered that HA with 20 wt. % α-TCP sintered at 1500°C obtained a relative density of about 90%, while α-TCP was difficult to be sintered at the same temperature. On the other hand, sintered HA with 40 wt. % α-TCP exhibited a relative density at 80% only. These findings indicated that there is a potential in improving the mechanical properties when combining HA and α-TCP as composite.

2.7 Summary

Hydroxyapatite (HA) has been successfully applied in medicine due to its excellent biocompatibility for decades. Unfortunately the low fracture toughness (<1 MPam$^{1/2}$) of the HA ceramics was the major drawback to be used as load-bearing implants. Therefore, the applications of HA are limited to non-load implants, fillers, coatings and low-loaded porous implants. To overcome this problem, many researches have been carried out to improve the mechanical properties of HA ceramics by forming a composite body. An overview of previous researchers' work on HA and HA composites are deliberated in this chapter. The composites can be divided into bioinert ceramics, bioactive ceramics and biodegrable ceramics. From the literature, magnesium orthosilicate has the potential to be mixed with HA to improve the mechanical properties as composite for load bearing implant purposes.

CHAPTER 3 - METHODOLOGY

3.1 Powder Synthesis

For the current research work, the preliminary powders i.e. hydroxyapatite (HA) powder was produced using a novel wet chemical method (Ramesh, 2004) and magnesium orthosilicate powder was produced via combination of ultrasonification and mechanical ball milling method. Then the HA-MO composites were finally prepared by using similar preparation method as magnesium orthosilicate.

3.1.1 Hydroxyapatite Powder

For the preparation of hydroxyapatite powder, a novel wet chemical method was used to synthesized pure HA (100g) with the use of precipitation from aqueous medium via titration process by reacting calcium ion with phosphate ion based on a molar ratio Ca/P = 1.67. During the titration process, the aqueous medium was maintained at a pH of about 10 – 12 by the addition of small amounts of ammonium (NH_3) solution (25% concentration) (Ramesh, 2004; Tian et al., 2008). The use of commercially available starting precursors such as calcium hydroxide, $Ca(OH)_2$ (98% purity, BDH) and orthophosporic acid, H_3PO_4 (85% purity, Merck) was in accordance with the chemical reactions as follows:

$$10Ca(OH)_2 + 6H_3PO_4 \rightarrow Ca_{10}(PO_4)_6(OH)_2 + 18H_2O \tag{3.1}$$

The synthesis process involved the preparation of orthophosphoric acid (H_3PO_4) and calcium hydroxide ($Ca(OH)_2$) solutions. The H_3PO_4 solution was prepared by diluting 69.19g of H_3PO_4 in a beaker containing 400ml of distilled water which was stirred for 10 minutes and subsequently contained in a titration funnel. This prepared acid solution has a pH of about 1. A similar procedure was used to prepare the $Ca(OH)_2$ solution, where 75.5g of $Ca(OH)_2$ measured was mixed into a beaker containing 750ml of distilled water and stirred for 10 minutes. The prepared $Ca(OH)_2$ solution has a pH of about 12. The solution was stored in a beaker which was then covered with cling film to minimize contamination including any reaction between carbon dioxide in air with the mixture.

The precipitation process began with H_3PO_4 solution dripped at a rate of 7 drops in 10 seconds into the $Ca(OH)_2$ solution which was still in stirred condition. The titration process usually takes about 3 hours. During the titration process, the pH of the mixture was monitored and kept above 10.5 by the addition of NH_3 solution. Once the titration process has completed, the solution was stirred for an additional 6 hours. The precipitate was allowed to settle overnight before filtration. The filtered precipitate was rinsed three times at every half hour interval using distilled water and dried in the oven at 60°C overnight. Finally the dried filtered cake was crushed and sieved (212µm) to obtain well-defined highly crystalline HA powder. The flow of this method is shown in Figure 3.1.

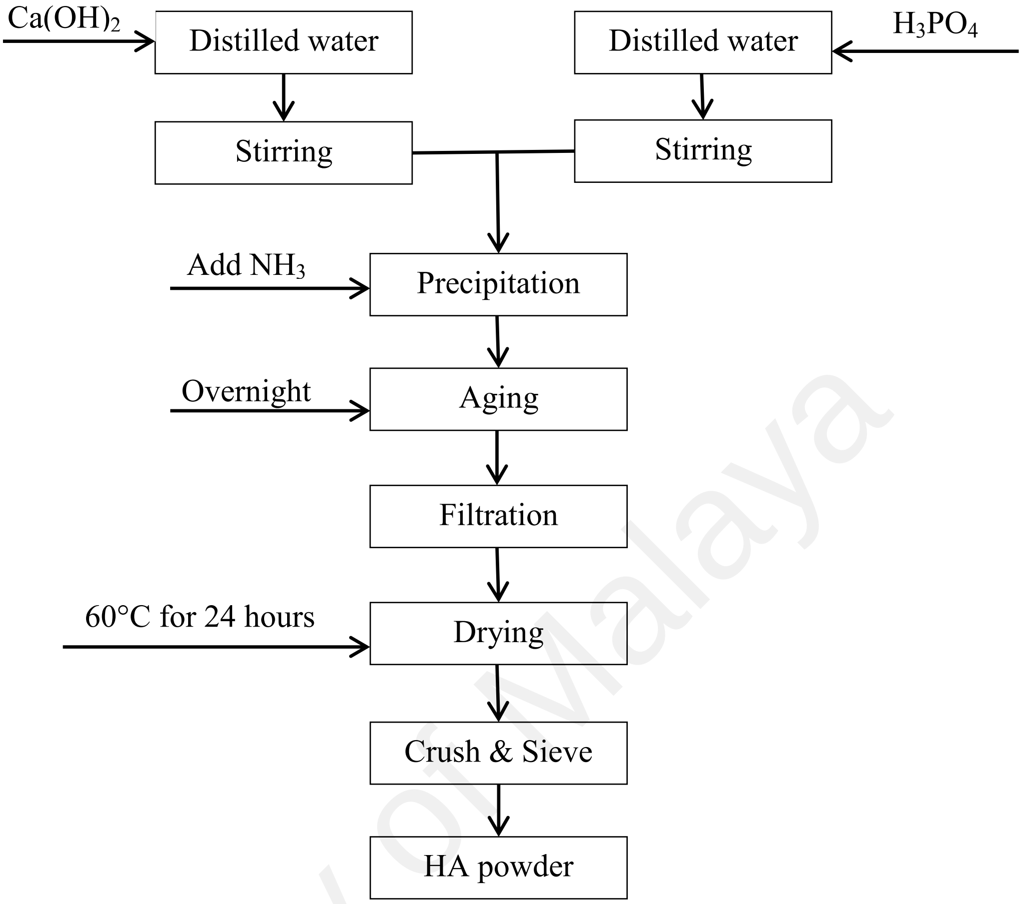

Figure 3.1: HA wet chemical method process flow.

3.1.2 Magnesium Orthosilicate Powder

Magnesium orthosilicate powder was produced via combination of ultrasonification and mechanical ball milling method. A conventional ball milling method was employed to mix and refine the powder particles. The starting precursors where 17.9016g of MgO and 33.6976g of $Mg_3Si_4O_{10}(OH)_2$ weighed were mixed individually into a beaker of 100ml ethanol and undergone ultrasonification for 2 minutes before finally mixing both of them in a beaker and ultrasonic for 30 minutes. The final solution was poured into a high density polyethylene (HDPE) bottle and ball milled with zirconia milling balls for 3 hours prior to the drying process. After 24 hours drying in the oven at 60°C, the dried cake of magnesium orthosilicate was sieved into powder form. Comprehensive details on the powder ratio can be obtained in Appendix A.

3.1.3 Hydroxyapatite-Magnesium Orthosilicatae Composite Powder

The HA-magnesium orthosilicate composite powders were prepared in 30 g for each batch of different weight percentage addition as shown in Table 3.1.

Table 3.1:HA-MO composition

	Forsterite (g)	**Hydroxyapatite (g)**
Undoped	0	30
10wt%	3	27
20wt%	6	24
30wt%	9	21
40wt%	12	18
50wt%	15	15

The HA powders were mixed with magnesium orthosilicate accordingly to the concentration from 10wt% to 50wt% using the ultrasonification and mechanical ball milling method. The first step in preparing the powder was to measure the accurate amount of powders needed for respective batches. Then both the HA and MO powders were mixed individually into a beaker of 100ml ethanol and undergone ultrasonification for 2 minutes before finally mixing both of them in a bigger beaker and ultrasonic for 30 minutes. The final solution was poured into a high density polyethylene (HDPE) bottle and ball milled with zirconia milling balls for 3 hours prior to the drying process and powder sieving.

3.2 X-Ray Diffraction (XRD)

X-Ray diffraction (XRD) is a versatile, non-destructive analytical technique for identification and quantitative determination of the various crystalline forms knows as phases of compounds present in powder and solid. Besides that, XRD method is capable of providing qualitative and quantitative information about the crystalline phase exists in the sample (Rahaman, 1995).

In the present work, the phases present in the powders as well as the sintered samples were determined at room temperature using X-Ray diffractometer with Cu-Kα ($\lambda = 0.15406$ nm) as the inception of the radiation using a scan speed and step scan of 6°/min and 0.02° respectively, at 35 kV and 15 mA.

The peaks obtained were compared to standard reference JCPDS-ICDD (Joint Committee of Powder Diffraction Standard – International Center for Diffraction Data) files for hydroxyapatite (09-0432) and magnesium orthosilicate (34-0189). The details of the said JCPDS-ICDD reference files are attached in Appendix B.

Besides the phase stability examination, the average crystallite size (d) can also be determined for the hydroxyapatite, magnesium orthosilicate and the composite powders from the peak broadening at the prominent XRD peaks at $2\theta = 28°$, $32°$ and $44°$ in the XRD diffraction pattern associated with a particular planar reflection from within the crystal unit cell using Scherrer's formula below (Cullity & Stock, 2001).

$$d = \frac{0.9\lambda}{\beta cos\theta} \tag{3.2}$$

Where,

d = Crystalline size (m)

λ = Wavelength (0.154056 nm)

β = Full width at half maximum

θ = Bragg angle

3.3 Fabrication of Samples

The as prepared HA-MO powders was uniaxial compacted at about 250 to 300 kPa into discs (20 mm diameter x 5 mm thickness) and into rectangular bars (32mm x 13mm x 6mm) using hardened steel mould and die set (Appendix C). For circular disc sample, 1.8 g of HA-MO powder was needed and for rectangular bar, about 2.0 g of HA-MO powder was used to form the green body. Throughout the pressing process, the cleanliness of the die was essential, so as not to contaminate the samples. To assure this, before the die is been used for the sample preparation it was cleaned with a penetrating oil liquid such as WD-40, in order to prevent powder lamination. The pressed samples were then labelled for identification purposes as shown in Table 3.2.

Table 3.2: Samples identifications

Temperature (°C)	**Pure HA**	**10wt%**	**20wt%**	**30wt%**	**40wt%**	**50wt%**
1000	A1	B1	C1	D1	E1	F1
1100	A2	B2	C2	D2	E2	F2
1200	A3	B3	C3	D3	E3	F3
1300	A4	B4	C4	D4	E4	F4

The green samples were subsequently cold isostatically pressed (CIP) at 200 MPa (Riken Seiki, Japan) in SIRIM Berhad, Malaysia. This step enables the samples to be more consistently compacted in all direction to induce a uniform shrinkage during the sintering process and ultimately improve the densification of the sintered samples besides preventing the samples from warping and cracking (Colling & Vasilos, 1995).

3.4 Sintering

Sintering is a process of making ceramic components from powder whereby the green body is heated in a sintering furnace to below its melting point to allow particles consolidation to occur. The process leads to decrease in the surface area, an increase in compact strength and in many cases shrinkage in the compact. The densification and grain growth can be controlled from the sintering manner. With better densification, porosity can be reduced in a sample thereby improving the mechanical properties.

In the present research work, the conventional pressureless sintering method was used to sinter the green compacts using standard rapid heating furnace (LT furnace, see Appendix C) at four different temperatures of 1000°C, 1100°C, 1200°C and 1300°C. A furnace ramp rate of 10°C/min (heating and cooling) and a holding time of 2 hours were used at each sintering. The sintering profile used in this work is schematically shown in Figure 3.2.

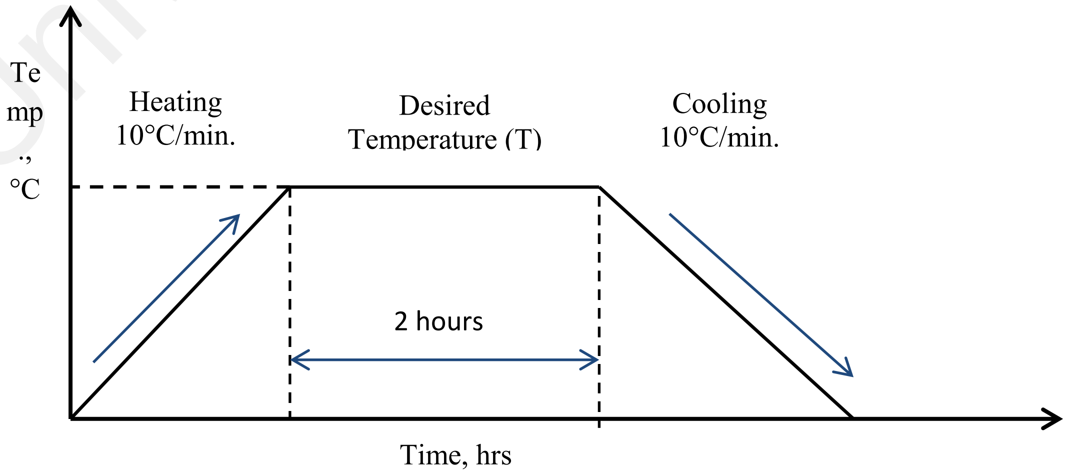

Figure 3.2: Sintering profile

3.5 Grinding and Polishing

The sintered HA-MO disc samples were firstly ground and then polished on one surface prior to density measurement, phases analysis, Vickers hardness testing and microstructural evaluation by Scanning Electron Microscopy (SEM). The process of surface grinding and polishing were done manually by means of the Imtech Grinder-Polisher (Appendix C). The samples were ground by SiC papers of 800, 1000 and 1200 grits successively, followed by polishing with 6μm and 1μm diamond paste to produce an optically reflective surface.

3.6 Bulk Density Measurement

The bulk densities of the samples in this research were measured using the water immersion technique based on Archimedes principle using a standard Mettler Toledo Balance AG204 densi-meter (Appendix C). The immersion medium used in the present research was distilled water.

The procedures to measure the bulk density can be summarized as follow:

1) Firstly, the weight of the sample in air was measured and recorded.
2) Then, the weight of the sample was measured by placing it in a dish immersed in water after zeroing the electronic balance. The measurement was recorded.
3) Measurement was taken with care due to the sensitivity of the balance to minor vibration. This can cause fluctuation of the reading.
4) Finally, the bulk density of the samples can be calculated using the equation (3.3).

$$\rho = \frac{W_a}{(W_a - W_w)} \rho_w \qquad (3.3)$$

Where

ρ = Bulk density of the sample

W_a = Weight of sample in air

W_w = Weight of sample in water

ρ_w = Density of distilled water. The temperature effect on the water density was taken into consideration using the table provided in Appendix D.

3.7 Young's Modulus Determination

The Young's modulus by sonic resonance technique was determined from rectangular samples using a commercial testing instrument (GridoSonic: MK5 "Industrial", Belgium). The resonant frequency of the samples was measured by monitoring and evaluating the vibrational harmonics of the sample by a transducer where the vibrations are physically induced in the sample by tapping. The block diagram of typical test apparatus is shown on Figure 3.3. The modulus of elasticity is calculated from the measured natural frequency, according to the standard test method (ASTM E1876-97). The Young's modulus or modulus of elasticity (E) is calculated using equation (3.4):

$$E = 0.9465\left(\frac{mF^2}{b}\right)\left(\frac{L}{t}\right)^3 T \qquad (3.4)$$

Where;

E = Young's modulus (Pa)

m = Mass of bar (g)

F = Fundamental resonant frequency of the bar in flexural (Hz)

b = Width of bar (mm)

L = Length of bar (mm)

t = Thickness of bar (mm)

T = Correction factor for fundamental flexural mode to account for finite thickness of bar and material's Poisson's ratio based on equation below:

$$T = 1 + 6.585(1 + 0.0752\mu + 0.8109\mu^2)\left(\frac{t}{L}\right)^2 - 0.868\left(\frac{t}{L}\right)^4 - \frac{8.34(1 + 0.2023\mu + 2.173\mu^2)\left(\frac{t}{L}\right)^4}{1 + 6.338(1 + 0.1408\mu + 1.536\mu^2)\left(\frac{t}{L}\right)^2}$$

Where;

μ = Poisson's ratio taken as 0.22 for ceramic body (Brook, 1991)

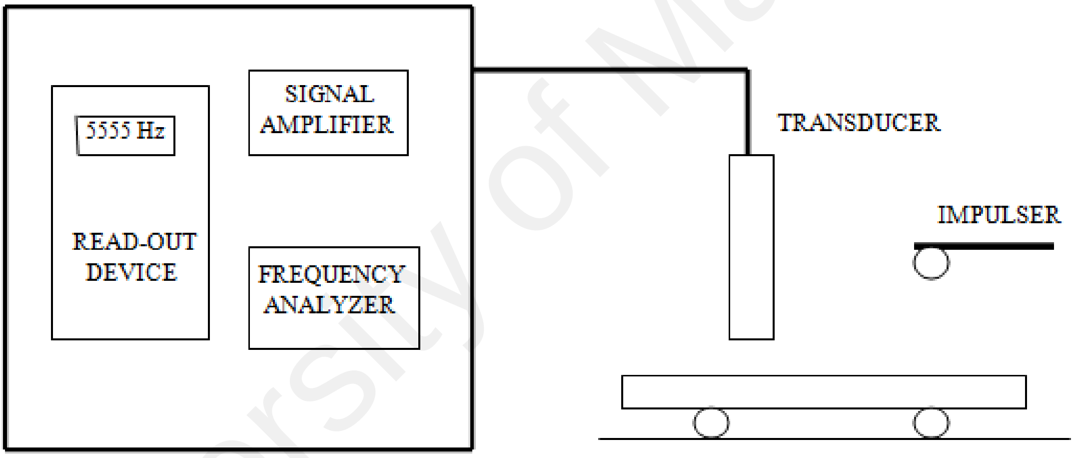

Figure 3.3: Block diagram of test apparatus for Young's modulus measurement (ASTM Standards E 1876-97)

3.8 Vickers Hardness Determination

The Vickers hardness testing method was employed to ascertain the hardness of the sintered samples. Hardness is defined as the ability of a material to resist denting as caused by a load bearing on the material using a dimensionally standardized probe. Indentations were made on the sintered samples using a pyramidal diamond indenter that has a 136° tip with an applied force of 0.5 kg.

During the test, the load is applied slowly, without impact, and held for approximately 10 seconds to create an impression. The physical quality of the indenter and the accuracy of the applied load as defined clearly in ASTM E384-99 and ISO 14705 must be controlled to get the correct results. The shape after indentation was then observed under microscope to measure the diagonal length d_1 and d_2 respectively. The shape of the diamond indenter and the indented shape are shown in Figure 3.4.

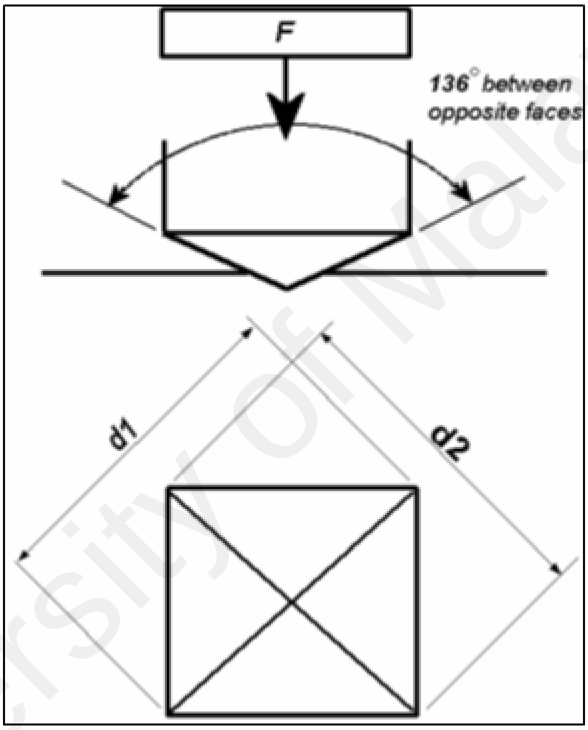

Figure 3.4: Schematic diagram of Vickers hardness indenter

Three indentations were made in order to obtain the average of the Vickers hardness value. The value of Vickers hardness can be calculated using equation 3.5.

$$H_v = \frac{1.854P}{d^2} \tag{3.5}$$

Where,

H_v = Vickers hardness

P = Applied load

d = average diagonal length = ([d1 + d2] /2)

3.9 Fracture Toughness Determination

The fracture toughness can be evaluated from the indentation method. The advantage of this method is the speed, ease of testing and sample preparation, relatively low cost, large numbers of indentation can be made quickly and the small volume of material required. Principally, the indentation method is similar to Vickers hardness testing procedures. Similar indentation pattern as shown in Figure 3.5 should be visible upon indentation with existence of crack propagation.

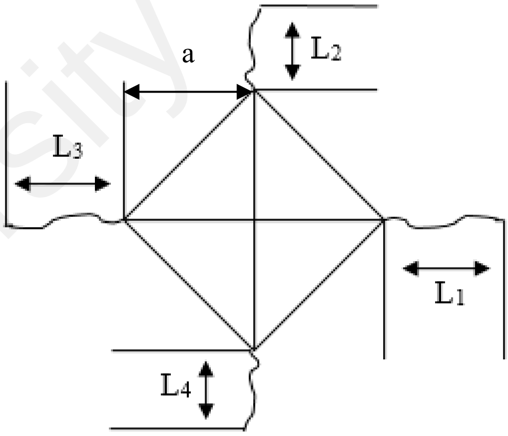

Figure 3.5: Crack propagation from indentation (L1, L2, L3, L4 = length of cracks).

Thus, the fracture toughness (K_{Ic}) was determined from the equation 3.6 derived by Niihara (1985);

$$K_{Ic} = 0.203\left(\frac{c}{a}\right)^{-1.5}(H_v)(a)^{0.5} \tag{3.6}$$

Where,

H_v = Vickers hardness (N/m^2)

c = Characteristics crack length (i.e. L + a)

a = Half diagonal of the indent, μm

3.10 Scanning Electron Microscopy and Grain Size Measurement

The synthesized HA and HA-MO powders were inspected by the scanning electron microscope (SEM). Carbon tapes were placed on metal SEM mounts and the HA and HA-MO powders were sprinkled onto the mount with a spatula. The powders were examined under SEM at accelerating voltage of 15 KV at magnifications up to 20,000X.

The microstructure development of the sintered samples were also examined under the SEM. The SEM function by focusing a small spot of electrons on a thick specimen and proceeds to scan across the specimen surface in a series of lines, using electrostatic or electromagnetic forces. Electrons emerging from the upper specimen surface are collected by an electron detector and used to produce image on a monitor as a series of line.

The average grain size of sintered samples was determined from scanning electron micrographs using the line intercept method. This technique requires measurements taken from polished sections. In a typical analysis, a known test line is drawn on an A4 size SEM micrograph of the selected polished section and the number of intercept between the test line and grain boundaries are counted. The test line should cover at least 50 grains and several lines are drawn and measure before average value is taken.

The average grain size is then calculated according to the equation proposed by Mendelson (1969):

$$\overline{D} = 1.56\overline{L} \tag{3.7}$$

where $\overline{D}$ is the average grain size and $\overline{L}$ is the measured average interception length over a large number of grains which can be represented by:

$$\overline{L} = \frac{C}{MN} \tag{3.8}$$

Where *C, M and N* are the total length of the test line, the magnification of the SEM micrograph and the number of intercepts respectively.

The technique used to count the number of intercepts was according to an international standard test method for intercept counting (ASTME E112-96, 2004). Essentially, the end point of a test line are not intersections and not counted unless the end appeared to exactly touch a grain boundary, when a ‘0.5’ intersection is scored. A tangential intersection with a grain boundary is scored as ‘1’ intersection while for intersection coinciding with the junction of 3 grain is scored as a ‘1.5’ intersection as shown in Figure 3.6.

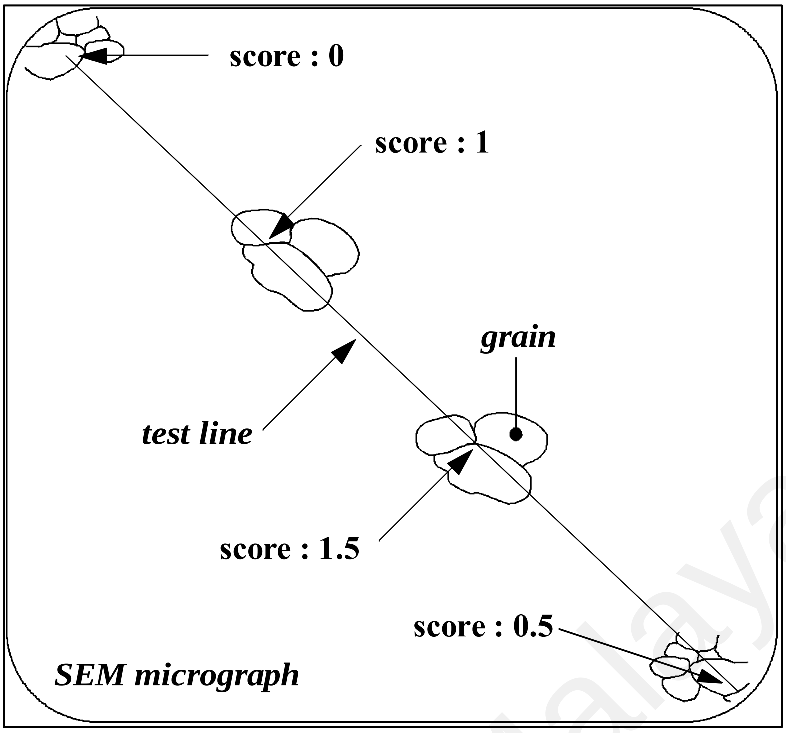

Figure 3.6: Schematic diagram showing the score given for the type of intersections (Ramesh, 1997)

CHAPTER 4 - RESULTS AND DISCUSSION

4.1 Introduction

For this research, studies were carried out to evaluate the densification behavior and properties of hydroxyapatite-magnesium orthosilicate (HA-MO) composite. The composite was prepared in various compositions, by varying the magnesium orthosilicate content from 10 wt. % to 50 wt. % via mechanical ball milling and conventional pressureless sintering at 1000°C to 1300°C, using ramp rate of 10°C / minute for 2 hours. Before sintering, synthesized magnesium orthosilicate, hydroxyapatite and hydroxyapatite-magnesium orthosilicate composite powders were identified through the x-ray diffraction (XRD) and scanning electron microscope (SEM) machine, likewise upon sintered, samples were characterized also. The mechanical properties such as relative density, Vickers hardness, Young's modulus and fracture toughness were evaluated through lab works.

4.2 Starting Powder

4.2.1 HA Powder

The hydroxyapatite (HA) powder was prepared by wet chemical method. The wet chemical method involved precipitation from an aqueous medium through the slow titration of an orthophosphoric acid solution to calcium hydroxide based on a molar ratio Ca/P = 1.67 where the solution was maintained at a pH of 10-12 through addition of small amounts of ammonium solution. The XRD result of hydroxyapatite powder before sintering as shown in Figure 4.1 is in good agreement with that of the standard JCPDS card No. 09-432. It was observed that the peaks were generally broad, signifying that the powder has low crystallinity. There were no other phases found in the powder. The Ca/P ratio of the starting powder is important as the reactivity, stability and mechanical properties of sintered HA can be affected as reported by Liu et al. (2008) and Raynaud et al. (2002a, b & c).

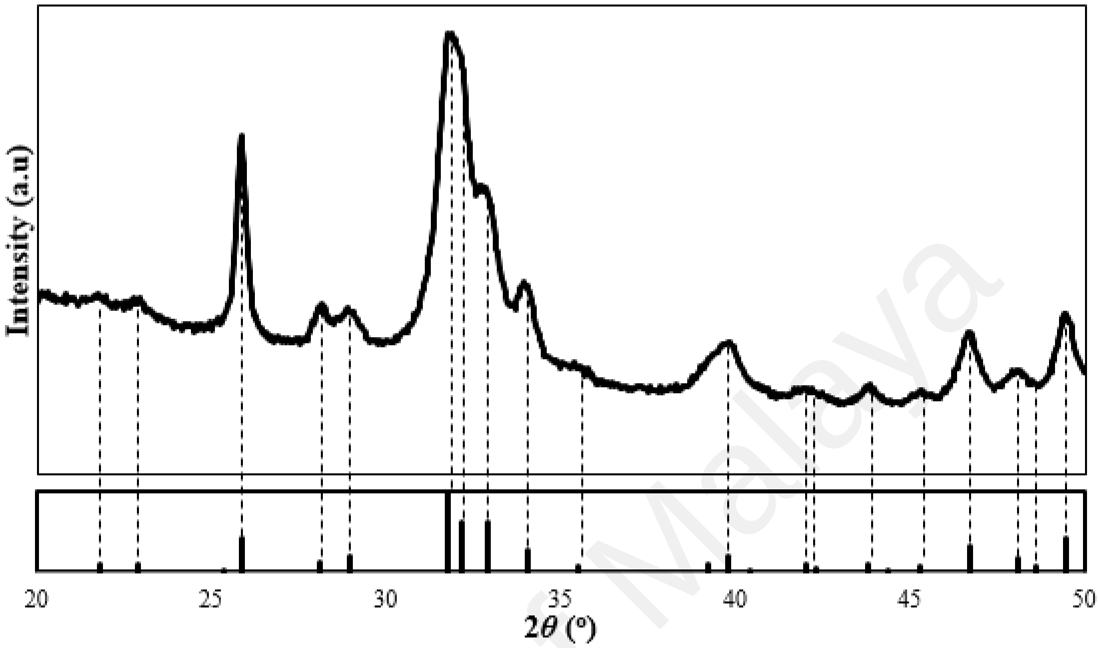

Figure 4.1: XRD traces of synthesized hydroxyapatite powder before sintering.

The SEM micrograph of HA powder shown in Figure 4.2a consists of small particles in the range of 1-3 µm and large particles in the range of 5-10 µm. Rougher surface was observed from the large agglomerate which consists of smaller particles. Similar observation was also reported by Ramesh et al. (2013), Gibson et al. (2001) and Saeri et al. (2003) for synthesized HA powder. The synthesized powder is also free of impurities as the energy dispersive x-ray (EDX) spectrum only displayed the element of HA which are Ca, P, and O in Figure 4.2b.

Besides, the formation of soft agglomerates which broke easily at low pressing pressure of 250 kPa during powder compaction can be due to the process of drying the filter cake of synthesized HA, even though the dried filter cake was grounded and sieved. Due to the soft nature of the powders, any attempts to use higher pressures during uniaxial pressing of the samples were futile as powders lamination on the die surface was observed and in some extreme cases, a layer of compacted powders separated immediately from the green body upon ejection from the mold.

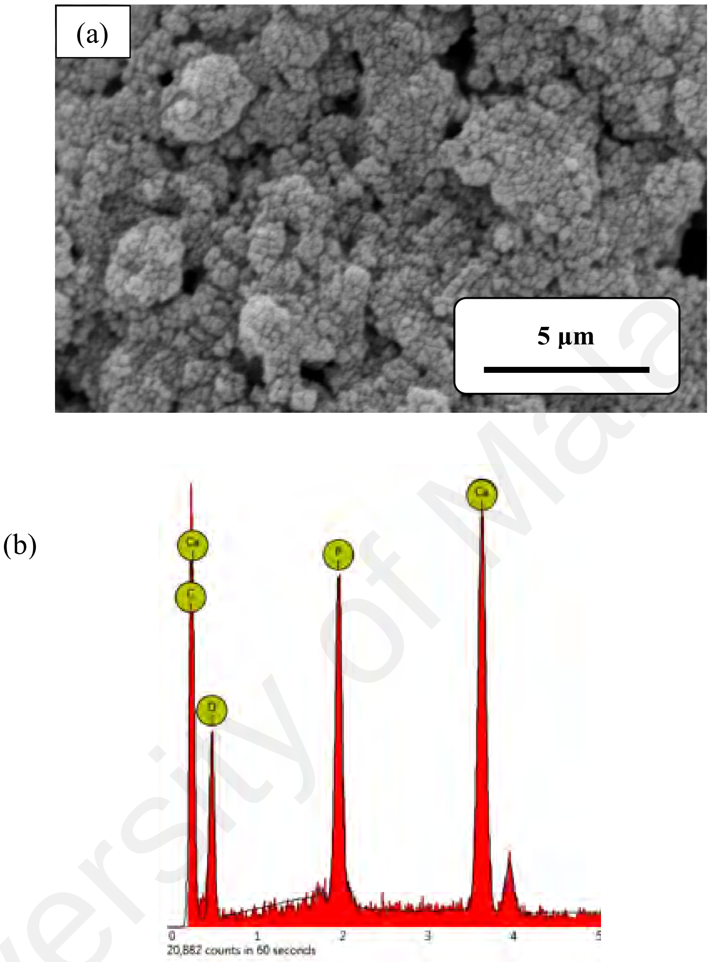

Figure 4.2: a) SEM analysis of synthesized hydroxyapatite powder, b) EDX of synthesized hydroxyapatite powder.

4.2.2 Magnesium Orthosilicate Powder

The magnesium orthosilicate (MO) powder was produced via combination of ultrasonification and mechanical ball milling method. A conventional ball milling method was employed for 3 hours to mix and refine the powder particles. The XRD results of magnesium orthosilicate as shown in Figure 4.3 before sintering exhibited peaks matching to the JCPDS card No. 34-0189. The SEM micrograph in Figure 4.4a shows characteristic of both MgO which show flake like morphology and talc with lamellar shape forming hard agglomerates. Figure 4.4b displayed the EDX spectrum result of magnesium orthosilicate which shows only elements of Mg, Si, and O were present.

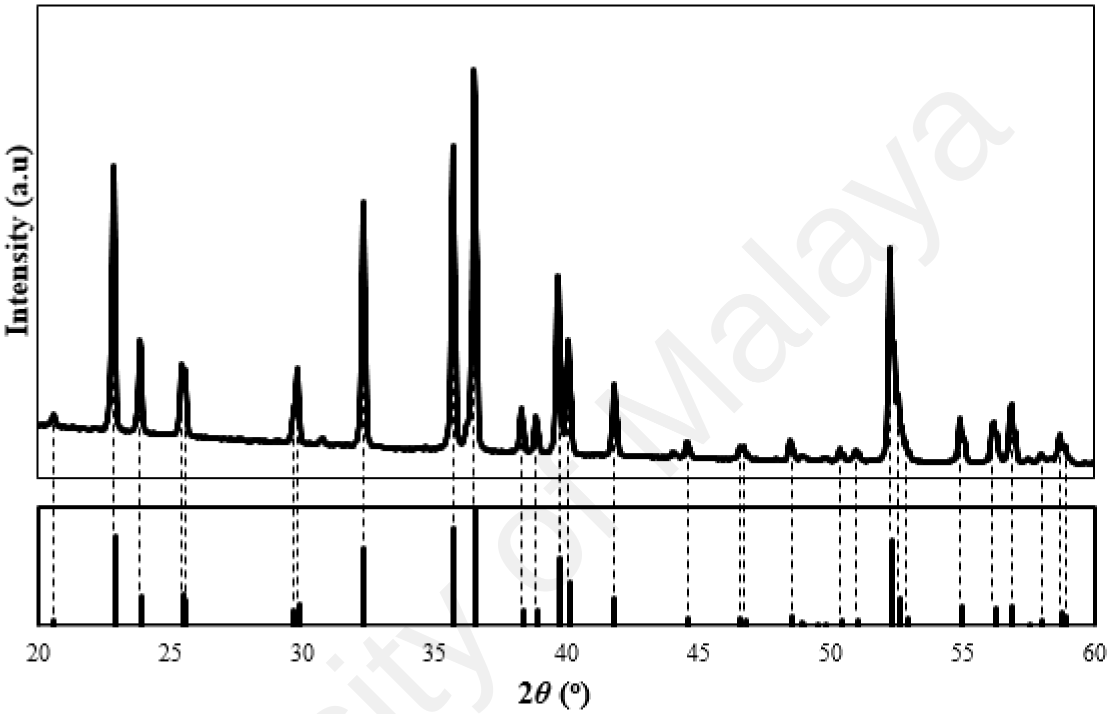

Figure 4.3: XRD traces of synthesized magnesium orthosilicate powder before sintering.

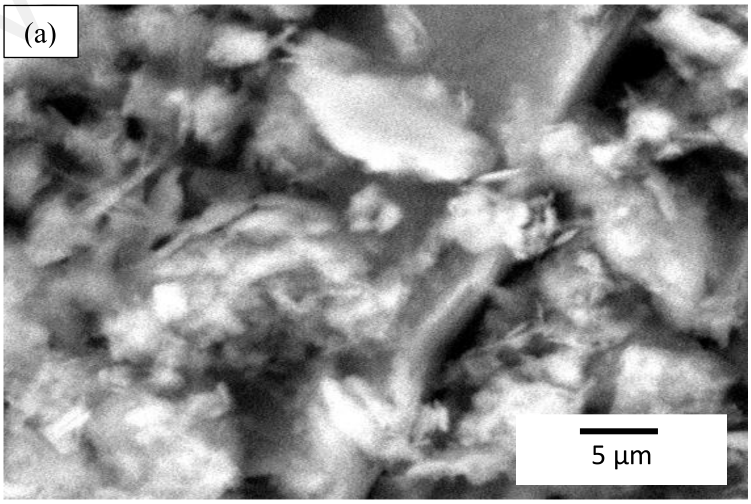

(b)

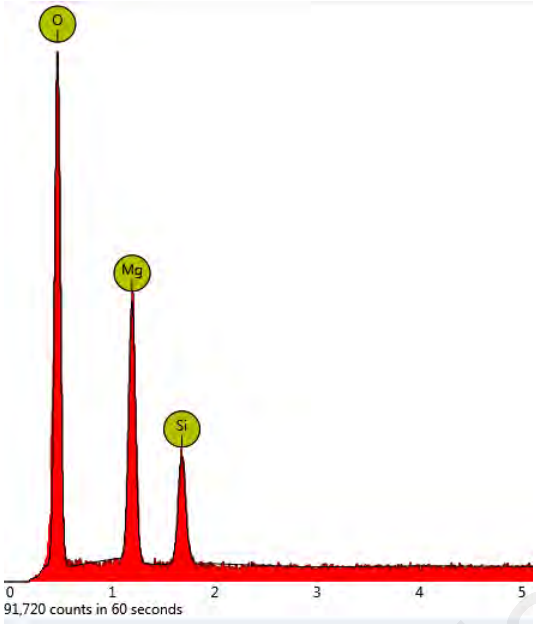

Figure 4.4: a) SEM analysis of synthesized magnesium orthosilicate powder, b) EDX of synthesized magnesium orthosilicate powder.

4.2.3 Hydroxyapatite-Magnesium Orthosilicate Powder

The hydroxyapatite-magnesium orthosilicate (HA-MO) powders were produced via combination of ultrasonification and mechanical ball milling method according to 10MO, 20MO, 30MO, 40MO and 50MO composition. A conventional ball milling method was employed for 3 hours to mix and refine the powder particles. The XRD signatures of HA-MO powders as shown in Figure 4.5 before sintering were found to be similar as that of the pure HA peaks matching to the JCPDS card N0. 09-0432. No major peak shifting was observed from the XRD traces of all the HA-MO powders.

Additionally, the SEM micrographs obtained for all the HO-MO powders indicated that the method employed to prepare the powders had negligible effect on the morphology and agglomeration of the starting HA powder. The powder particles of both powders (HA & HA-50MO) were in the range of 1 to 3 µm diameters as shown in Figure 4.6. Figure 4.7 displayed the EDX spectrum result of HA-MO powder (10MO – 50MO) which shows only elements of Mg, Si, O, Ca, and P were present regardless of the various MO content.

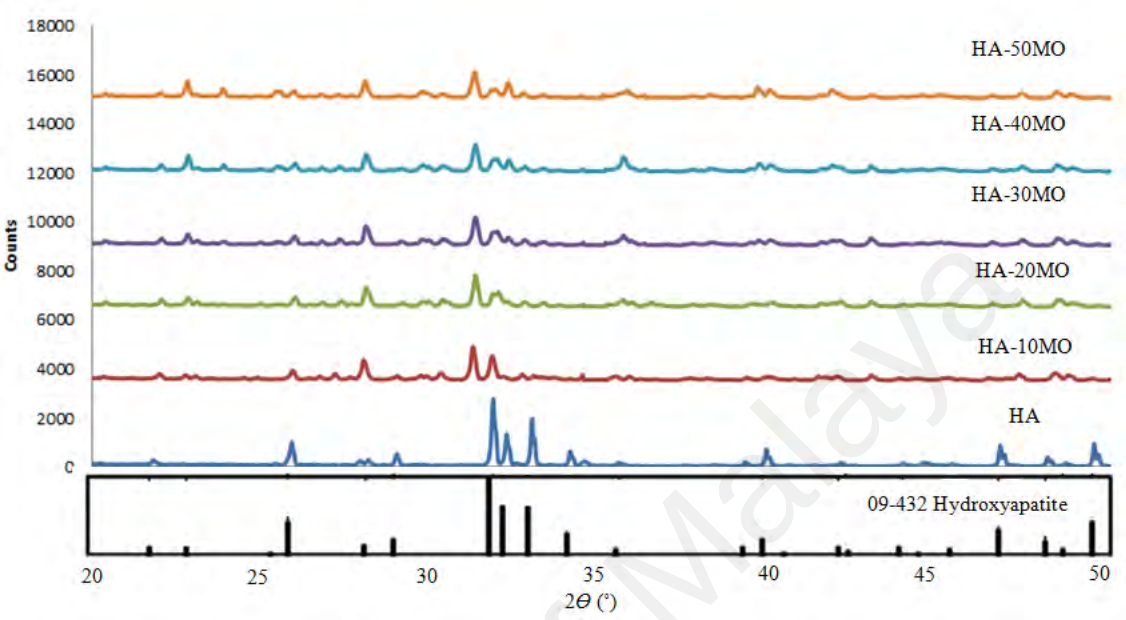

Figure 4.5: XRD traces of HA-MO powders before sintering.

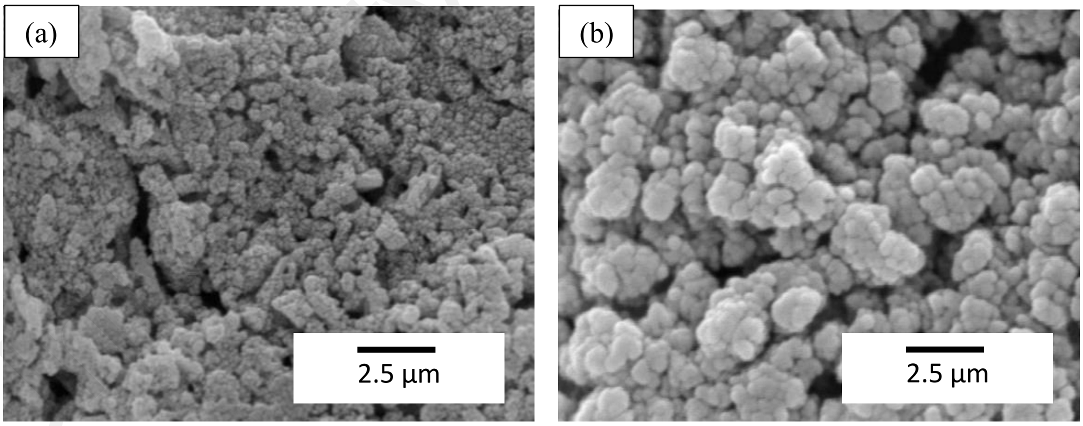

Figure 4.6: SEM micrographs of (a) Pure HA and (b) HA-50MO powder.

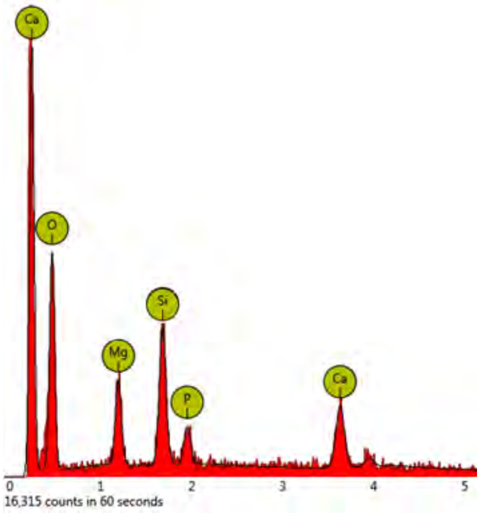

Figure 4.7: EDX of HA-MO powder.

4.3 HA-MO Composite Evaluation

In the present study, the HA-MO composite with various concentration from 10wt.% to 50wt.% were pressureless sintered at four different temperatures of 1000°C, 1100°C, 1200°C and 1300°C with ramp rate of 10°C/minute (heating and cooling) and a holding time of 2 hours. Upon sintering, the HA-MO bulk samples were ground and polished on one surface to 1μm prior to properties measurement such as phase analysis, shrinkage, densification, Young's modulus, hardness, fracture toughness, and microstructure evaluation.

4.3.1 Phase Analysis

The phase stability of the sintered samples were evaluated via XRD for sintering temperatures of 1000°C, 1100°C, 1200°C, and 1300°C and are summarized in Table 4.1.

Table 4.1: Phases present in the sintered HA and HA-MO composites. *For keys:* HA = Hydroxyapatite, MO = Magnesium orthosilicate, W = Whitlockite.

Comp. Sintering Temperature	**HA**	**HA-10MO**	**HA-20MO**	**HA-30MO**	**HA-40MO**	**HA-50MO**
1000°C	HA	HA+MO+W	HA+MO+W	HA+MO+W	HA+MO+W	HA+MO+W
1100°C	HA	HA+MO+W	HA+MO+W	HA+MO+W	HA+MO+W	HA+MO+W
1200°C	HA	HA+MO+W	HA+MO+W	HA+MO+W	HA+MO+W	HA+MO+W
1300°C	HA	HA+MO+W	HA+MO+W	HA+MO+W	HA+MO+W	HA+MO+W

Results from these four sintering temperatures indicated that complete crystalline phase of hydroxyapatite-magnesium orthosilicate composite were obtained after cooling down to room temperature. The comparison between XRD patterns obtained for the sintered HA-MO composite samples are shown in Figure 4.8 to Figure 4.11.

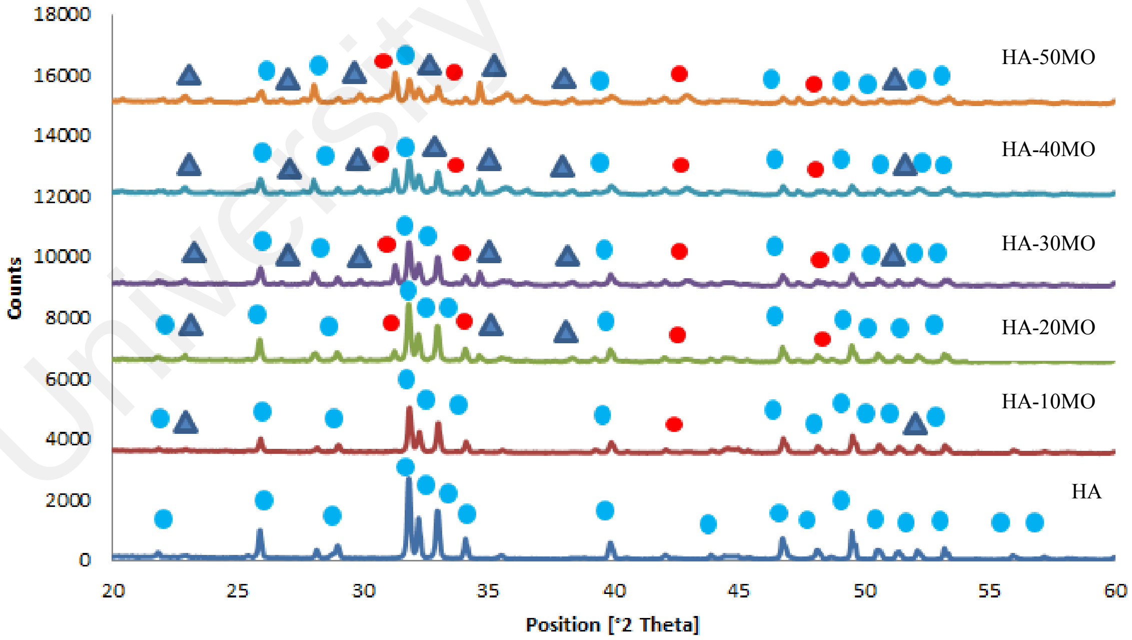

Figure 4.8: XRD patterns of HA-MO samples sintered at 1000°C. *For keys*: 🔵 = HA, 🔴 = whitlockite, ▲ = magnesium orthosilicate.

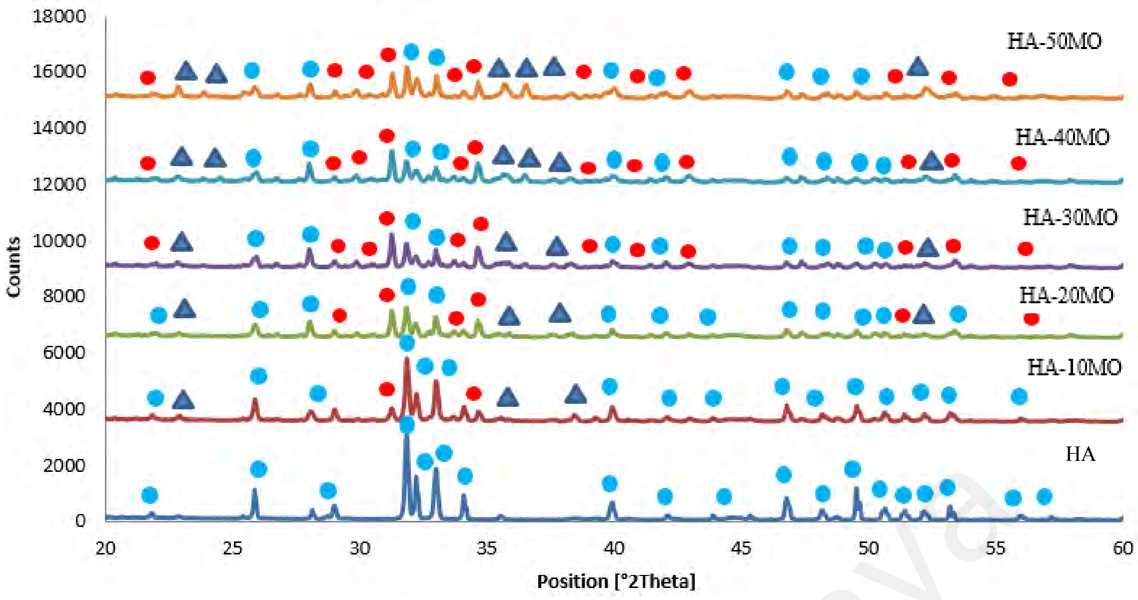

Figure 4.9: XRD patterns of HA-MO samples sintered at 1100°C. *For keys*: 🔵 = HA, 🔴 = whitlockite, ▲ = magnesium orthosilicate.

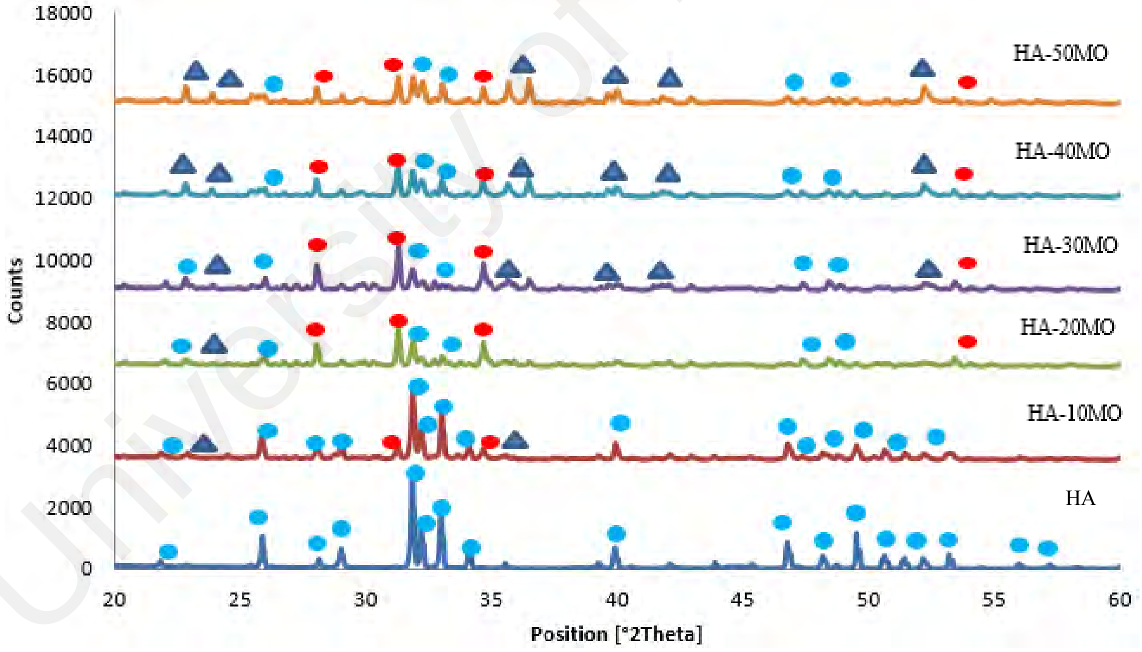

Figure 4.10: XRD patterns of HA-MO samples sintered at 1200°C. *For keys*: 🔵 = HA, 🔴 = whitlockite, ▲ = magnesium orthosilicate.

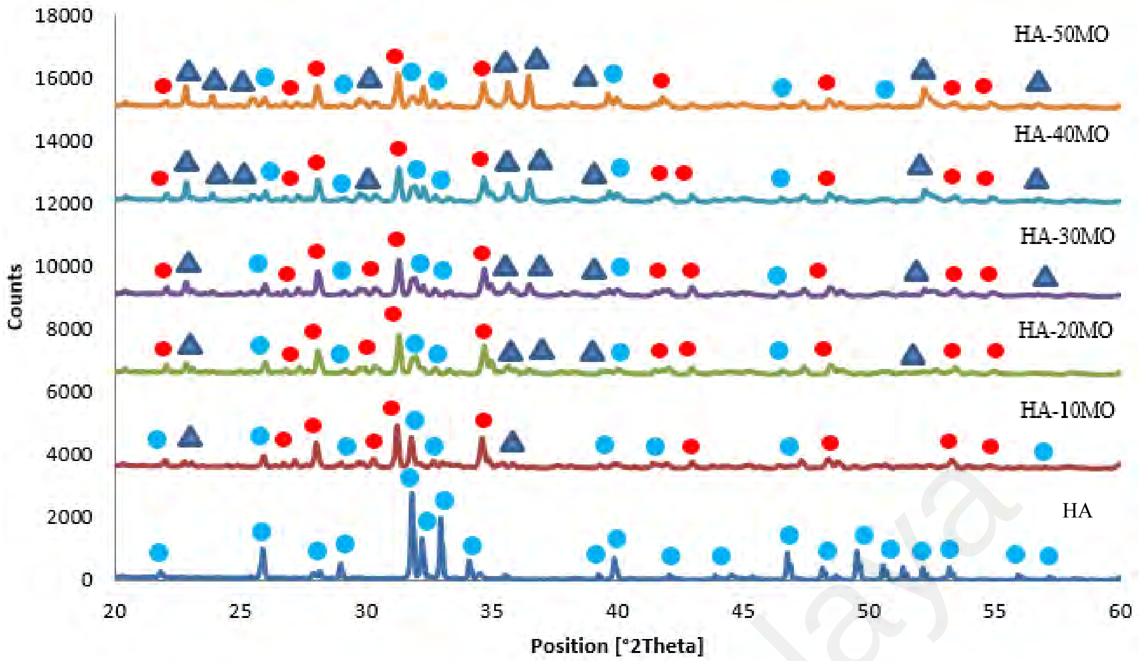

Figure 4.11: XRD patterns of HA-MO samples sintered at 1300°C. *For keys*: ● = HA, ● = whitlockite, ▲ = magnesium orthosilicate.

The XRD phase analysis of monolithic HA in Figure 4.8 to Figure 4.11 indicated that only pure HA was obtained when sintered at 1000°C to 1300°C. The HA peak is in accordance to the standard JCPDS card No. 09-432. The higher the intensity of HA peak indicates the level of crystallinity phase attained. No secondary phase was formed in the pure HA sintered samples. At 1000°C, magnesium orthosilicate was observed to be present in all the composites (10wt. % - 50wt. %). The intensity of MO peak increases as amount of MO increased in the composite. Similar trend of MO peaks were also attained in the sintering temperature between 1100°C and 1300°C, where the peak intensity of MO appeared to increase with increasing MO content, but the difference was minimal. The MO peaks observed are in accordance to the JCPDS card No. 34-0189. However, secondary phase was observed to be present in all the HA-MO composites as shown in Figure 4.8 to Figure 4.11. The addition of MO into HA promotes the decomposition of HA to whitlockite (also known as β-TCP). This observation was also reported by Emadi et al. (2010) where the transformation of HA to whitlockite is associated with a chemical reaction with MO during sintering which lead to partial thermal decomposition. It is believed that the presence of MO has caused the dehydroxylation and decomposition to takes place. The water vapor was considered as a product from the dehydroxylation and decomposition and the speed of the reactions would depend on the partial pressure of H_2O in the sintering atmosphere (Bernache-Assollant et al., 2003). During the sintering of the composite samples, HA would have loss the OH radicals which resulted to the decomposition to whitlockite.

It is also believed that the MO which contains magnesium where it inhibits apatite crystallization in solution can act as a stabilizer for the whitlockite phase which promotes the decomposition of HA (Ma et al., 2012; Cacciotti & Bianco, 2011; Nikaido et al., 2015). Bigi et al. (1993) also confirmed that the presence of magnesium prevented the transformation of calcium phosphate into HA when magnesium entered the prenuclei structures of HA which caused distortion and prevented the growth of HA from the structural mismatch that occurred. The decomposition of the HA to whitlockite phase becomes obvious with the increase of the MO contents. Therefore, the composite with higher amount of MO causes the HA to be more unstable.

4.3.2 Shrinkage

The assessment of the shrinkage was taken as the average of the diameter and the thickness of the disc samples with respect to sintering temperatures. The resulting shrinkage of the sintered samples is shown in Figure 4.12. Generally, the monolithic HA samples attained higher shrinkage across the investigated range of sintering temperatures.

The HA and HA-MO composites displayed an increasing trend manner in the shrinkage when sintered at 1000°C, 1100°C and 1200°C. At low temperature of 1000°C, the sintered HA attained a shrinkage of 15.8%, while the HA-MO composites (10MO - 50MO) in the range of ~3% to ~12%. However, at 1100°C, the shrinkage increased significantly for the sintered HA, attained at 19.1%. For the HA-MO composites, the shrinkage increased in a linear manner till 1200°C, where a significant increase in shrinkage were attained from ~7% to ~17% range at above 1200°C. A maximum shrinkage of 19.7% was attained from HA sintered at 1300°C, while the composite (HA-20MO) managed to attain about 17.7% shrinkage at the same temperature. In addition, it was observed that shrinkage of HA-MO composites (10MO, 30MO, 50MO) showed increasing trend and attained shrinkage of between ~15% to ~17% at 1300°C.

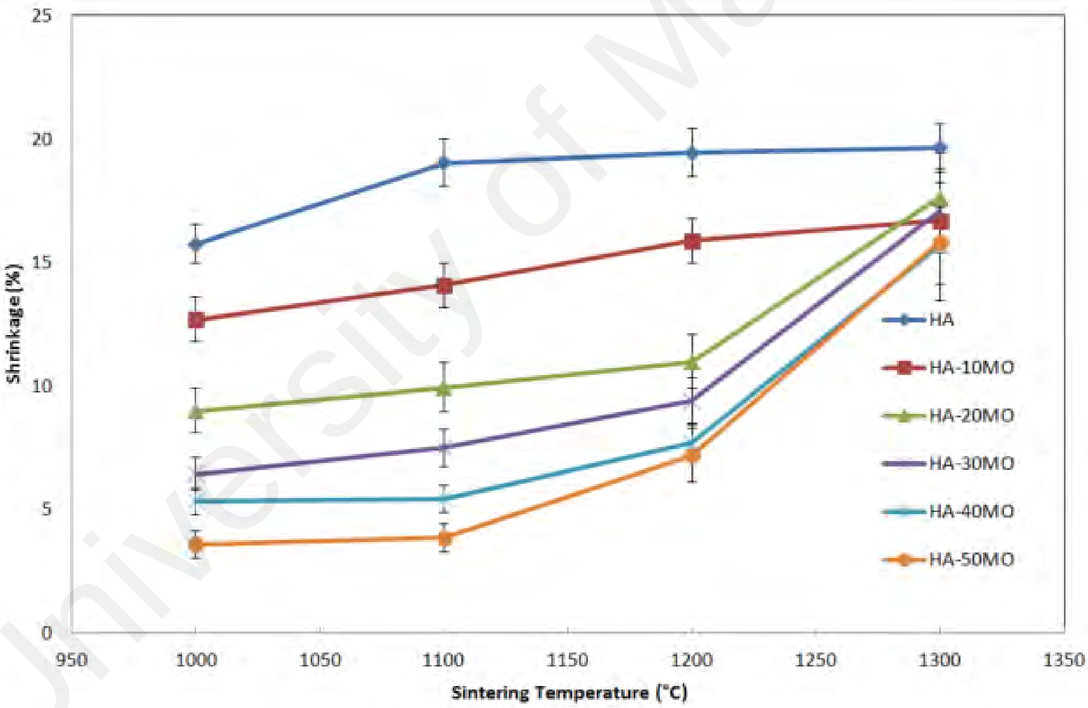

Figure 4.12: Shrinkage of different sintered samples as a function of sintering temperature.

4.3.3. Bulk Density

The effect of sintering on the bulk density of the HA and HA-MO composites is shown in Figure 4.13. The results indicated that HA samples exhibited higher bulk density than HA-MO composites regardless of the sintering temperature used. The bulk density of the HA sintered at 1000°C was 2.7 g/cm^3 and attained a final density of above 3 g/cm^3 when sintered at 1200°C - 1300°C. Generally, sintering across the four range of sintering temperatures (1000°C - 1300°C) resulted in very small increased in density for the HA sintered samples.

Conversely, the HA-MO composites (10MO to 50MO) exhibited lower bulk density across the sintering temperatures when compared to monolithic HA. For HA-10MO only exhibited a bulk density of 2.2 g/cm^3 at 1000˚C and 2.4 g/cm^3 at 1300˚C which showed a small increment. For HA-MO composites with 30MO – 50MO exhibited bulk density in the range of ~1.7 g/cm^3 to ~2.5 g/cm^3 when sintered across 1000˚C to 1300˚C. This range of densities of the composites with 30MO – 50MO were generally low when sintered below 1200˚C due to the inability of MO to consolidate and densify. The MO requires a higher amount of activation energy to diffuse into HA. Besides, another factor could be attributed to the hard agglomerates of magnesium orthosilicate, which could have led to a lower packing density in the green state and also decomposition of the HA phase in the composite matrix from the addition of MO. Hence among the composites, HA-20MO exhibited the optimum value with a bulk density of 1.9 g/cm^3 at 1000°C and 2.7 g/cm^3 at 1300°C.

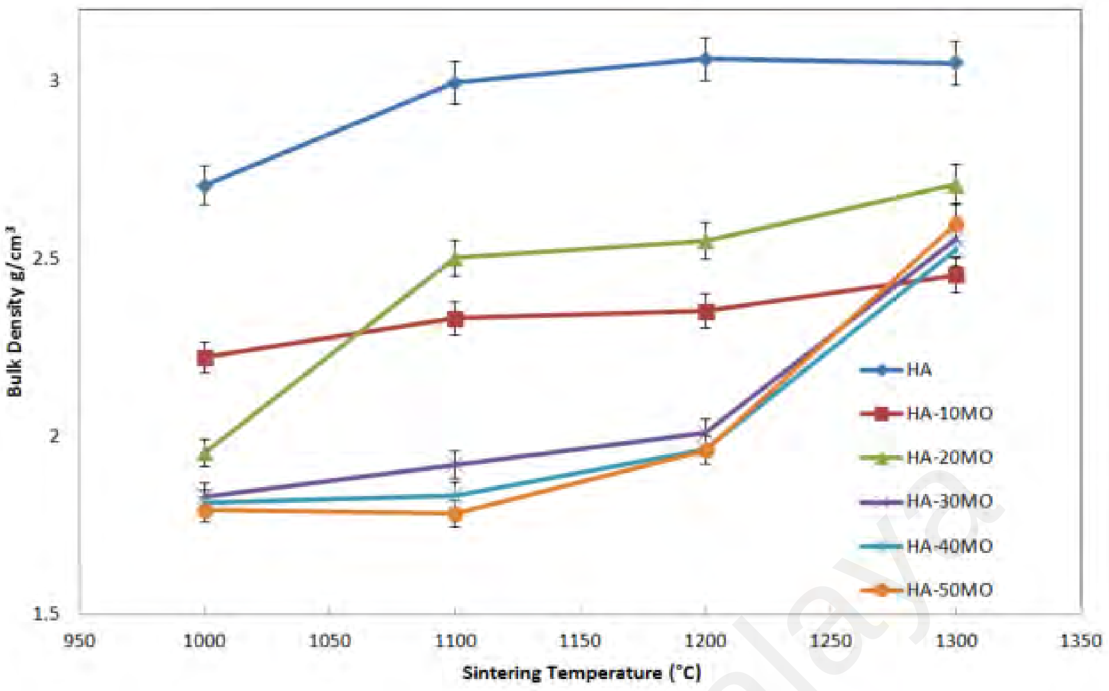

Figure 4.13: Bulk density variation as a sintering temperature and MO content.

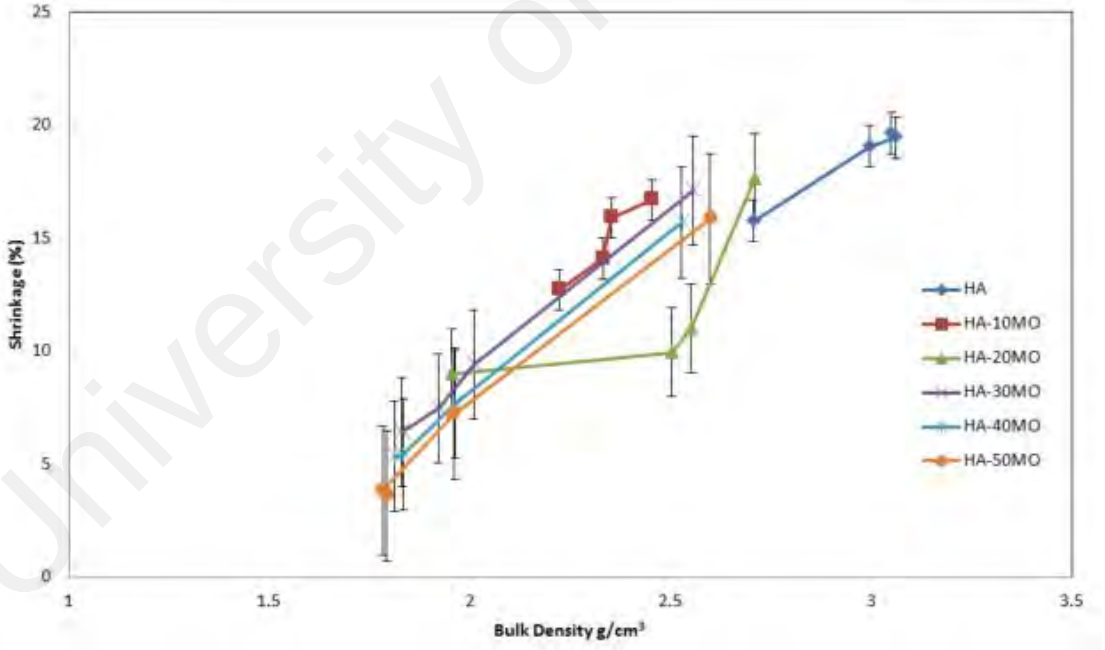

Figure 4.14: Variation in bulk density with shrinkage of the HA and HA-MO composites.

Figure 4.14 exhibited the relationship between shrinkage and bulk density of the sintered bodies, whereby linear shrinkage of the sintered bulks is reported to be a major influence which affects the resulting densification values. It was observed that as the shrinkage values increase, the bulk density values followed to increase in linear manner except for HA-20MO composite. The onset of densification, indicated by a sharp increase in the bulk density, for HA-20MO was between ~9% to ~17%. Generally, all the composite shrinkage findings were lower than monolithic HA due to the complexity of the three phases (HA, MO, whitlockite) that exist upon sintered accompanied with porosities that make the composite to be less dense.

4.3.4 Young's Modulus

Study carried out on the Young's modulus (*E*) of HA-MO sintered samples is shown in Figure 4.15. The HA-50MO composite exhibited a higher Young's modulus than monolithic HA regardless of sintering temperature. The Young's modulus of the monolithic HA varied almost linearly from 90 GPa at 1000°C to about 111 GPa at 1300°C. Conversely, composites containing less than 50wt. % MO exhibited a lower Young's modulus than the monolithic HA when sintered at 1000°C. Typical values recorded for the composites were 29 GPa for HA-10MO, 35 GPa for HA-20MO, 64 GPa for HA-30MO and 82 GPa for the HA-40MO samples when sintered at 1000°C. At 1300˚C, HA-10MO attained 98 GPa, HA-20MO attained 105 GPA, HA-30MO attained 115 GPa and HA-40MO attained 116 GPa.

However, the elastic modulus of the composites increased rapidly with increasing sintering temperature to attain values above 90 GPa. The maximum Young's modulus of 118 GPa was measured for the HA-50MO composite when sintered at 1300°C. The increasing in Young's modulus also reflects the reduce in porosity (Xiao et al., 2005).
These values exhibited by the composites could be beneficial when the composites are used as implant material given their comparable value to human bones.

According to Figure 4.16, the Young's modulus of the HA-MO composites are not governed by the bulk density. This finding is a bit unusual as normally the decreased in bulk density will reflect the decline in flexural modulus of elasticity. However, thru this result, the inclusion of MO in HA, in an increasing manner was found to be beneficial in enhancing the stiffness of the sintered HA-MO composite as depicted by the higher Young's modulus attained. The pores that exist in the composite of the three phases (HA, MO and whitlockite) could have caused more dislocation in the material which it can be perceived that the pores had provided a mechanical interlock leading to firmer fixation of the composite giving it better stiffness.

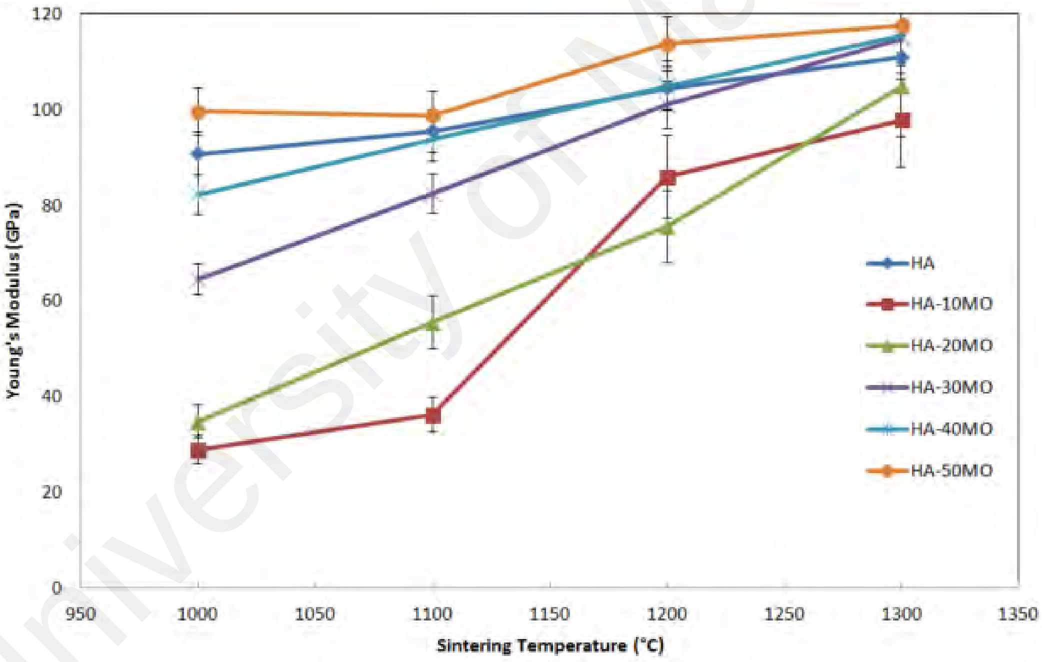

Figure 4.15: Young's modulus variation with sintering temperature.

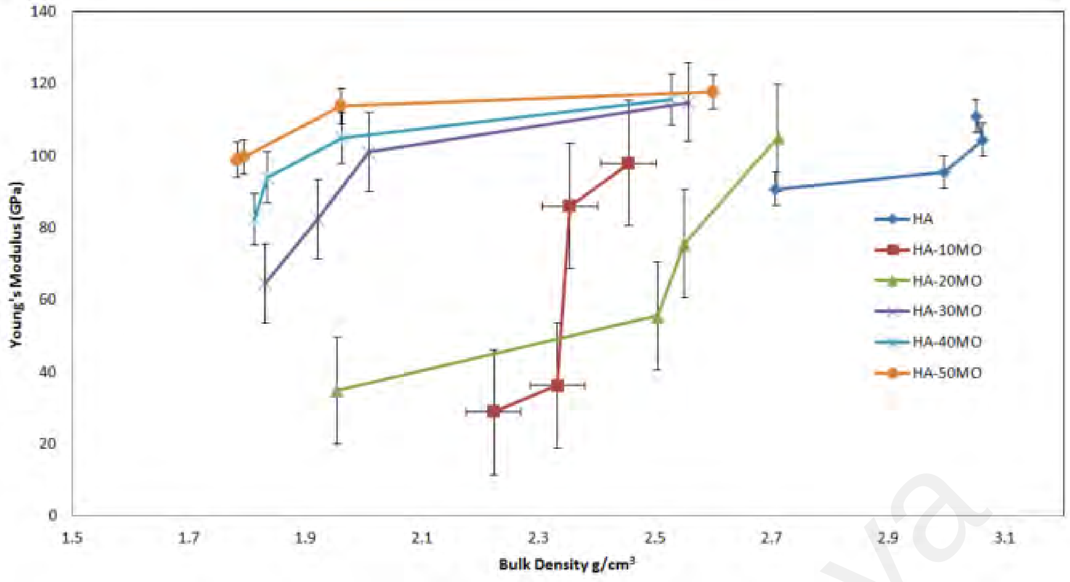

Figure 4.16: Young's modulus variation with bulk density.

4.3.5 Vickers Hardness

The effect of combining HA and MO and sintering temperatures on the Vickers hardness of composites (HA-MO) are shown in Figure 4.17. The HA samples exhibited higher hardness than the composites throughout the sintering regime. The hardness trend attained displays the similar trend found in the bulk density results. At low temperature of 1000°C, the hardness value of HA was at 3.7±0.1 GPa while the HA-MO composites (10wt. % - 50wt. %) were in the range of ~ 0.4 to ~ 1.6 GPa. The increment of hardness in the HA-MO composites were small when sintered in the range of 1000°C to 1200°C. The obvious increment were only noticeable for the composites when sintered at 1300°C. An optimum hardness of 7.1 ± 0.2 GPa was attained for monolithic HA when sintered at 1300°C. Conversely, the highest hardness attainable for the composite containing 20wt. % MO was 2.9±0.1 GPa when sintered at 1300°C. The hardness values of HA-MO composites (10wt. % - 50wt. %) sintered at above 1100°C were in the range of ~1.9 to ~2.7 GPa which are still higher than cortical bone lower limit which is about 0.2 GPa (Pramanik et al., 2007). Therefore, the composite has the potential for biomedical application. The lower hardness observed for the composites is associated with the lower bulk density of the sintered body as depicted in Figure 4.18. Tancred et al. (2001) also reported that the hardness and bulk density of HA composite was found decreased with additive addition. Decomposition of phase and pores that exist in the composite could be the factor of the low hardness and bulk density too.

Another attribute to the higher hardness value of the sintered samples is the grain size. It was observed that as the grain size decreased in HA, the hardness value increased when sintered from 1000˚C to 1300˚C. Similar observations were also found on the HA-MO composites. Even though the composites exhibited lower hardness value than monolithic HA, as the amount of MO increases in the composite, smaller grains were found to be closely packed in the bimodal grain distribution resulted in higher hardness value for the HA-MO composites.

From the results obtained and also reported by Ramesh et al. (2007b), Veljovic et al. (2008) and Li et al. (2008b), it can be suggested that provided the grain does not exceed a critical grain size limit, the hardness of sintered samples would be governed by bulk density or porosity. However, once the grains exceeded the critical grain size, the controlling parameter would be the grain size rather than bulk density.

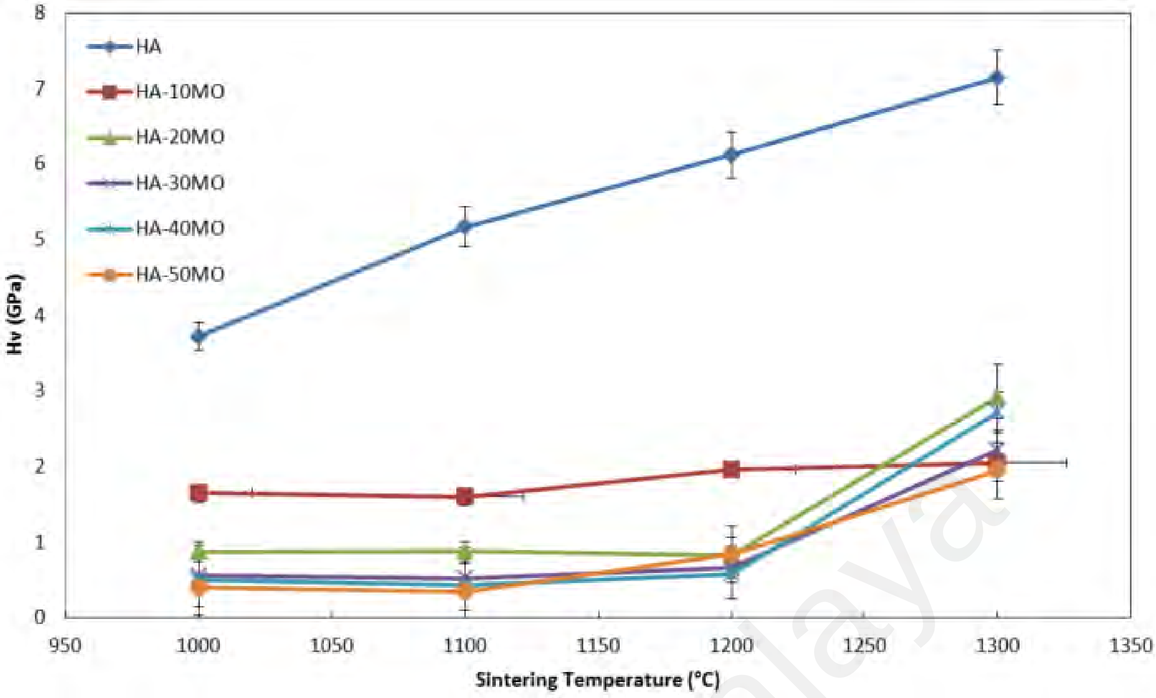

Figure 4.17: Vickers hardness variation with MO addition as a function of sintering temperature.

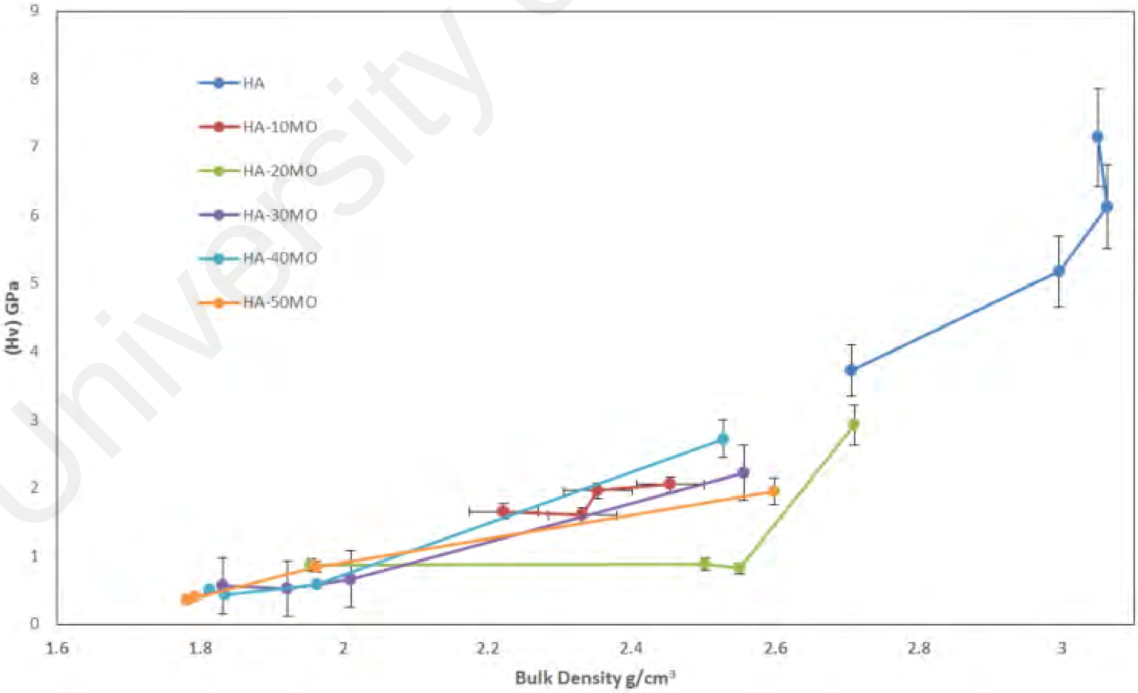

Figure 4.18: Vickers hardness variation with MO addition as a function of bulk density.

4.3.6 Fracture Toughness

The fracture toughness (K_{Ic}) of the sintered samples were attained via indentation method and are summarized in Table 4.2. In general, the monolithic HA sintered samples displayed a poor fracture toughness of 0.55 to 0.99 MPam$^{1/2}$ in comparison to magnesium orthosilicate (1.6 – 3.61 MPam$^{1/2}$) (Kharaziha & Fathi, 2009; Sara et al., 2012; Muralithran & Ramesh, 2000) when sintered from 1000°C to 1300°C. From this study, it was observed that the use of magnesium orthosilicate as reinforcement has effectively improved the fracture toughness of monolithic HA. The trend of improvement can be observed in Figure 4.19, where the HA-MO composites (10wt. % - 20wt. %) attained higher fracture toughness at any sintering temperatures compared to monolithic HA sintered samples. The monolithic HA exhibited toughness value of 0.5±0.1 MPam$^{1/2}$ when sintered at 1000°C and attained maximum of 0.9±0.1 MPam$^{1/2}$ when sintered at 1300°C which is still in the low side. The incorporation of higher amount of magnesium orthosilicate into the HA matrix seems to bring improvement in fracture toughness.

Table 4.2: Fracture toughness of HA and HA-MO composites sintered at different temperature.

	HA (MPam$^{1/2}$)	HA-10MO (MPam$^{1/2}$)	HA-20MO (MPam$^{1/2}$)	HA-30MO (MPam$^{1/2}$)	HA-40MO (MPam$^{1/2}$)	HA-50MO (MPam$^{1/2}$)
1000°C	0.55	0.99	1.01	0.72	0.56	0.47
1100°C	0.79	1.02	1.02	0.69	0.5	0.43
1200°C	0.88	1.45	0.96	0.82	0.63	0.89
1300°C	0.98	2.41	2.5	2.03	1.99	1.55

In particular, the addition of 10-20wt. % MO exhibited a much higher toughness than the monolithic HA when sintered at 1200°C and above. The HA-10MO sample exhibited toughness of greater than 1.0 MPam$^{1/2}$ when sintered at 1100°C and attained a maximum of 2.4±0.1 MPam$^{1/2}$ when sintered at 1300°C. The highest fracture toughness of 2.5±0.1 MPam$^{1/2}$ was measured at 1300°C for HA composite containing 20wt. % MO. The HA-30MO, HA-40MO and HA-50MO only exhibited toughness in the range of ~1.5 to ~2.0 MPam$^{1/2}$ when sintered at 1300˚C as anything below exhibited low fracture toughness value. The toughness values were in the range of ~0.5 to ~0.8 MPam$^{1/2}$. This could be due to the grain boundary that was not properly formed at low sintering temperatures.

On the other hand, the improvement in the fracture toughness of HA-10MO and HA-20MO can be associated with the pores and presence of TCP in the composite matrix that could have interact with the propagating crack through a stress absorption mechanism, although the presence of such a secondary phase has been reported to be generally detrimental to the properties of HA (Veljovic et al., 2011). Figure 4.20 indicated that the fracture toughness of the HA-MO composites was not governed by bulk density. As discussed earlier in the attribute that help improved the stiffness of the composites was due to grain size, and presence of the pores whereby the pores provided the mechanical interlock which lead to the firmer fixation of the material, also contributed to the improvement of the composites' toughness. The fracture toughness values for most monolithic HA reported in the literature varied at 0.6-1 MPam$^{1/2}$ (Ramesh et al., 2013; Monika, 2015; Ramesh et al., 2012) and HA doped with different additives such zirconia (Li et al., 1993); Kim et al., 2003), titania (Manjubala and Kumar, 2000), and alumina (Champion et al., 1996) only attained a fracture toughness in the range of 1.0 to 1.4 MPam$^{1/2}$.

The indentation fracture toughness of HA-MO composites obtained in this study was appreciably higher than those reported in many studies on dense HA ceramics. This finding is encouraging because it creates opportunities for these HA composites to be used for biomedical load-bearing implants.

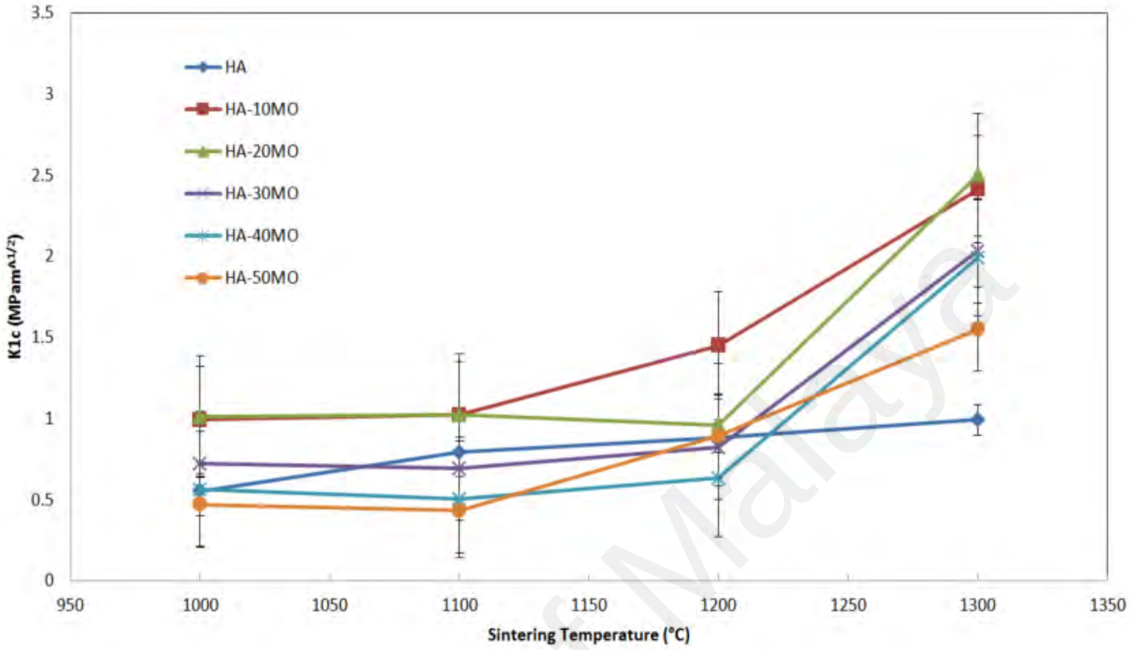

Figure 4.19: Fracture toughness of sintered samples as a function of sintering temperature and MO addition.

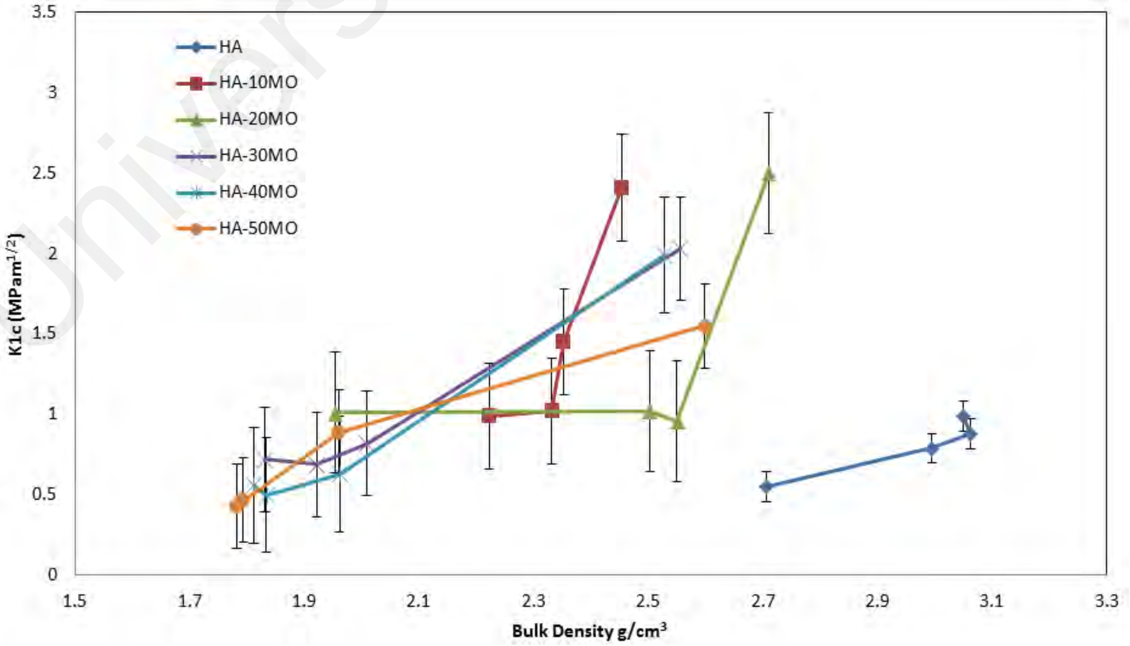

Figure 4.20: Fracture toughness variation with MO addition as a function of bulk density.

4.3.7 Microstructure Evaluation

Scanning electron micrographs (SEM) of HA, and HA-MO composites (10wt. % MO, 20wt. % MO, 30wt. % MO, 40wt. % MO, 50wt. % MO) sintered at 1000°C to 1300°C are shown in Figure 4.21 to 4.24. The ramification of magnesium orthosilicate on the grain size and microstructure of HA-MO composites can be observed in the SEM micrographs.

For the monolithic HA sintered samples, grain growth were observed to have taken place when the temperature of the sintering increased. This was due to the improvement in the homogeneity of the HA powder with increasing sintering temperature. The grain growth of monolithic HA in Figure 4.21 (a) was not obvious when sintered at 1000°C. As the temperature increases, the grain growth and grain boundary became more visible. At 1200°C, the grain growth and grain boundary became visible in the sintered monolithic HA sample as shown in Figure 4.23 (a). It was also observed that at higher sintering temperature, the porosity reduces as compared to those sintered at 1100°C and below, which corresponds to the formation of solid bridges between grains. The HA grains was observed to have grown rapidly, roughly ten times from an average of 0.55µm at 1200°C to approximately 5.5µm at 1300°C as depicted in Figure 4.23 (a) and Figure 4.24 (a). The monolithic HA exhibited a bimodal distribution of grains.

The micrographs of the HA-MO composites in Figure 4.21 (b-f) – Figure 4.24 (b-f) (10wt. % MO, 20wt. % MO, 30wt. % MO, 40wt. % MO and 50wt. % MO) were also observed upon sintering (1000°C - 1300°C). For HA-MO composites sintered at below 1200°C tend to display large amount of pores and well defined grains could not be observed. The HA-MO composites sintered at 1000˚C and 1100˚C as shown in Figure 4.21 (b-f) and Figure 4.22 (b-f) indicated that the fusion state is still incomplete, hence no clear grain boundaries were observed. This is partly due to the inability of MO to consolidate and densify when sintered at low temperature (Fathi & Kharaziha, 2008). The MO requires a higher amount of activation energy and thermal energy for grain growth to takes place in the HA-MO composite. Activation energy is the minimum energy needed to overcome the energy barrier of the atoms present in the lattice. In Figure 4.23 (b-f), the micrographs of the HA-MO composites sintered at 1200˚C start to display more grain formation and visible grain boundary especially from HA-50MO.

On the other hand, the composite tends to display lesser porosity in the samples that contain higher amount of MO. However, the addition of MO is found to promote the decomposition of HA as indicated in the XRD results. Therefore, the decomposition will liberate the hydroxyl in the HA matrix which increases the pore formation. As a result, the HA-MO exhibited higher amount of porosity than monolithic HA. These observations corresponded well to the shrinkage and bulk density of the sintered composites discussed earlier.

Sintering at 1300°C resulted in the formation of a denser microstructure, with well-formed grains being visible particularly for all the HA-MO composites. The average grain sizes of the composites were much smaller than 0.55 µm. The beneficial effect of magnesium orthosilicate in suppressing the grain growth of HA was revealed. The higher fracture toughness exhibited by the composites could be attributed to the fine grain size of the sintered body. However, with the existence of the molten phase which consists of HA, MO and whitlockite upon sintering, no proper boundary was able to form among the grains thus leaving some pores formation as observed in Figure 4.24 (b-f). This finding could be the factor contributing to the low mechanical properties of the HA-MO composites such as shrinkage, bulk density, and hardness due to the complexity of the molten phase as observed in the micrographs but the pores that exist had helped improved the stiffness and toughness of the HA-MO composites thru the mechanical interlock mechanism as discussed earlier. In spite of the fact that a fully dense HA-MO composite was not achieved, an advantageous ceramic composite body that has improved fracture toughness and has potential for load-bearing clinical implant has been produced. Furthermore, as reported by others that bone tissue grows well into the pores and thus increasing the strength of the implant making this HA-MO composite as the viable bioceramics.

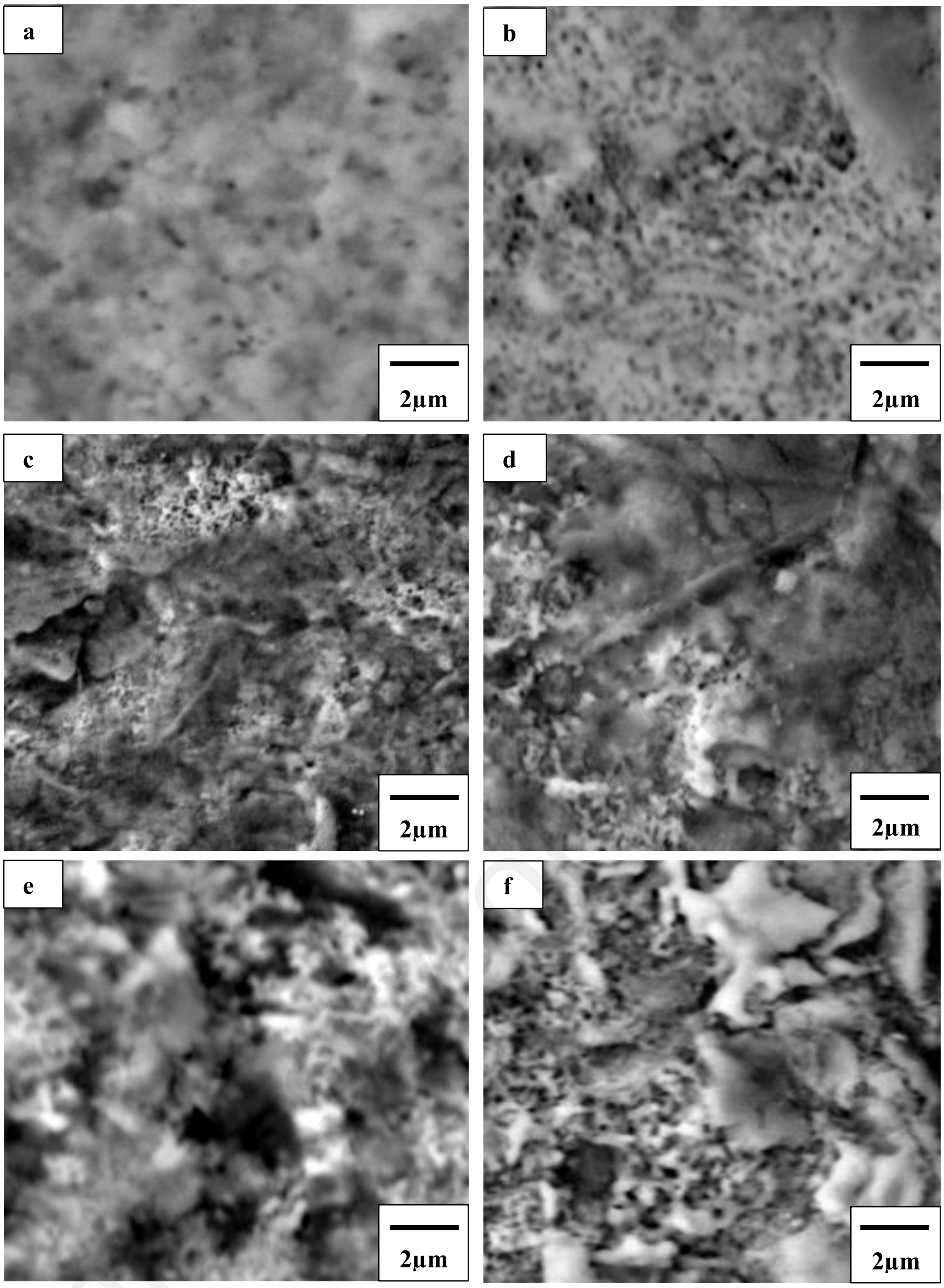

Figure 4.21: SEM images of samples sintered at 1000°C. (a) HA, (b) HA-10MO, (c) HA-20MO, (d) HA-30MO, (e) HA-40MO, (f) HA-50MO.

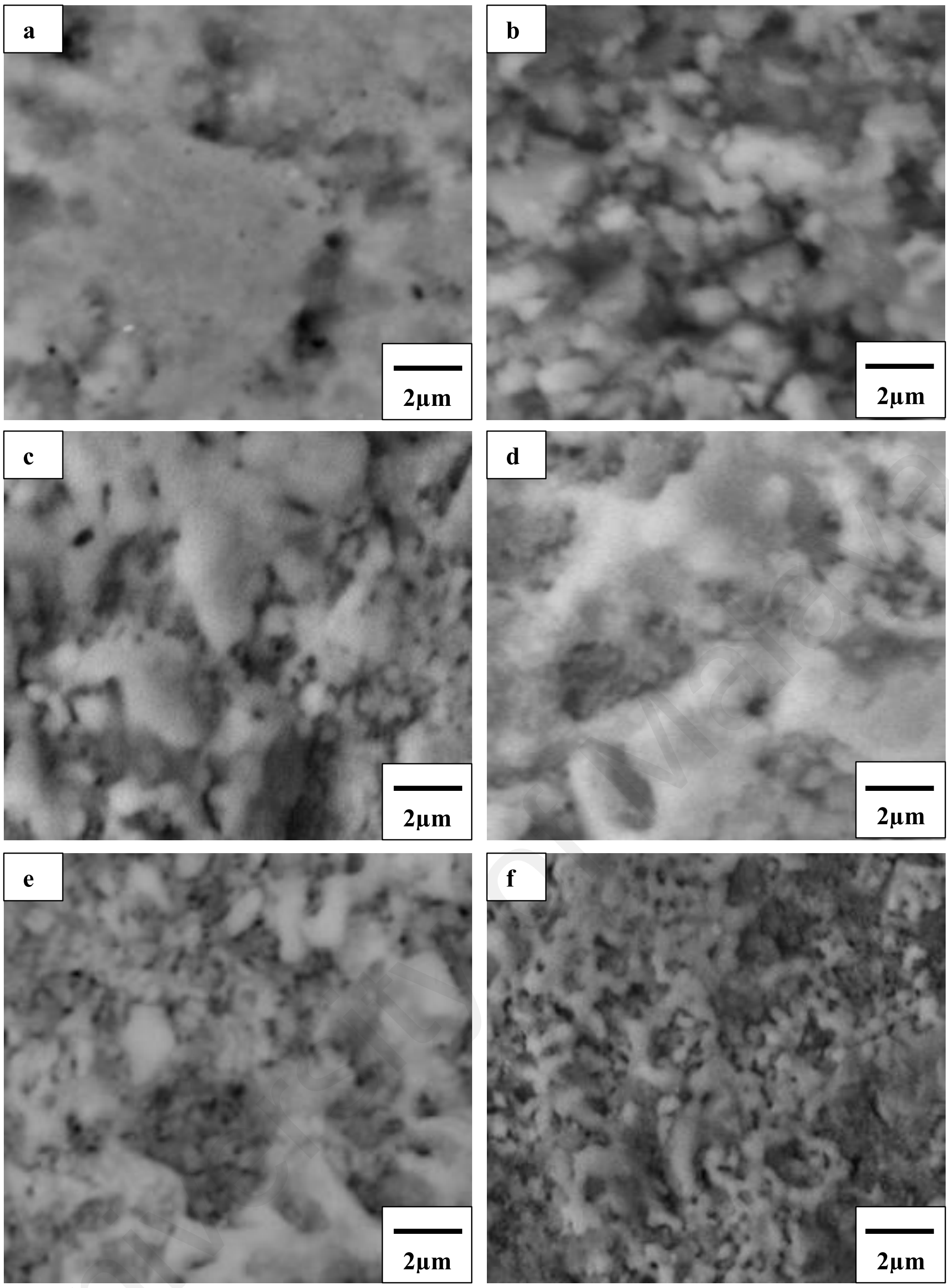

Figure 4.22: SEM images of samples sintered at 1100°C. (a) HA, (b) HA-10MO, (c) HA-20MO, (d) HA-30MO, (e) HA-40MO, (f) HA-50MO.

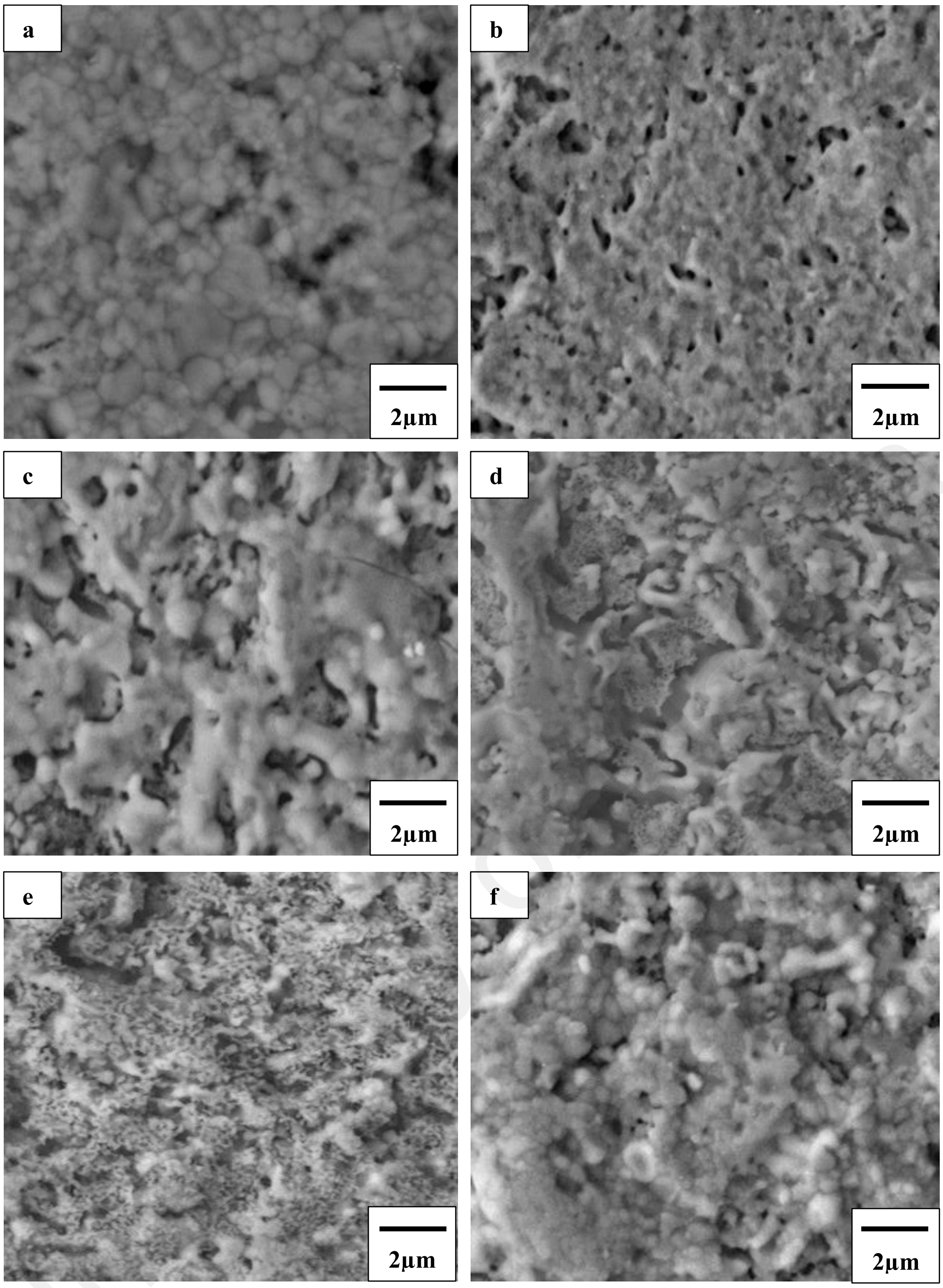

Figure 4.23: SEM images of samples sintered at 1200°C. (a) HA, (b) HA-10MO, (c) HA-20MO, (d) HA-30MO, (e) HA-40MO, (f) HA-50MO.

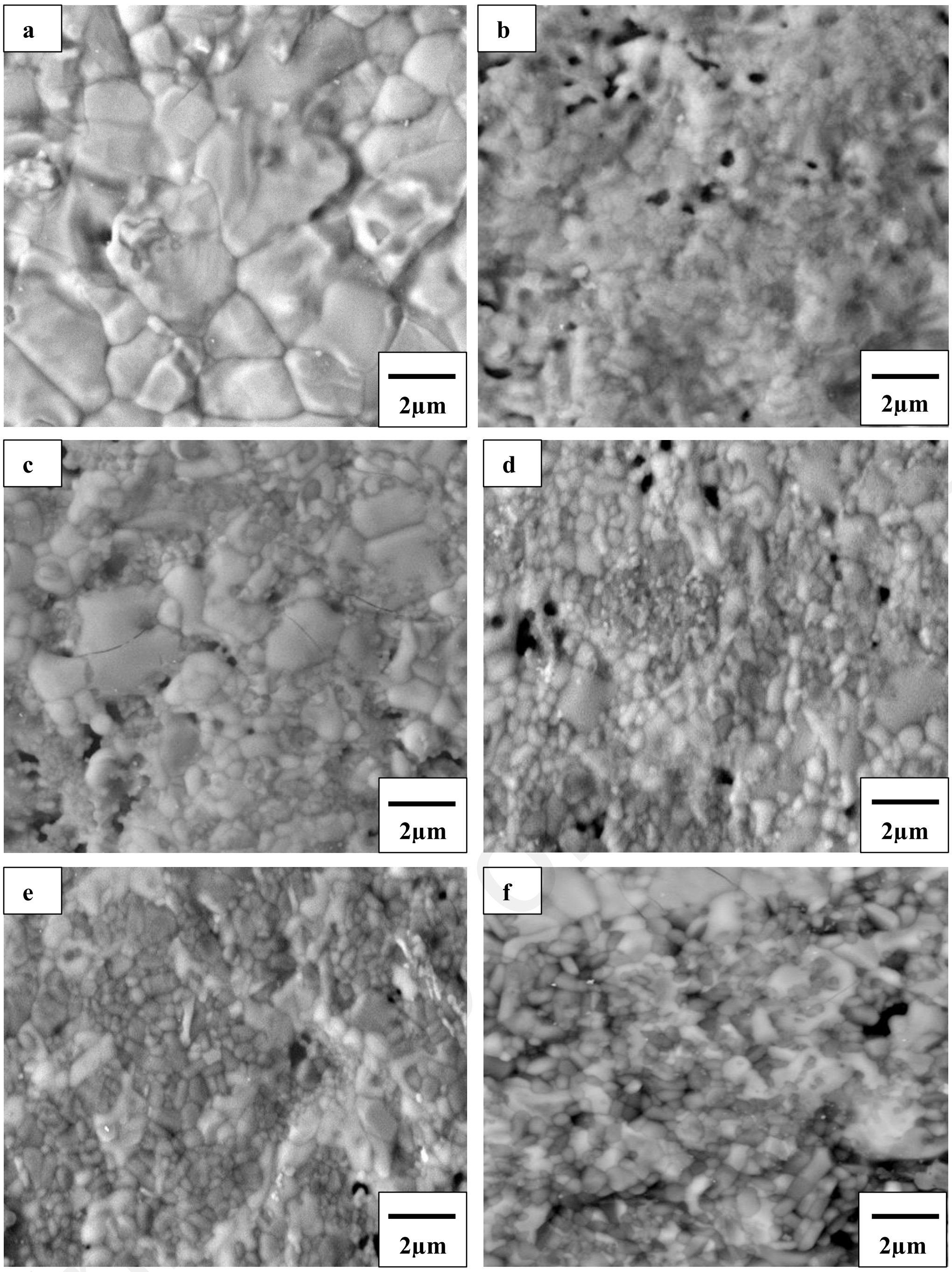

Figure 4.24: SEM images of samples sintered at 1300°C. (a) HA, (b) HA-10MO, (c) HA-20MO, (d) HA-30MO, (e) HA-40MO, (f) HA-50MO.

4.4 Toughening Effect of MO

The enormous improvement in fracture toughness in HA-MO composites can be viewed in different perspectives. The decomposition of HA to whitlockite or better known as β-TCP was being observed throughout the sintering range studied has contributed to the high toughness of the HA-MO composites which also considered as new knowledge in the bioceramics field. Furthermore, evidence from SEM analysis for monolithic HA and HA-20MO sintered at 1300˚C as shown in Figure 4.25 indicated that the bimodal grains of HA-20MO were the result from the three phases formed (HA, MO, whitlockite) distributed quite evenly which also consist of smaller grains as observed compared to monolithic HA when sintered at the same temperature.

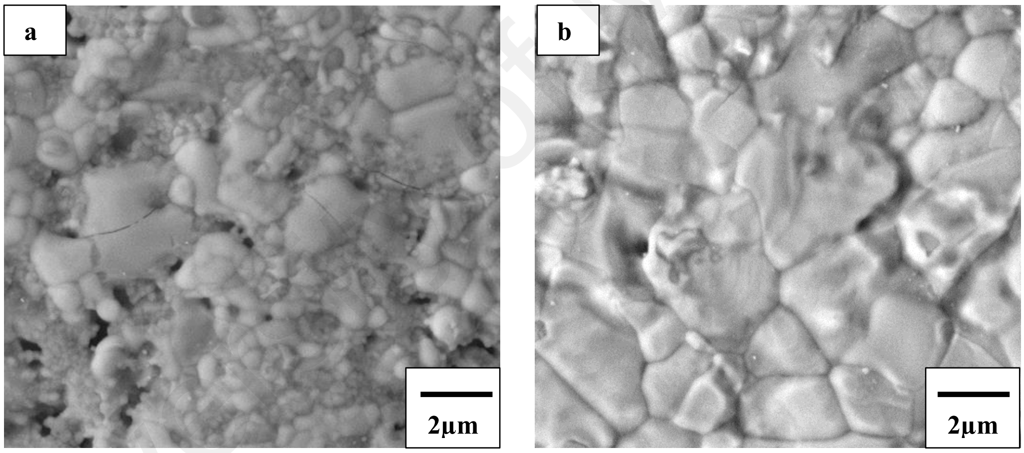

Figure 4.25: SEM images of samples sintered at 1300°C. (a) HA-20MO, (b) HA

As shown in Figure 4.13, the bulk density of sintered HA-20MO was lower than HA when sintered at 1300˚C. However, the latter exhibited higher fracture toughness as depicted in Figure 4.19. Usually, grain size is believed to be the dominant factor controlling the high fracture toughness of the composites. According to Hall-Petch equation, $\sigma_f = \sigma_o + kd^{-1/2}$, where σ_f is the fracture strength, d is the grain size, k and σ_o are constants, the strength decreases with increasing grain size. From fracture mechanics point of view, the fracture toughness of the ceramic could be correlated with its fracture strength. Thus, the present results indicated that MO plays an important role in suppressing grain growth and this will lead to higher fracture strength and hence higher fracture toughness.

The incorporation of MO into HA was observed to be beneficial as the effect of MO in suppressing the grain coarsening of HA was evident when the material was sintered at higher temperature as typically shown in Figure 4.26. As shown in Figure 4.26 (a), the average grain size measured for monolithic HA is about 5.5 µm when sintered at 1300˚C. The grain size decreased to less than 5.5µm with the addition of 10MO as shown in Figure 4.26 (b) and further down to less than 0.55 µm with the addition of 20MO as shown in Figure 4.26 (c). Figure 4.6 (c) indicated the presence of bimodal grain size from the three phases formed upon sintered (HA, MO, whitlockite).

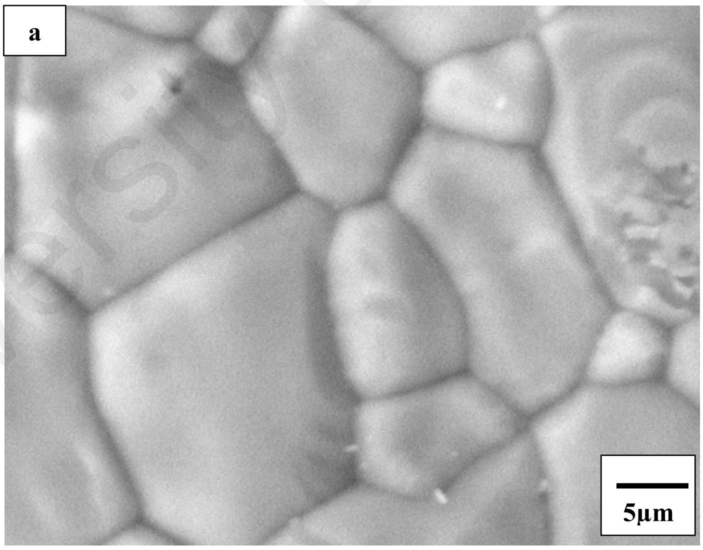

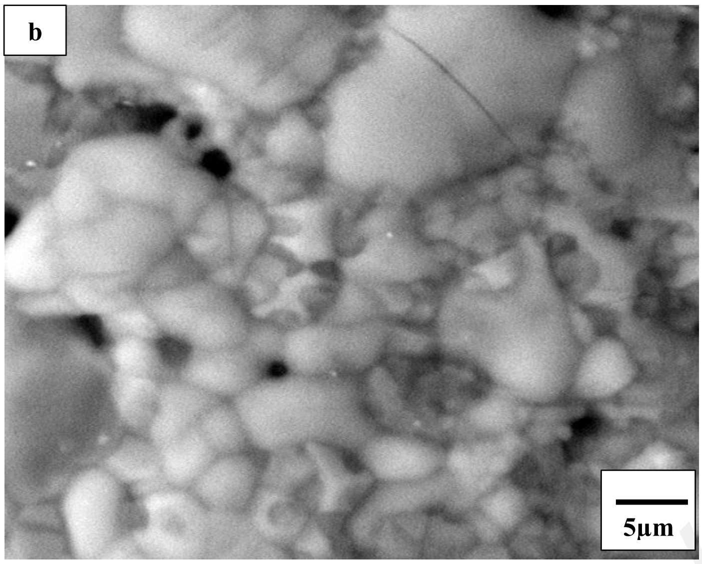

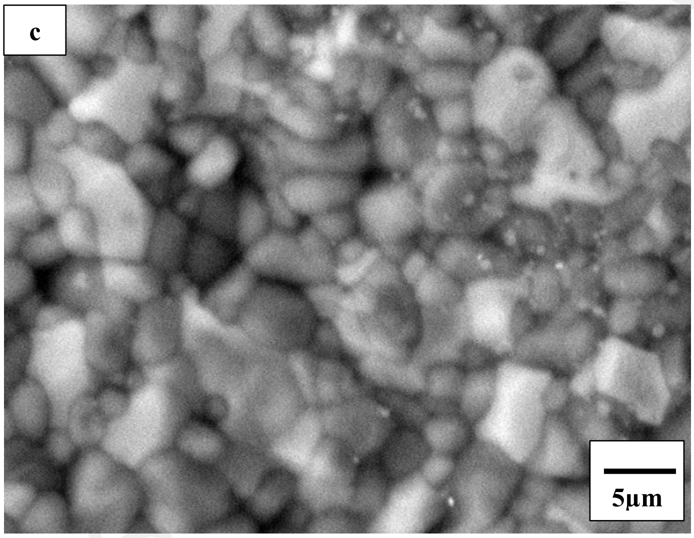

Figure 4.26: SEM images of (a) HA, (b) HA-10MO, (c) HA-20MO, sintered at 1300˚C.

A polished HA-20MO with the typical Vickers indent is shown in Figure 4.27. The micrograph shown in Figure 4.27 (b) displayed the brittle nature of the material evidently as the cracks propagating form the edge of the indent. When viewed under higher magnifications, the cracks were observed to be intergranular fracture as the cracks propagate in a “zig-zag” path rather than straight line.

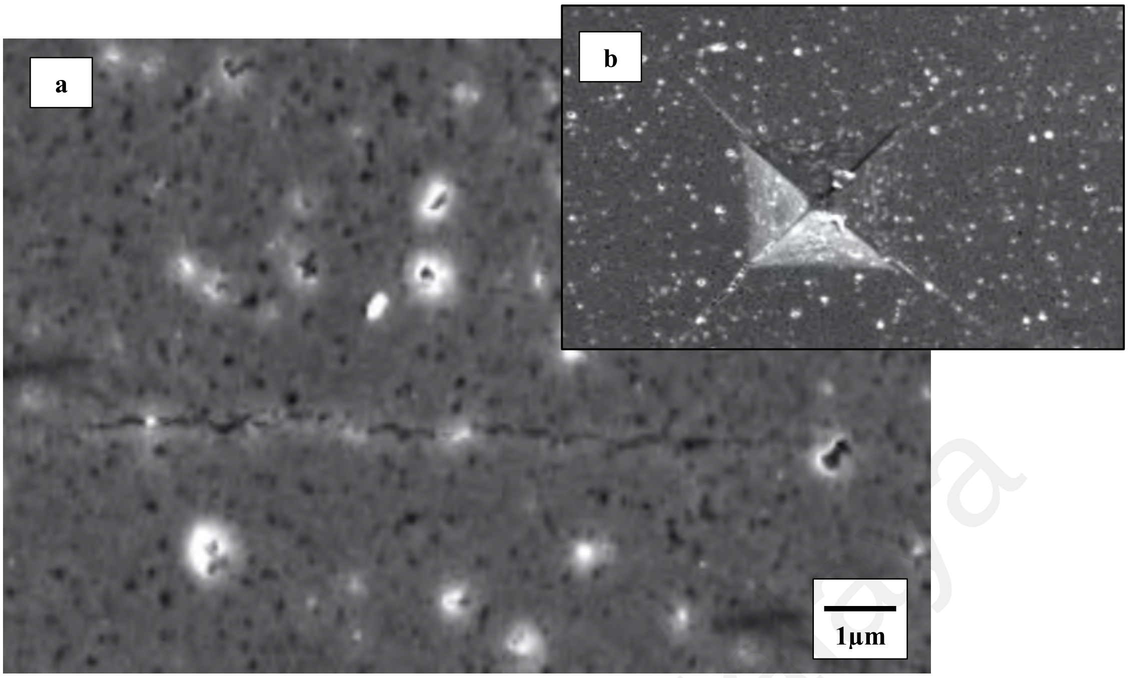

Figure 4.27: (a) Propagating crack from the indent (b) Diamond shaped Vickers indentation accompanied with side cracks.

In contrast, the monolithic HA exhibited typical transgranular fracture, suggesting the grain boundary was more resistant than the grain interior as shown in Figure 4.28. Therefore, it can be suggested that with the introduction of MO into HA matrix, the grain boundaries are weakened and there is a change in fracture mode from transgranular to intergranular fracture, leading to an improvement in the fracture toughness of the HA-MO composites.

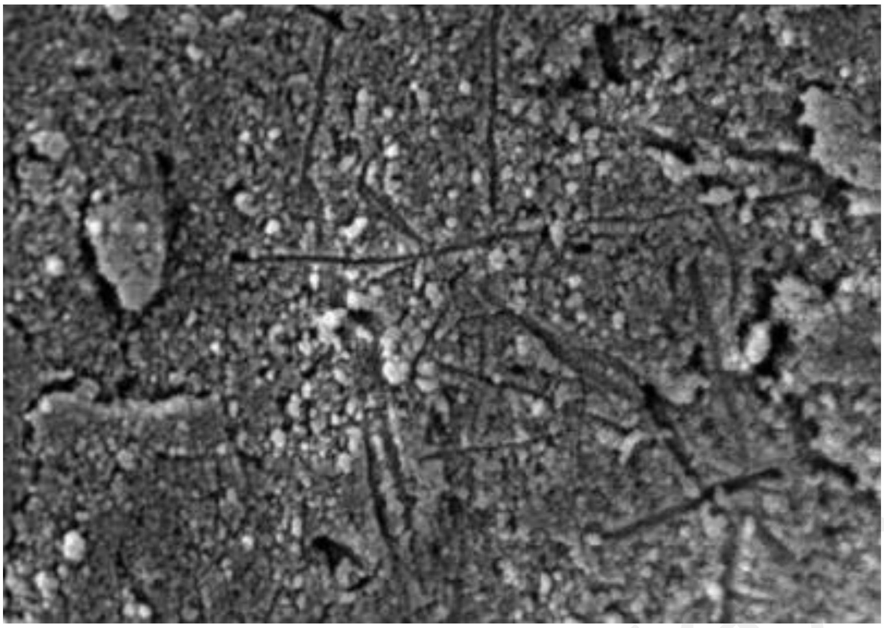

Figure 4.28: SEM image of fracture surface of monolithic HA.

The observation of highest fracture toughness of 1.45 MPam$^{1/2}$ for HA-10MO when sintered at 1200˚C as compared to 0.88 MPam$^{1/2}$ for monolithic HA has prompted further work to investigate the effect by increasing the temperature to 1300˚C. As a result, the sintering behaviour of HA with 20MO, 30MO, 40MO and 50MO sintered at 1300˚C were studied.

The phase analysis of all the MO addition samples sintered at 1300˚C is shown in Figure 4.29. It was found that the introduction of MO content did cause the secondary phase to occur. Nevertheless, the MO peak that corresponded to JCPDS card No. 34-0189 was detected in these samples with the increased in intensity when more MO was added into HA matrix. From the point of view of clinical applications as implant material, the presence of Mg ions could be beneficial as a number of studies have shown that there was an increased in interfacial strength for implant with HA surfaces enriched with magnesium (Kuwahara et al., 2001; Staiger et al., 2006).

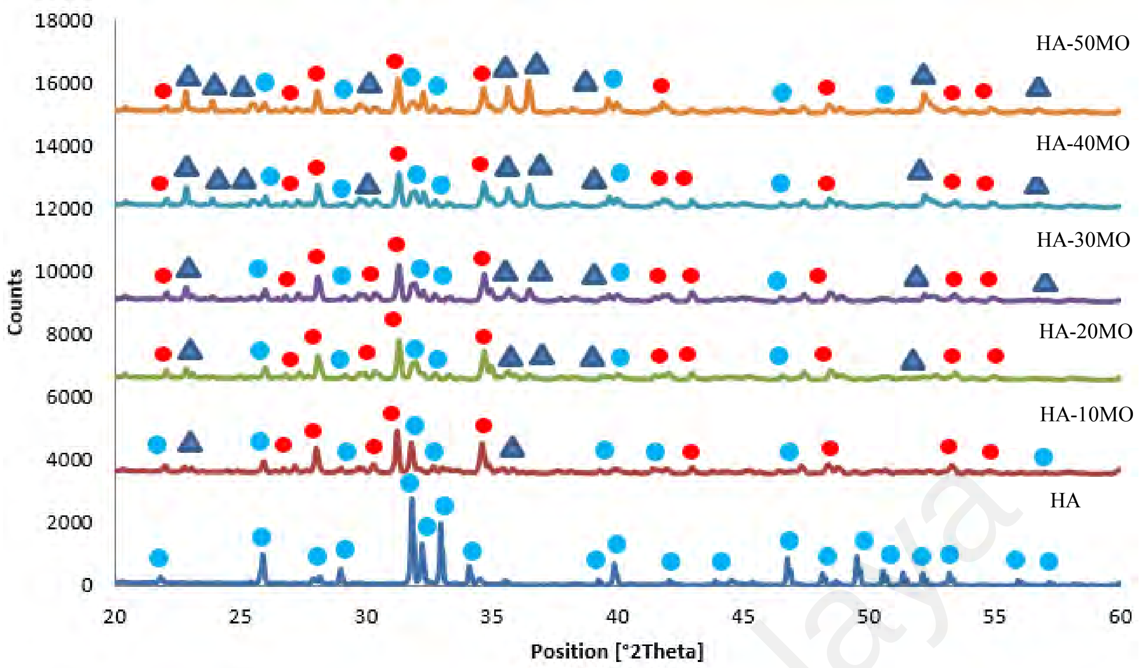

Figure 4.29: XRD patterns of HA-MO samples sintered at 1300°C. *For keys*: 🔵 = HA, 🔴 = whitlockite, ▲ = magnesium orthosilicate.

The shrinkage, bulk density, Young's modulus, Vickers hardness and fracture toughness of the composites with various MO concentrations displayed some increasing and decreasing trend of mechanical properties as shown in Figure 4.30 to Figure 4.34 respectively. The shrinkage and bulk density of HA-MO composites was generally lower than monolithic HA as shown in Figure 4.30 and Figure 4.31. The HA-MO composite in Figure 4.30 was displaying an increase trend initially from 10MO to 20MO composition and peaked at 17.7% before the shrinkage began to decrease as the MO content increased. Similarly, the bulk density as shown in Figure 4.31 of the HA-MO composite initially displayed an increase in bulk density in the sample from 10MO to 20MO before decreasing as the MO composition increased. These results could be due to the lower packing density from the hard agglomerates of MO and the complexity of the three phases (HA, MO, whitockite) that exist accompanied with porosities as explained earlier. The bimodal grains from the three phases formed in the HA-20MO were observed to be more evenly distributed compared to the composite with 50MO when sintered at 1300˚C, thus resulted to lesser porosities as shown in Figure 4.32. The pores are indicated by the red circles as shown in Figure 4.32 (b). The microstructure observed from the SEM images can be regarded as some unusual bimodal grain distribution from the 3 phases of the HA-MO composite (HA, MO, whitlockite).

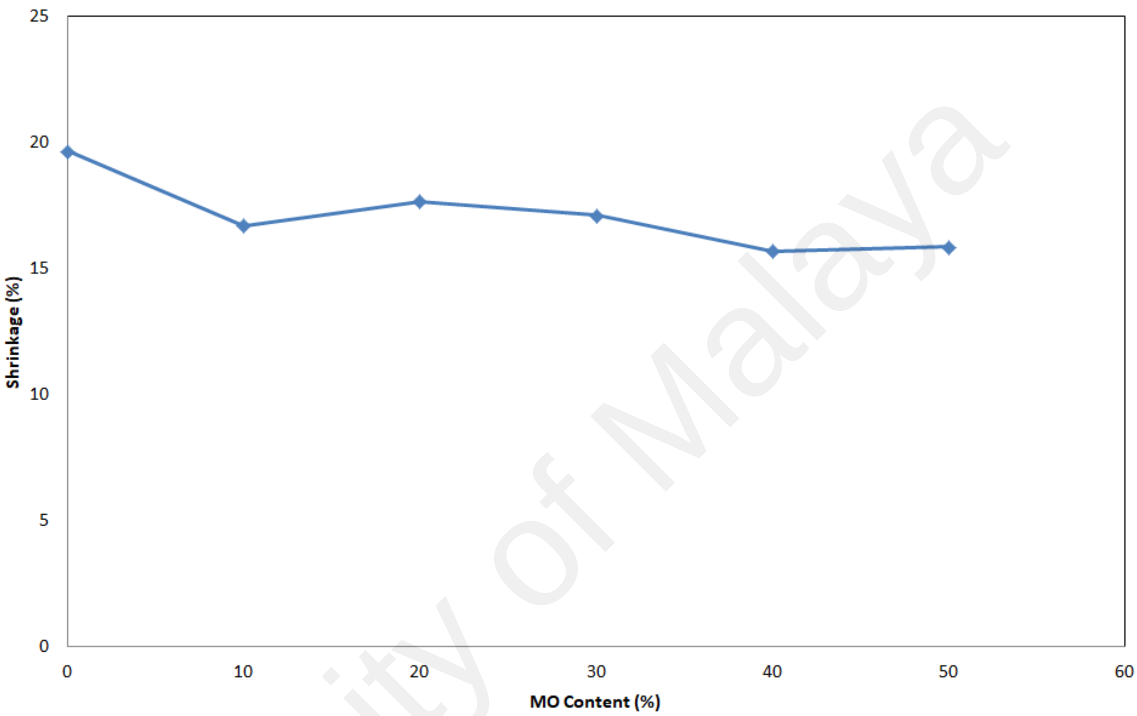

Figure 4.30: The effect of MO on the relative density of HA when sintered at 1300˚C.

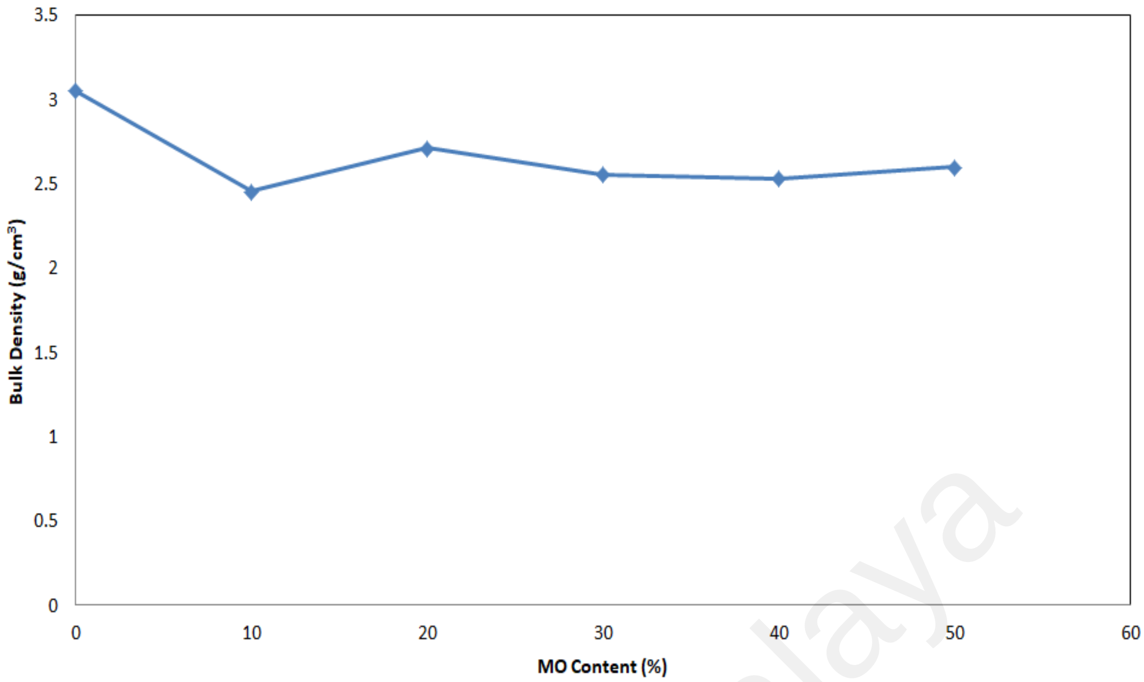

Figure 4.31: The effect of MO on the bulk density of HA when sintered at 1300˚C.

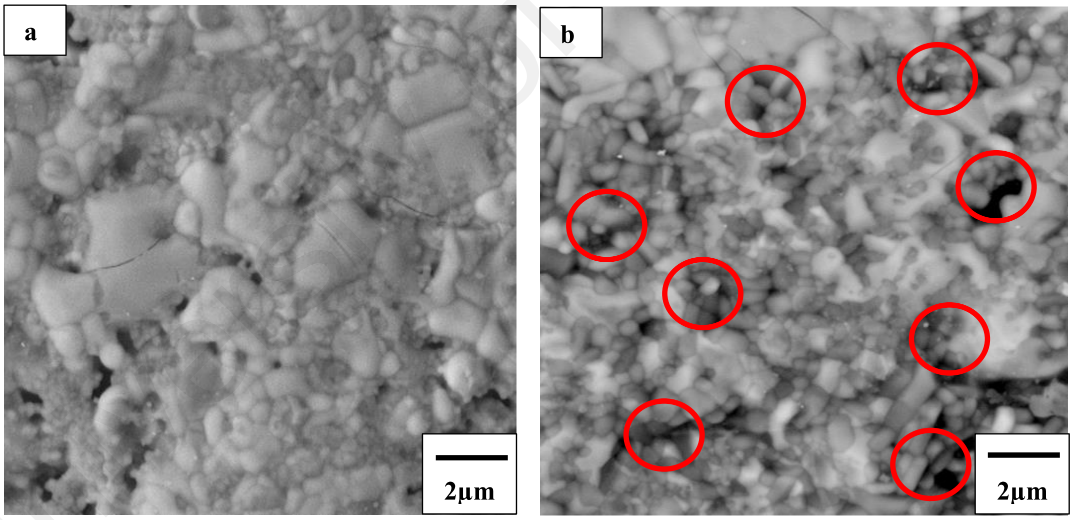

Figure 4.32: SEM images of samples sintered at 1300°C. (a) HA-20MO, (b) HA-50MO.

Although the bulk density usually influences the mechanical properties, the Young's modulus of the HA-MO composite displayed an increasing trend in Figure 4.33 compared to the decreasing trend of bulk density as the amount of MO increased. The HA-50MO displayed the optimum Young's modulus at 118 GPa. The Young's modulus of the remaining other HA-MO composites were still higher than those for natural bone

(*E* = 10-22 GPa) and enamel (*E* = 40-84 GPa) (Hench, 1991; LeGeros, 1993). It is believed that the composite could have caused more dislocation in the bimodal grains distribution of the material leading to firmer fixation. The mechanical interlock from the pores which involved the arrangement of the atoms of the three phases (HA, MO, whitlockite) could have inhibited the crack propagation by redistributing the stresses in the regions adjacent to the crack tips thus improving the stiffness of the HA-MO composites.

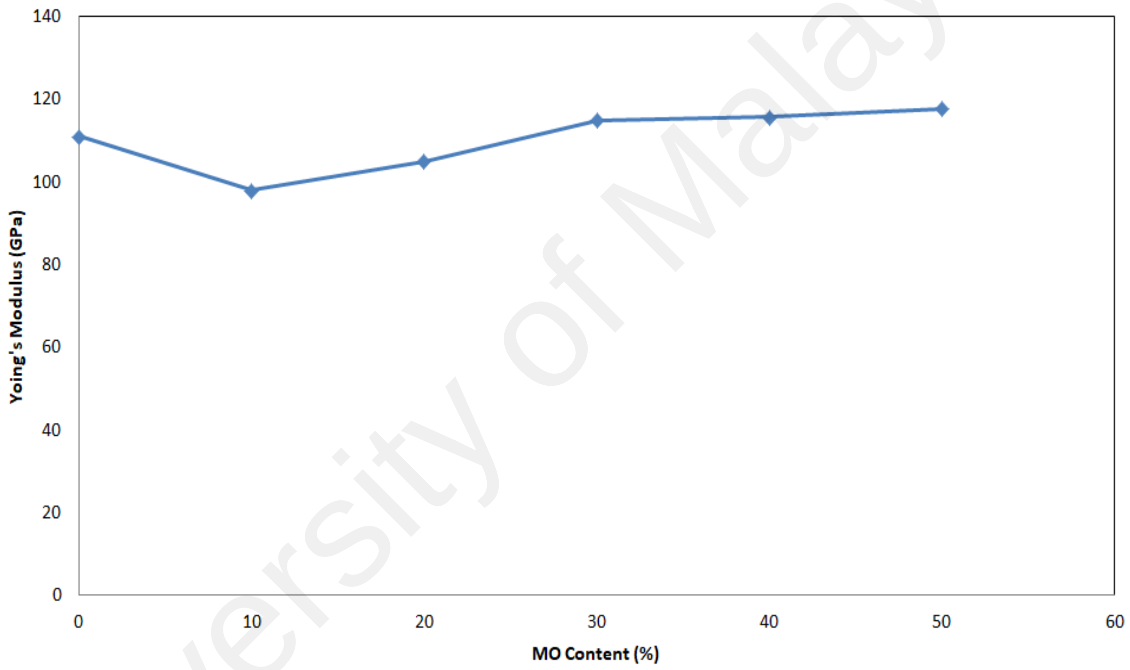

Figure 4.33: The effect of MO on the Young's modulus of HA when sintered at 1300˚C.

However, Figure 4.34 displayed an inconsistent decreasing trend in hardness for the HA-MO composites while monolithic HA exhibited highness hardness of 7.1 ± 0.2 GPa when sintered at 1300˚C. The HA-MO composites were generally much lower than the monolithic value but still above the cortical bone lower limit (0.2 GPa). This finding was expected as the bulk density also exhibited decreasing trend when MO composition increased. The inconsistency of the hardness value in the composite could be due to the bimodal grain size distributed accompanied by various pores' size in the material. The molten phase that exist from HA, MO and whitlockite upon sintered cannot form proper grain boundary hence leading to random dislocation in the crystal structure leading to the inconsistency of the hardness findings as well. Here, the addition of MO did not bring beneficial effect to the hardness.

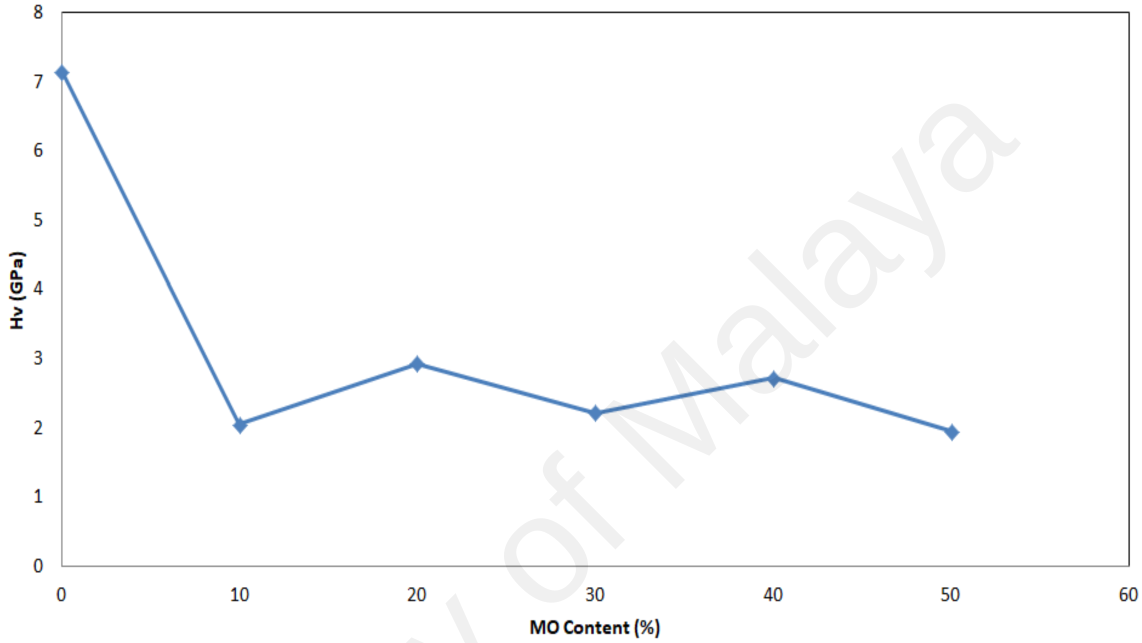

Figure 4.34: The effect of MO on the hardness of HA when sintered at 1300˚C.

The effect of adding MO into HA on the fracture toughness of sintered samples is shown in Figure 4.35. It could be observed that the toughness of 0.9±0.1 MPam$^{1/2}$ for monolithic HA has been increased to 2.5±0.1 MPam$^{1/2}$ when incorporated with 20MO when sintered at 1300°C. Any further addition of MO resulted to decrease in fracture toughness. This increased in fracture toughness could be attributed to the entire phase formation mechanism which took place in this HA-MO composite which resulted to smaller bimodal grain which been distributed evenly to form bridges across crack faces acting as stress absorption mechanism which help improved the toughness of the material.

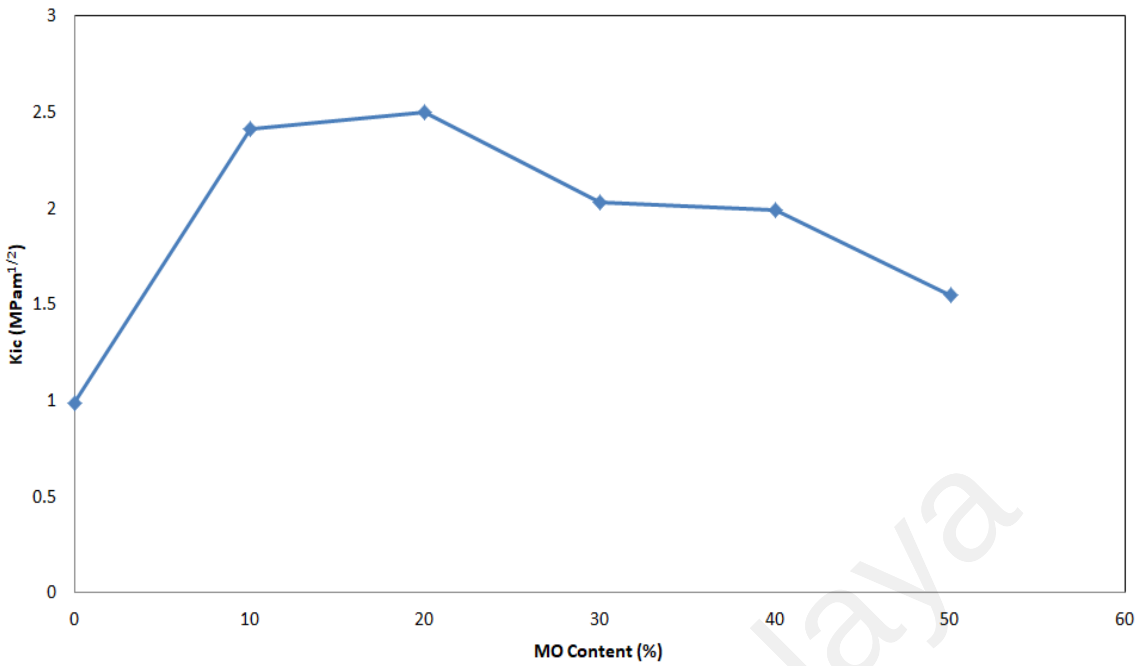

Figure 4.35: The effect of MO on the fracture toughness of HA when sintered at 1300˚C.

It has been concluded that the HA-MO composites show a promising direction in improvement of fracture toughness which will definitely contribute to the new knowledge of HA composite as few work has been done incorporating MO into HA.

CHAPTER 5 - CONCLUSIONS & FURTHER WORK

5.1 Conclusions

In the present work, the densification behavior and properties of hydroxyapatite-magnesium orthosilicate (HA-MO) composite were investigated. The amount of magnesium orthosilicate in the green body was varied from 10wt. %, 20wt. %, 30wt. %, 40wt. % and 50wt. % and pressureless sintered from 1000°C to 1300°C for 2 hours. The effects of incorporating MO with HA have been compared with the pure HA via phase analysis, bulk density, linear shrinkage Vickers hardness, Young's modulus, fracture toughness and microstructural investigation. The results obtained can be concluded that:

1. The HA powder synthesized by the wet chemical precipitation method is in good agreement with the JCPDS card. There were no other phases found in the powder.

   However, the peaks of the XRD trace were generally broad, which indicates that the powder has low crystallinity. Large and small particles were observed from the micrograph which formed the agglomerates.

2. The MO powder which was produced via combination of ultrasonification and mechanical ball milling method is in good agreement with the JCPDS card. No secondary phase was observed from the XRD result. The micrograph of MO displayed flake like morphology and also lamellar shape forming hard agglomerates.

3. The effect of incoporating magnesium orthosilicate (MO) to form the composites regardless of various amount of MO (10wt. % to 50wt. %) and sintering temperatures resulted to the decomposition of the HA phase to

whitlockite phase (also known as β-TCP). The whitlockite phase becomes more prominent when higher amount of MO was incorporated. The decomposition of the composites was due to chemical reaction with MO during sintering. The MO which contains magnesium inhibits apatite crystallization in solution which can act as a stabilizer for the whitlockite phase which in return promotes the decomposition of HA. Similar observation was also reported by Emadi et al. (2010).

4. The HA-MO composites still exhibited higher amount of porosity than monolithic HA however the HA-MO composites tend to display lesser porosity in samples that contain higher amount of MO when sintered across the increasing temperatures (1000°C - 1300°C). Large amount of pores and not well defined grain size were observed in composites sintered at below 1200°C regardless of MO contents due to the inability of MO to consolidate and densify when sintered at low temperature. The average grain size of the composites were found to be smaller than 0.55µm.

5. The grain growth and grain boundary for HA were only visible when sintered at 1200°C. The grains were observed to have grown rapidly, about ten times from an average of 0.55µm at 1200°C to 5.5µm at 1300°C. A bimodal distribution of grains was displayed by the HA grains.

6. Generally, the monolithic HA sintered samples attained higher shrinkage across the sintering temperatures. A maximum shrinkage of 19.7% was attained from monolithic HA while HA-20MO attained at about 17.7% shrinkage when

sintered at 1300°C. The other HA-MO composites only attained shrinkage in the range of ~7% to ~15%.

7. The monolithic HA sintered samples exhibited higher bulk density than HA-MO composites regardless of the sintering temperature used. A maximum bulk density of above 3 g/cm^3 was attained by monolithic HA when sintered at 1300°C while the HA-20MO is the highest among the other composites to have achieved bulk density of 2.7 g/cm^3 at the same sintering temperature. The hard agglomerates of magnesium orthosilicate and decomposition of the HA phase could have led to the lower packing density in the green state.

8. For the Young's modulus study, the HA-50MO composite exhibited a higher Young's modulus than monolithic HA regardless of sintering temperature. A maximum Young's modulus of 118 GPa was attained from the HA-50MO composite when sintered at 1300°C while the monolithic HA attained at about 111 GPa at the same sintering temperature. The increase in Young's modulus as the temperatures increase reflect the reduce in porosity.

9. The hardness trend attained displays the similar trend found in the bulk density results where the monolithic HA displays higher hardness value than the composites. The monolithic HA hardness attained an optimum value of 7.1± 0.2 GPa when sintered at 1300°C. Conversely, the highest hardness attained by the composite containing 20wt. % MO was 2.9± 0.1 GPa when sintered at 1300°C. The hardness values of HA-MO composites (10wt. % - 50wt. %) sintered at above 1100°C are still higher than cortical bone lower limit which is about 0.2 GPa.

10. The use of magnesium orthosilicate has effectively improved the fracture toughness of monolithic HA. In general, monolithic HA displays fracture toughness in the range of 0.55 to 0.99 $MPa \cdot m^{1/2}$. The highest fracture toughness of 2.5 ± 0.1 $MPa \cdot m^{1/2}$ was attained from HA-20MO composite sintered at 1300°C. This improvement in fracture toughness can be associated with the presence of TCP in the composite matrix that could have interact with the propagating crack through a stress absorption mechanism, although the presence of such secondary phase is usually detrimental to the properties of HA. With the fracture toughness improvement, the composite will create opportunities to be used for biomedical load-bearing implants.

5.2 Further Work

Following are some suggestions for further work:

1. The use of other sintering methods such as microwave sintering and hot pressing to prepare the HA-MO composite could be explored and compared with the results obtained using pressureless sintering method.

2. A TEM study could be an avenue for further studies especially in elucidating the sintering mechanism of HA-MO composite.

3. The use of two step sintering method as a possible way to suppress grain growth of HA-MO composite in the final sintering stage. It would be interesting to investigate if the two step sintering method could aid the densification of the present composite.

4. An in vitro testing through the use of simulated body fluid (SBF) can be performed to evaluate the biocompatibility of the current HA-MO composite samples.

5. A more insightful study of the dihydroxylation phenomenon of the composite and the relation to XRD peak shifting of the present work could be obtained by carrying out Raman spectroscopy studies.

6. To use various ramp rate, 5°C/minute and 15°C/minute for sintering and also various holding time of 1 minute and 1 hour to observe the outcome on the HA-MO composites in terms of its mechanical properties.

REFERENCES

Adamopoulus, O. & Papadopoulus, T. (2007). Nanostructured bioceramics for maxillofacial applications. *Journal of Materials Science: Materials in Medicine*, *18*: 1587-1597.

Afshar, A., Ghorbani, M., Ehsani, N., Saeri, M. R. & Sorrell, C. C. (2003). Some important factors in the wet precipitation process of hydroxyapatite. *Materials and Design*, *24*: 197-202.

Agrawal, D. K. (1998b). Microwave processing of ceramics. *Current Opinion in Solid State & Materials Science*, *3*: 480-485.

Akira, O., Tetsuo, H., Hiroyuki, K., Naoki, K., Wenguang, G., Takeshi, K. & Naoto, E. (2004). Comparison of hydroxyapatite and beta tricalcium phosphate as bone substitutes after exicison of bone tumors. *Journal of Biomedical Materials Research*, *42*: 1411-1420.

Aizawa, M., Hanazawa, T., Itatani, K., Howell, F. S. & Kishioka, A. (1999). Characterisation of hydroxyapatite powders prepared by ultrasonic spray-pyrolysis technique. *Journal of Materials Sci*ence, *34*: 2865-2873.

Akao, M., Aoki, H. & Kato, K. (1981). Mechanical properties of sintered hydroxyapatite for prosthetic applications. *Journal of Material Science*, *16*: 809-812.

Almirall, A., Larrecq, G., Delgado, J. A., Martinez, S., Planell, J. A. & Ginebra, M. P. (2004). Fabrication of low temperature macroporous hydroxyapatite scaffolds by foaming and hydrolysis of an α-TCP paste. *Biomaterials*, *25*: 3671-3680.

Aminzare, M., Eskandari, A., Baroonian, M. H., Berenov, A., Hesabi, R., Taheri, M. & Sadrnezhaad, S. K. (2013). *Ceramics International*, *39*: 2197-2206.

An, G. H., Wang, H. J., Kim, B. H., Jeong, Y. G., & Choa, Y. H. (2007). Fabrication and characterisation of a hydroxyapatite nanopowder by ultrasonic spray pyrolysis with salt-assisted decomposition. *Materials Science and Engineering*, *44*: 821-824.

Aykul, A., Kutbay, I., Evis, Z. & Usta, M. (2013). Effect of YF_3 on the phase stability and sinterability of hydroxyapatite – Partially stabilized zirconia composites. *Ceramics International*, *39*: 7869-7877.

Bandyopadhyay, A., Bernard, S., Xue, W., Bose, S. (2006). Calcium phosphate-based resorbable ceramics: Influence of MgO, ZnO, and SiO_2 Dopants. *Journal of the American Ceramic Society*, *89*: 2675-2688.

Ben-Nissan, B., Miley, A. & Vago, R. (2004). Morphology of sol-gel derived nano coated coralline hydroxyapatite. *Biomaterials*, *25*: 4971-4975.

Bernache-Assollant, D., Ababou, A., Champion, E., & Heughebaert, M. (2003). Sintering of calcium phosphate hydroxyapatite $Ca_{10}(PO_4)_6(OH)_2$. Calcination and particle growth. *Journal of the European Ceramic Society*, *23* (2): 229-241.

Best, S. & Bonfield, W. (1994). Processing behavior of hydroxyapatite powders with contrasting morphology. *Journal of Materials Science: Materials in Medicine, 5*: 516-521.

Best, S. M., Porter, A. E., Thian, E. S. & Huang, J. (2008). Bioceramics: Past, present and for the future. *Journal of Materials Science: Materials in Med*icine, *5*: 516 – 521.

Bhaduri, S. & Bhaduri S. B. (1998). Recent developments in ceramic nanocomposites. *Journal of the Minerals, Metals, and Materials Society*, *50*: 44-51.

Bianco, A., Cacciotti, I., Lombardi, M., Montanaro, L. & Gusmano, G. (2007). Thermal stability and sintering behaviour of hydroxyapatite nanopowders. *Journal of Thermal Analysis and Calorimetry*, *88* (1): 237-243.

Bigi, A., Falini, G., Foresti, E., Ripamonti, A., Gazzano, M., & Roveri, N. (1993). Magnesium influence on hydroxyapatite crystallization. *Journal of Inorganic Biochemistry*, *49* (1): 69-78.

Binyamin, G., Shafi, B. M. & Carlos, M. M. (2006). Biomaterials: A primer for surgeons. *Seminar in Pediatric Surgery*, *15*: 276-283.

Bogdanoviciene, I., Beganskiene, A., Tonsuaadu, K., Glaser, J., Meyer, H. J. & Kareiva, A. (2006) Calcium hydroxyapatite, Ca¬10(PO4)6(OH)2 ceramics prepared by aqueous sol-gel processing. *Materials Research Bulletin*, *41*: 1754-1762.

Bogdanov, B. I., Pashev, P. S., Hristov, J. H. & Markovska, I. G. (2008). Bioactive fluorapatite-containing glass ceramics. *Ceramics International*, 35: 1651-1655.

Bohner, M. (2000). Calcium orthophosphates in medicine: from ceramics to calcium phosphate cements. *International Journal of the Care of the Injured*, *31*: S-D37-D47.

Boskey, A. L. & Coleman, R. (2010). Critical reviews in oral biology & medicine: Aging and Bone. *Journal of Dental Research, 89*(12):1333-1348.

Cacciotti, L. & Bianco, A. (2011). High thermally stable Mg-substituted tricalcium phosphate via precipitation. *Ceramics International*, *37*: 127-137.

Calafiori, A. R., Di Marco, G., Martino, G. & Marotta, M. (2007). Preparation and characterization of calcium phosphate biomaterials. *Journal of Materials Science: Materials in Medicine*, *18*: 2331 - 2338.

Carlisle, E. M. (1970). Silicone: a possible factor in bone calcification. *Science 167*: 279-280.

Carlisle, E. M. (1988). Silicon as a trace nutrient. *Science of The Total Environment*, *73*: 95-106.

Carolina, T., Chayuda, C., David, E. D. & George, V. F. (2016). Mechanical strength and damage tolerance of highly porous alumina ceramics produced from sintered particle stabilized foams. *Ceramics International*, *42*: 8478-8487.

Cao, N., Bai, Y., Ma, Q., Sui, J., Li, M. (2008). Biological behaviour of hydroxyapatite coatings on carbon/carbon composites produced by plasma spraying. *New Carbon Materials*, *23* (2): 144-148.

Cao, W. & Hench, L. L. (1996). Bioactive Materials. *Ceramics International*, *22*: 493-507.

Cengiz, B., Gokce, Y., Yildiz, N., Aktas, Z. & Calimli, A. (2008). Synthesis and characterization of hydroxyapatite nanoparticles. *Colloids and Surfaces A: Physicochemical and Engineering Aspects*, *322*: 29-33.

Chai, C. S. & Ben-Nissan, B. (1999). Bioactive nanocrystalline sol-gel hydroxyapatite coatings. *Journal of Materials Science: Materials in Medicine*, *10*: 465-469.

Chen, C. W., Oakes, C. S., Byrappa, K., Riman, R. E., Brown, K., TenHuisen, K. S. & Janas, V. F. (2004). Synthesis, characterization, and dispersion properties of hydroxyapatite prepared by mechanochemical-hydrothermal methods. *Journal of Materials Chem*istry A, *14*: 2425-2432.

Chen, Q. Z., Thompson, I. D. & Boccaccini, A. R. (2006). 45S5 Bioglass derived glass ceramic scaffolds for bone tissue engineering. *Biomaterials*, *27*: 2414-2425.

Chern, L., Liu, M. L., Chen, K. S. & Ju, C. P. (1993). Plasma-sprayed hydroxyapatite-bioactive glass coatings on Ti6A14V. *Ceramic Engineering and Science Proceedings*, *14*: 971-981.

Chiu, C., Hsu, H. C. & Tuan, W. H. (2007). Effect of zirconia addition on the microstructural eveloution of porous hydroxyapatite. *Ceramics International*, *33*: 715-718.

Chu, C., Xue, X., Zhu, J. & Yin, Z. (2004). Mechanical and biological properties of hydroxyapatite reinforced with 40 vol. % titanium particles for use as hard tissue replacement. *Journal of Materials Science: Materials in Medicine*, *15*: 665-670.

Colling, D.C. & Vasilos, T. (1995). Industrial materials: Polymers, ceramics and composites. Vol 2. *New Jersey: Prentice Hall, Inc*.

Dee, K. C., Puleo, D. A. & Bizios, R. (2003). Biomaterials: An introduction to tissue biomaterial interactions. *John Wiley & Sons, Inc.*: 13.

Dobradi, A., Bodogh, M. E., Kovacs, K. & Balczar, I. (2015). Structure and properties of bio-glass ceramics containing natural bones. *Ceramics International*, *41*: 4874-4881.

Donadel, K., Laranjeira, M. C. M., Goncalves, V. L., Favere, V. T., de Lima, J. C. & Prates, L. H. M. (2005). Hydroxyapatite produced by wet-chemical methods. *Journal of the American Ceramic Society*, *88* (8): 2230-2235.

Dorozhkin, S. V. (2007). Calcium orthophosphates. *Journal of Materials Science*, *42*: 1061-1095.

Dorozhkin, S. V. (2008). Calcium phosphate cements for biomedical application. *Journal of Material Science*, *43*: 3028-3057.

Dorozhkin, S. V. (2010). Bioceramics of calcium orthophosphates. *Biomaterials*, *31*: 1465-1485.

Drdlik, D., Slama, M., Hadraba, H. & Cihlar, J. (2015). Hydroxyapatite/zirconia microfiber composites with controlled microporosity and fracture properties prepared by electrophoretic deposition. *Ceramics International*, *41*: 11202-11212.

El Briak-BenAbdeslam, H., Ginebra, M. P., Vert, M. & Boudeville, P. (2008). Wet or dry mechanichemical synthesis of calcium phosphates? Influence of the water content on DCPC-CaO reaction kinetics. *Acta Biomaterialia*, *4*: 378-386.

Encinas-Romero, M. A., Aguayo-Salinas, S., Valenzuela-Garcia, J. L., Payan, S. R. & Castilon-Barraza, F. F. (2010). Mechanical and bioactive behavior of hydroxyapatite wollastonite sintered composites. *International Journal of Applied Ceramic Technology*, *7*: 164-177.

Evis, Z. (2007). Reactions in hydroxyapatite-zirconia composites. *Ceramics International*, *33*: 987-991.

Fathi, M. H., Hanifi, A. & Mortazavi, V. (2008). Preparation and bioactivity evaluation of bone-like hydroxyapatite nanopowder. *Journal of Materials Processing Technology*, *202*: 536-542.

Fathi, M. H. & Kharaziha, M. (2009). Two step sintering of dense, nanostructural forsterite. *Material Letters*, *63*: 1455-1458.

Fathi, M. H. & Hanifi, A. (2007). Evaluation and characterisation of nanostructure hydroxyapatite powder prepared by simple sol-gel method. *Materials Letters*, *61*, 3978-3983.

Fernandez, E., Gil, F. J., Ginebra, M. P., Driessens, F. C. M., Planell, J. A. & Best, S. M. (1999a). Calcium phosphate bone cements for clinical applications. Part I: Solution chemistry. *Journal of Materials Science: Materials in Medicine*, *10*: 169-176.

Galea, L. G., Bohner, M., Lemaitre, J., Kohler, T. & Muller, R. (2008). *Biomaterials*, *29*: 3400-3407.

Giannoudis, P. V., Dinopoulus, H. & Tsiridis, E. (2005). Bone substitutes: An update. *International Journal of the Care of the Injured*, *365*: 520-527.

Gibson, I. R., Ke, S., Best, S. M. & Bonfield, W. (2001). Effect of powder characteristics on the sinterability of hydroxyapatite powders. *Journal of Materials Science: Materials in Medicine*, *12*: 163-171.

Goller, G., Demirkiran, H., Oktar, F. N. & Demikersen, E. (2003). Processing and characterization of bioglass reinforced hydroxyapatite composites. *Ceramics International*, *29*: 721-724.

Gu, Y. W., Loh, N. H., Khor, K. A., Tor, S. B. & Cheang, P. (2002). Bone-like apatite layer formation on hydroxyapatite prepared by spark plasma sintering (SPS). *Biomaterials*, *25*: 4127-4134.

Habibovic, P. & Barralet, J. E. (2011). Bioinorganics and biomaterials: bone repair. *Acta Biomaterialia*. *7*: 3013-3026.

Hafezi, M., Talebi, A. R., Miresmaeili, S. M., Sadeghian, F. & Fesahat, F. (2013). Histological analysis of bone repair in rat femur via nanostructured merwinite granules. *Ceramics International*, *39*: 4575-4580.

Han, J. K., Song, H. Y., Saito, F. & Lee, B. T. (2006). Synthesis of high purity nano-sized hydroxyapatite powder by microwave-hydrothermal method. *Materials Chemistry and Phy*sics, *99*: 235-239.

He, L. H., Standard, O. C., Huang, T. T. Y., Latella, B. A. & Swain, M. V. (2008). Mechanical behaviour of porous hydroxyapatite. *Acta Biomaterialia*, *4*: 577-586.

Hench, L. L., Splinter, R. J., Allen, W. C., & Greenlee, T. K. (1972). Bonding mechanisms at the interface of ceramic prosthetic materials. *Journal of Biomedical Materials Research*, *2*: 117-141.

Hench, L. L., Wilson J, eds. (1993). An introduction to bioceramics. *World Scienctific*, : 1-24.

Hench, L. L. (1998). Bioceramics. *Journal of the American Ceramic Society*, *81*: 1705-1728

Hench, L. L. (2000). The challenge of orthopaedic materials. *Current Orthopaedics*, *14*: 7-15.

Hench, L. L. (1991). Bioceramics: From concept to clinic. *Journal of the American Ceramic Society*, *74*: 1487-1510.

Hench, L. L. (2006). The story of bioglass. *Journal of Materials Science: Materials in Medicine*, *17*: 967-978.

Heyman, D. & Passuti, N. (1999). Bone substitutes: new concept. *European Journal of Orthopaedic Surgery & Traumatology*, *9*: 179-184.

Hsieh, M., Perng, L., Chin, T. & Perng, H. (2001). Phase purity of sol-gel-derived hydroxyapatite ceramic. *Biomaterials*, *22*: 2601-2607.

Ioku, K, Goto, S., Kurosawa, H., Shibuya, K., Yokozeki, H., Hayashi, T., Nakagawa, T. (1996). Reaction of porous β-TCP with different micro-structure in vivo. *Bioceramics*, *9*: 201-204.

Jagdale, P.N. & Bamane, SR. (2011). Calcium hydroxyapatite bioceramics and evaluation of their in vitro biocompatibility. *Research Journal of Pharmaceutical, Biological and Chemical Sciences, 2*: 180-186.

Jagwiga, B. M., Krzysztof, H., Maciej, S., Miroslaw, M. B., Beata, M. & Radoslaw, L. (2016). Natural and synthethic hydroxyapatite/zirconia composites: A comparative study. *Ceramics International*, *42*: 11126-11135.

Jokanovic, V., Izvonar, D., Dramicanin, M. D., Jokanovic, B., Zivojinovic, V., Markovic, D. & Dacic, B. (2006). Hydrothermal synthesis and nanostructure of carbonated calcium hydroxyapatite. *Journal of Materials Science: Materials in Medicine*, *17*: 539-546.

Juang, H. Y. & Hon, M. H. (1996). Effect of calcination in the sintering of hydroxypapatite. *Biomaterials*, *17*: 2059-2064.

Jun, I. K., Song, J. H., Choi, W. Y., Koh, Y. H., Kim, H. E. & Kim, H. W. (2007). Porous hydroxyapatite scaffolds coated with bioactive apatite wollastonite glass ceramics. *Journal of the American Ceramic Society*, *90*: 2703-2708.

Kalita, S. J., Bhardwaj, A. & Bhatt, H. A. (2007). Nanocrystalline calcium phosphate ceramics in biomedical engineering. *Materials Science and Engineering: C*, *27*: 441-449.

Kalmodia, S., Goenka, S., Laha, T., Lahiri, D., Basu, B., & Balani, K. (2010). Microstructure, mechanical properties and in vivo biocompatibility of spark plasma sintered hydroxyapatite-aluminum oxide carbon nanotube composite. *Material Science and Engineering*, *30*: 1162-1169.

Kangasniemi, I. M. O. (1993). Development of Ca, P-ceramic containing bioactive glass composites. *Master Thesis, University of Leiden*, *The Netherlands*.

Kharaziha, M. & Fathi, M. (2009). Synthesis and characterization of bioactive forsterite nanopowder. *Ceramics International*, *35* (6): 2449-2454.

Kharaziha, M. & Fathi, M. H. (2010). Improvement of mechanical properties and biocompatibility of forsterite bioceramic addressed to bone tissue engineering materials. *Journals of the mechanical behavior of biomedical materials, 3*: 530 – 537.

Khorsand, S., Fathi, M. H., & Amirkhanlou, S. (2014). Hydroxyapatite/alumina nanocrystalline composite powders synthesized by sol-gel process for biomedical applications. *International Journal of Minerals, Metallurgy, and Materials*, *21* (10): 1033-1036.

Kien, P. T., Ishikawa, K. & Tsuru, K. (2015). Setting reaction of α-TCP spheres and an acidic calcium phosphate solution for the fabrication of fully interconnected macroporous calcium phosphate. *Ceramics International*, *41*: 13525-13531.

Kim, H. M. (2001). Bioactive ceramics: challenges and perspectives. *Journal of the Ceramic Society of Japan*, *109* (4): 49-57.

Kokubo, T., Kim, H. M. & Kawashita, M. (2003). Novel bioactive materials with different mechanical properties. *Biomaterials*, *24*: 2161-2175.

Kokubo, T. (1990). Surface chemistry of bioactive glass ceramics. *Journal of Non Crystalline Solids*, *120*: 138-151.

Kokubo, T., Kim, H. M., Kawashita, M. & Nakamura, T. (2004). Bioactive metals: preparation and properties. *Journal of Materials Science*, *15*: 99-107.

Kokubo, T., Shigematsu, M., Nagashima, Y., Tashiro, M., Nakamura, T., Yamamuro, T. & Higashi, S. (1982). Apatite and wollastonite containing glass ceramics for prosthetic applications. *Bulletin of the Institute for Chemical Research*, *60*: 260-268.

Kobayashi, S. & Murakoshi, T. (2013). Characterization of mechanical properties and bioactivity of hydroxyapatite/β-tricalcium phosphate composites. *Advanced Composite Materials*, *23*: 163-177.

Kosanic, C., Stubicar, N., Tomasic, N., Bermanec, V., & Stumicar, M. (2005). Synthesis of forsterite powder by combined ball milling and thermal treatment. *Journal of Alloys and Compounds*, *389*: 306-309.

Kulkarni, S. S., Yong, Y., Rys, M. J. & Lei, S. (2013). Machining assessment if nano-crystalline hydroxyapatite bio-ceramic. *Journal Manufacturing Processes*, *15*(4): 666-672.

Kumta, P. N., Sfeir, C., Lee, D. H., Olton, D. & Choi, D. (2005). Nanostructured calcium phosphates for biomedical applications: novel synthesis and characterization. *Acta Biomaterialia*, *1*: 65-83.

Laczka, M., Cholewa, K. & Osyczka, A. M. (2016). Bioactivity and osteoinductivity of glasses and glassceramics and their material determinants. *Ceramics International*, *42*: 14313-14325.

Lala, S., Satpati, B. & Pradhan, S. K. (2016). Sintering behavior and growth mechanism of β-TCP in nanocrystalline hydroxyapatite synthesized by mechanical alloying. *Ceramics International*, *42*: 13176-13182.

Landi, E. Tampieri, A., Celotti, G. & Sprio, S. (2000). Densification behaviour and mechanisms of synthetic hydroxyapatites. *Journal of European Ceramic Society*, *20*: 2377-2387.

LeGeros, R. Z. (1991). Calcium phosphates in oral biology and medicine. *Monographs in Oral Science*, *15*: 1-201.

LeGeros, R. Z.& LeGeros, J.P. (1993). Dense hydroxyapatite: In An Introduction to Bioceramics. Ed. By Hench, L. L & Wilson. *J. (World Scientific Singapore)*, *9*: 139-180.

LeGeros, R. Z., Lin, S., Rohanizadeh, R., Mijares, D. & LeGeros, J. P. (2003). Biphasic calcium phosphate bioceramics: preparation, properties and applications. *Journal of Materials Science: Materials in Medicine*, *14*: 201-209.

Le Huec, Schaeverbeke, T., Clement, D., Faber, J. & Le Rebeller, A. (1995). Influence of porosity on the mechanical resistance of hydroxyapatite ceramics under compressive stress. *Biomaterials*, *16*: 113-118.

Li, J., Liao, H. & Hermansson, L. (1996). Sintering of partially-stabilized zirconia and partially stabilized zirconia-hydroxyapatite composites by hot isostatic pressing and pressureless sintering. *Biomaterials*, *17*: 1787-1790.

Li, J., Fartash, B. & Hermansson, L. (1995). Hydroxyapatite-alumina composites and bone bonding. *Biomaterials*, *16*: 417-422.

Li, J., Wang, Q., Liu, J. H., & Li, P. (2009). Synthesis process of forsterite refractory by iron ore tailings. *Journals of environmental sciences supplement*, *16*: 92-295.

Liu, Y., Hou, D. & Wang, G. (2004). A simple wet chemical synthesis and characterization of hydroxyapatite nanorods. *Materials Chemistry and Physics*, *86*: 69-73.

Liu, Y. & Wang, M. (2007). Developing a composite material for bone tissue repair. *Current Applied Physics*, *7*: 547-554.

Liu, H., Yazici, H., Ergun, C., Webster, T. J. & Bermek, H. (2008). An in vitro evaluation of the Ca/P ratio for the cytocompatibility of nano to micron particulate calcium phosphates for bone regeneration. *Acta Biomaterialia*, *4*: 1472-1479.

Lugo, G. J., Mazon, P. & De Aza, P. N. (2016). Material processing of a new calcium silicophosphate ceramic. *Ceramics International*, *42*: 673-680.

Ma, J., Chen, C. Z., Wang, D. G., Shao, X., Wang, C. Z. & Zhang, H. M. (2012). Effect of MgO addition on the crystallization and in vitro bioactivity of glass ceramics in the CaO-MgO-SiO_2-P_2O_2 system. *Ceramics International*, *38*: 6677-6684.

Mano, J. F., Sousa, R. A., Boesel, L. F., Neves, N. M. & Reis, R. L. (2004). Bioinert, biodegradable and injectable polymeric matrix composites for hard tissue replacement: state of the art and recent developments. *Composites Science & Technology*, *64*: 789-817.

Mendelson, M. I. (1969). Average grain size in polycrystalline ceramics. *Journal of the American Ceramic Society*, *52*: 443-446.

Mobasherpour, I., Heshajin, M. S., Kazemzadeh, A. & Zakeri, M. (2007). Synthesis of nanocrystalline hydroxyaptite by using precipitation method. *Journal of Alloys and Compounds*, *430*: 330-333.

Mobasherpour, Hashjin, M. S., Toosi, S. S. & Kamachali, R. D. (2009). Effect of the addition ZrO_2-Al_2O_3 on nanocrystalline hydroxyapatite bending strength and fracture toughness. *Ceramics International*, *35*: 1569-1574.

Monika, S. (2015). Substituted hydroxyapatite for biomedical applications: A review. *Ceramics International*, *41*: 9203-9231.

Muralithran. G. & Ramesh. S. (2000). The effects of sintering temperature on the properties of hydroxyapatite. *Ceramics Intternational*, *26*: 221-230.

Murugan, R. & Ramakrishna, S. (2005). Aqueous mediated synthesis of bioresorbable nanocrystalline hydroxyapatite. *Journal of Crystal Growth*, *274*: 209-213.

Narasaraju, T. S. B. & Phebe, D. E. (1996). Review: Some physico-chemical aspects of hydroxylapatite. *Journal of Material Science*, *31*: 1-21.

Niihara, K. (1985). Indentation microfracture of ceramics – Its application and problems. *Ceramic Society of Japan*, *20*: 12-18.

Nikaido, T., Tsuru, K., Munar, M., Maruta, M., Matsuya, S., Nakamura, S. & Ishikawa, K. (2015). Fabrication of β-TCP foam: Effects of magnesium oxide as phase stabilizer on its properties. *Ceramics International*, *32*: 617-621.

Nursen, K., Muharrem, T. & Feza, K. (2004). Fabrication and characterization of porous tricalcium phosphate ceramics. *Ceramics International*, *30*: 205-211.

Orlovskii, V.P., Komlev, V.S. & Barinov, S. M. (2002). Hydroxyapatite and hydroxyapatite-based ceramics. *Inorganic Materials*, *38*: 973-984.

Paul, C. (2004). Bone structure and function. *Retrieved from https://deps.washington.edu/bonebio/ASBMRed/structure.html*.

Pramanik, S., Agarwal, A. K., Rai, K. N. & Garg, A. (2007). Development of high strength hydroxyapatite by solid-state sintering process. *Ceramics International*, *33*: 419-426.

Rabiee, S. M., Nazpar, N., Azizian, M., Vashaee, D. & Tayebi, L. (2015). Effect of ion substitution on properties of bioactive glasses: A review. *Ceramics International*, *41*: 7241-7251.

Rahaman, M.N. (1995). Ceramic processing and sintering (2nd ed). *New York: Marcel Dekker, Inc*.

Ramesh, S., Aw., K. L., Tolouei, T., Amiriyan, M., Tan, C. Y., Hamdi, M., Purbolaksono, J., Hassan, M. A. & Teng, W. D. (2013). Sintering properties of hydroxyapatite powders prepared using different methods. *Ceramics International*, *39*: 111-119.

Ramesh, S., Tan, C. Y., Tolouei, R., Amiriyan, M., Purbolaksono, J., Sopyan, I. & Teng, W. D. (2012). Sintering behavior of hydroxyapatite prepared from different routes. *Materials and Design*, *34*: 148-154.

Ramesh, S., Tan, C. Y., Bhaduri, S. B., Teng, W. D. & Sopyan, I. (2008). Densification behaviour of nanocrystalline hydroxyapatite bioceramics. *Journal of Materials Processing Technology*, *206*: 221-230.

Ramesh, S., Tan, C. Y., Sopyan, I., Hamdi, M. & Teng, W. D. (2007a). Consolidation of nanocrystalline hydroxyapatite powder. *Science and Technology of Advanced Materials*, *8*: 124-130.

Ramesh, S., Tan, C. Y., Bhaduri, S. B. & Teng, W. D. (2007b). Rapid densification of nanocrystalline hydroxyapatite for biomedical applications. *Ceramics Int*ernational, *33*: 1363-1367.

Ramesh, S. (1997). The influence of transition metal oxide additions on the manufacturing behavior & properties of yttria-tetragonal zirconia polycrystals. (Doctoral Dissertation, University of Sundreland).

Ramesh, S. (2004). A method for manufacturing hydroxyapatite bioceramic. *Malaysia Patent.* No. PI. 20043325.

Raynaud, S., Champion, E., Bernache-Assollant, D., & Thoma, P. (2002a). Calcium phosphate apatites with variable Ca/P atomic ratio I. Synthesis, characterization and thermal stability of powders. *Biomaterials*, *23*: 1065-1072.

Raynaud, S., Champion, E., & Bernache-Assollant, D. (2002b). Calcium phosphate apatites with variable Ca/P atomic ratio II. Calcination and sintering. *Biomaterials*, *23*: 1073-1080.

Raynaud, S., Champion, E., Bernache-Assollant, D., & Lafon, J. P. (2002c). Calcium phosphate apatites with variable Ca/P atomic ratio III. Mechanical properties and degradation in solution of hot pressed ceramics. *Biomaterials*, *23*: 1081-1089.

Rodriguez-Lorenzo, L. M., Vallet-Regi, M. & Ferreira, J. M. F. (2001). Fabrication of hydroxyapatite bodies by uniaxial pressing from a precipitated powder. *Biomaterials*, *22*: 583-588.

Roeder, R. K., Converse, G. L., Kane, R. J. & Yue, W. (2008). Hydroxyapatite reinforced polymer biocomposites for synthetic bone substitutes. *Biomaterials*, *60*: 38-45.

Ruys, A. J., Wei, M., Sorrell, C. C., Dickson, M. R., Brandwood, A. & Milthorpe, B. K. (1995a). Sintering effects on the strength of hydroxyapatite. *Biomaterials*, *16*: 405-415.

Ryu, H. S., Lee, J. K., Kim, H. & Hong, K. S. (2005). New type of bioactive materials: Hydroxyapatite/α-wollastonite composites. *Journal of Materials Research, 20*: 1154-1163.

Saeri, M. R., Afshar, A., Ghorbani, M., Ehsani, N. & Sorrell, C. C. (2003). The wet precipitation process of hydroxyapatite. *Materials Letters*, *57*: 4064-4069.

Santos, M. H., de Oliveira, M., de Freitas Souza, L. P., Mansur, H. S. & Vasconcelos, W. L. (2004). Synthesis control and characterization of hydroxyapatite prepared by wet precipitation process. *Materials Research Bulletin*, *7* (4): 625-630.

Sara, L. K. Y, Christopher, C. K. M., Ramesh, S., Tan, C. Y., Teng, W. D. & Sopyan, I. (2012). Characterization of forsterite bioceramics. *Advanced Materials Research*, *576*: 195-198.

Schwarz, K., & Milne, D. (1972). Growth promoting effects of Si in rats. *Nature*, *4*: 293-333.

Schwarz, K. & Milne, D. (1972). Fluorine requirement for growth in the rat. *Bioinorganic Chemistry*, *1* (4): 331-338.

Sebdani, M. M., & Fathi, M. H. (2011). Novel hydroxyapatite forsterite bioglass nanocomposite coatings with improved mechanical properties. *Journal of alloys and compound*, *509*: 2273-2276.

Sebdani, M. M. & Fathi, M. H. (2011). Fabrication and characterization of hydroxyapatite-forsterite bioactive glass composite nanopowder for biomedical applications. *International Journal of Applied Ceramic Technology*, *8* (3): 553-559.

Sivakumar, R. (1999). On the relevance of biomaterials. *Bulletin of Materials Science*, *22* (3): 647-655.

Shirtliff, V. J. & Hench, L., L. (2003). Bioactive materials for tissue engineering, regeneration and repair. *Journal of Materials Science*, *38*: 4697-4707.

Siyu, N., Lee, C., & Jiang, C. (2007). Preparation and characterization of forsterite bioceramics. *Ceramics International*, *33*: 83-88.

Slosarcyzk, A., Stobierska, E. Paszkiewicz, Z. & Gawlicki, M. (1996). Calcium phosphate materials prepared from precipitates with various calcium-phosphorus molar ratio. *Journal of the American Ceramic Society., 79* (10): 2539-2544.

Suchanek, W., Yashima, M., Kakihana, M. & Yoshimura, M. (1997). Hydroxyapatite ceramics with selected sintering additives. *Biomaterials*, *18*: 923-933.

Suchanek, W. L., Shuk, P., Byrappa, K., Riman, R. E., TenHuisen, K. S. & Janas, V. F. (2002). Mechanochemical hydrothermal synthesis of carbonated apatite powders at room temperature. *Biomaterials*, *23*: 699-710.

Suchanek, W. & Yoshimura, M. (1998). Processing and properties of hydroxyapatite-based biomaterials for use as hard tissue replacement implants. *Journal of Materials. Research*, *13*: 94-116.

Sung, Y. M., Lee, J. C. & Yang, J. W. (2004). Crystallization and sintering characteristics of chemically precipitated hydroxyapatite nanopowder. *Journal of Crystal Growth*, *262*: 467-472.

Sugiyama, T., Tsunooka, T., Kakimoto, K., & Ohsato, H. (2006). Microwave dielectric properties of forsterite-based solid solutions. *Journals of the European Ceramic*

Tampieri, A., Celloti, G., Sprio, S. & Mingazzini, C. (2000). Characteristics of synthetic hydroxyapatites and attempts to improve their thermal stability. *Materials Chemistry Physics*, *64*: 54-61.

Tancred, D. C., Carr, A. J. & McCormack, B. A. O. (2001). The sintering and mechanical behavior of hydroxyapatite with bioglass additions. *Journal of Materials Science: Materials in Medicine*, *12* (1): 81-93.

Tancred, D. C., McCormack, B. A. O, & Carr, A. J. (1998). A quantitative study of the sintering and mechanical properties of hydroxyapatite/phosphate glass composites. *Biomaterials*, *19*: 1735-1743.

Tavangarian, F., & Emadi, R. (2010). Effects of fluorine ion and mechanical activation on nanostructure forsterite formation mechanism. *Powder Technology*, *203*: 180-186.

Tavangarian, F., & Emadi, R. (2011). Improving degradation rate and apatite formation of nanostructure forsterite. *Ceramics International*, *38*: 2275- 2280.

Teamey, G. J., Boppart, S. A., Bouma, B., Brezinski, M. E., Golubovic, B., Southern, J. F., Swanson, E. A., & Fujimoto, J. G. (1996). *Conference on Lasers and Electra-Optics,* OSA Technical Digest Series, *9*: 57.

Thamaraiselvi, T. V. & Rajeswari, S. (2004). Biological evaluation of bioceramic materials – A review. *Trends in Biomaterials & Artificial* Organs, *18*: 9-17.

Thurmer, M. B., Diehl, C. E. & Santos, L. A. (2016). Calcium phosphate cements based on alpha-tricalcium phosphate obtained by wet method: Synthesis and milling effects. *Ceramics International*, *13*: 1330-1245.

Tian, T., Jiang, D., Zhang, J. & Lin, Q. (2008). Synthesis of Si-substituted hydroxyapatite by a wet mechanochemical method. *Materials Science and Engineering*: *C*, *28*, 57-63.

Tony, M. K., Elise, F. M & Oscar, C. Y. (2003). Standard handbook of biomedical engineering & design. Bone Mechanics. *Mc-Graw-Hill Professional*.

Vallet-Regi, M. & Gonzalez-Calbet, J. M. (2004). Calcium phosphate as substitution of bone tissues. *Progress in Solid State Chemistry*, *32*: 1-31.

Veljovic, Dy., Jancic-Haneman, R., Balac, I., Jokie, B., Putic, S., Petrovic, R., Janackonic, Dj. (2011). The effect of the shape and size of the pores on the mechanical properties of porous HAP-based bioceramics. *Ceramics International*, *37*: 471-479.

Viswanath, B. & Ravishankar, N. (2006). Interfacial reactions in hydroxyapatite/alumina nanocomposites. *Scripta Materialia*, *55*: 863-866.

Viswanath, B., Raghavan, R., Ramamurty, U. & Ravishankar, N. (2007). Mechanical properties and anisotropy in hydroxyapatite single crystals. *Scripta Materialia*, *57*: 361-364.

Vitale-Brovarone, C., Verne, E., Robligio, L., Martinasso, G., Canuto, R. A. & Muzio, G. (2008). Biocompatible glass-ceramics materials for bone substitution. *Journal of Materials Science: Materials in Medicine*, *19*: 471-478.

Wang, F., Li, M., Lu, Y. & Qi, Y. (2005). A simple sol-gel technique for preparing hydroxyaptite nanopowders. *Materials Letters*, *59*: 916-919.

Wang, X., Fan, H., Xiao, Y., & Zhang, X. (2006). Fabrication and characterization of porous hydroxyapatite / β-tricalcium phosphate ceramics by microwave sintering. *Materials Letters, 60*: 455-458.

Wang, P. E. & Chaki, T. K. (1993). Sintering behaviour and medical properties of hydroxyapatite and dicalcium phosphate. *Journal of Mateirals Science: Mateirals in Medicine*, *4*: 150-158.

Wang, M. (2003). Developing bioactive composite materials for tissue replacement. *Biomaterials*, *24*: 2133-2151.

Williams, D. F. (2003). Biomaterials and tissue engineering in reconstructive surgery. *Sādhanā*, *28*: 563-574.

Williams, D. F. (2008). On the mechanism of biocompatibility. *Biomaterials*, *29*: 2941-2953.

Witte, F., Feyerabend, F., Maier, P., Fischer, J., Stormer, M., Blawert, C., Dietzel, W. & Hort, N. (2007). Biodegradable magnesium-hydroxyapatite metal matrix composites. *Biomaterials*, *28*: 2163-2174.

Xiao, F., Ye, J., Wang, Y. & Rao, P. (2005). Deagglomeration of HA during precipitation synthesis. *Journal of Materials Science*, *40*: 5439-5442.

Xie, Y., Zhai, W., Chen, L., Chang, J., Zheng, X. & Ding, C. (2009). Preparation and in vitro evaluation of plasma sprayed Mg_2SiO_4 coating on titanium alloy. *Acta Biomaterialia*, *5*: 2331-2337.

Xu, P. K. & Wei, G. Z. (2005). New process technology for refractory. *Metallurgy Industry Press, Beijing, 4*: 2-5.

Xu, Y., Wang, D., Yang, L. & Tang, H. (2001). Hydrothermal conversion of coral into hydroxyapatite. *Materials Characterization*, *47*: 83-87.

Yamanaka, A., Yokoyama, Y. & Iwamoto, H. (2006). Biomaterials in ophthalmology. *Journal of Artificial Organs*, *9*: 67-70.

Yamamuro, T., Kokubo, T. & Ohtsuki, C. (1992). Mechanism of apatite formation on CaO-SiO_2-P_2O_5 glasses in a simulated body fluid. *Journal of Non-Crystalline Solids*, *143*: 84-92.

Yasuda, H. Y., Mahara, S., Terashita, N. & Umakoshi, Y. (2002). Preparation of porous hydroxyapatite/alpha tricalcium phosphate composites by a colloidal process. *Materials Transaction*, *43*: 1332-1335.

Zakaria, S.M., Sharif, S.H., Othman, M. R., Yang, F., Jansen, J.A. (2013). Nano-phase hydroxyapatite as a biomaterial in advanced hard tissue engineering. *Tissue Engineering Part B Reviews*, *19* (5): 431-441.

Zhang, C., Zhang, X., Liu, C., Sun, K., & Yuan, J. (2016). Nano – alumina/hydroxyapatite composite powders prepared by in-situ chemical precipitation. *Ceramics International*, *42*: 279-285.

Zhang, S. & Gonsalves, K. E. (1997). Preparation and characterisation of thermally stable nanohydroxyapatite. *Journal of Materials Science: Materials in Medicine*, *8*: 25-28.

Zhang, Y., Wang, Y., Shi, B. & Cheng, X. (2007). A platelet derived growth factor releasing chitosan/coral composite scaffold for periodontal tissue engineering. *Biomaterials*, *28*: 1515-1522.

LIST OF PUBLICATIONS

1) Densification behavior of magnesium orthosilicate-hydroxyapatite composite. Journal of Ceramic Processing Research. 17(6): 620-625 (2016).

2) Sintering behavior and properties of magnesium orthosilicate-hydroxyapatite ceramic. Ceramics International. 42: 15756-15761 (2016).